Characterisation of the innate immune sensor MDA5



Antonio Gregorio Dias Jr.

Radcliffe Department of Medicine
Lincoln College
University of Oxford

Supervisors: Jan Rehwinkel, Ph.D.
Christian Eggeling, Ph.D.

Thesis submitted for the degree of Doctor of Philosophy in Medical Sciences

Trinity Term 2017

ACKNOWLEDGEMENTS

I am extremely grateful to my supervisors Profs. Dr. Jan Rehwinkel and Dr. Christian Eggeling. First for the great opportunity to join their labs for a 4-year DPhil program in Oxford. But also for their immense support, care, friendship, and professional development I had the chance to be exposed to.

I would like to dedicate my thesis and all of the happiest moments of my life to my mother, Edite Dias (*in memoriam*), and my father, Antonio Gregorio. I also want to express my feelings and love to all my family members and close ones: Elaine Dias, Eliane Dias, Ediane Dias, Yasmin Quaresma, Paulo Victor, Edite Maria, Gabriela Prata, and Edna Paiva.

To CNPq from the Brazilian government for funding my studies through a “Science Without Borders Scholarship” in Oxford for 4 years.

I would like to thank Profs. Dr. Vincenzo Cerundolo (WIMM, University of Oxford) and Dr. Quentin Sattentau (Sir Dunn School of Pathology, University of Oxford) as members of my Thesis Committee meetings. All feedback and criticism on my work were very well appreciated.

I also received valuable comments and feedbacks from Profs. Dr. Hal Drakesmith (WIMM, University of Oxford) and Dr. Ervin Fodor (Sir Dunn School of Pathology, University of Oxford) as members of my Transfer of Status and Confirmation of Status.

To Lincoln College for the academic and social support. I also want to thank the Lincoln Blue Funds board for the financial support to play Volleyball for the University of Oxford for the past three years.

To Prof. Yanick Crow (University of Manchester) for providing us with primary human skin fibroblast used in this study.

To Profs. Tao Dong (WIMM, University of Oxford) and Dr. Jin Boquan’s group (Department of Immunology, Fourth Military Medical University, China) for helping us with the generation of human MDA5 antibodies used in this study.

To the examiners of this thesis for the taking their time to evaluate and criticise my work: Profs. Dr. Castello Palomares (University of Oxford, UK) and Dr. Katherine Fitzgerald (UMass, USA).

To all my friends and colleagues from both laboratories of Profs. Rehwinkel and Eggelling. In particular, I would like to thank all those members which friendship

and collaboration were relevant for my academic training and to this thesis: Dr. Alice Mayer, Jonny Hertzog, Dr. Rachel Rigby, Chiara Cursi, Tamara Davenne, Dr. Jonathan Maelfait, Dr. Natalia Sampaio, Dr. Jakub Chojnakci, Dr. Silvia Galiani, and Dr. Erdinc Sezgin.

To Oxford University Volleyball Club (OUVC) members for providing me with a great and joyful distraction, and right level of physical exercise to help me to keep up with a healthy routine. In addition to achieve a Varsity Blues Certificate and many great friends, I have also developed several team building and leadership skills. The same applies to the Oxford Volleyball Club (OVC), Maite Braud and Martijan Stroo, for the chance to play Beach Volleyball in a “sunny” city of Oxford.

To all my beloved friends that had a great importance in most of my days in Oxford: Luiza, Neele, Deborah, Flavia Filocreao, Tom, Florian, Kathie, Lena, Vanessa, Tess, Layal, Priscila, Simonas, Itziar, Lauren, Uli, Cecilia, Michael, Pei Jin, and so many others I had the pleasure to meet and share so many unforgettable moments.

ABSTRACT

Melanoma Differentiation-Associated gene 5 (MDA5) is a cytosolic RNA receptor. Its activation triggers the production of the antiviral cytokines type I and III Interferons (IFN). It is believed that MDA5 detects viral and/or cellular RNAs. The latter case may be relevant in the context of cancer treatment with DNA demethylating agents, and in autoinflammatory and autoimmune diseases. In all these settings, physiological MDA5 agonists have not been identified. To identify MDA5-stimulatory RNAs, we generated mouse monoclonal antibodies against human MDA5. We showed that some of these antibodies are specific and detect MDA5 protein by Western Blot, in immunofluorescence, and work in immunoprecipitation (IP). To identify MDA5's RNA ligands in living cells, we employed the UV-crosslinking and IP (iCLIP) technique. Interestingly, we found that MDA5 associated with RNAs regardless of virus infection. Sequencing and characterisation of these RNA species will be performed in the future. MDA5 overexpression led to IFN-I induction, which could be explained by MDA5 binding to cellular RNAs. Indeed, two bioassays developed here suggest that MDA5 can sense RNAs from uninfected human cells and tissues. In a second project, we demonstrated that Zika Virus (ZIKV) replication generated MDA5 and, RIG-I immunostimulatory RNAs. RIG-I-dependent IFN-I induction was sensitive to alkaline phosphatase treatment, in line with the requirement for 5'-ppp groups for RIG-I activation. Furthermore, by using a mini-screen of ZIKV proteins, we identified the non-structural protein 5 (NS5) as a potent inhibitor of the type I IFN signalling pathway. We show that this inhibitory mechanism is unrelated to: i) NS5's nuclear localisation, ii) mutations found in strains of the current outbreak, and iii) a conserved residue in the methyltransferase domain. In sum, we provide novel insights into the biology of MDA5, new reagents for the studies of MDA5,

as well as data on the role of RNA sensors in detecting ZIKV infection and evasion of innate immunity by ZIKV.

Table of Contents

CHAPTER 1 **15**

1 INTRODUCTION **15**
1.1 INNATE IMMUNE PATTERN RECOGNITION RECEPTORS SENSE PAMPS AND DAMPS 15
1.2 THE TYPE I AND III INTERFERON SYSTEMS INDUCE INTERFERON-STIMULATED GENES 19
1.3 THE RIG-I-LIKE RECEPTOR FAMILY 20
1.4 THE AGONISTS FOR RIG-I 23
1.5 ACTIVATION AND CONTROL OF RIG-I-LIKE RECEPTOR SIGNALLING PATHWAY 26
1.6 THE DISCOVERY OF MELANOMA DIFFERENTIATION-ASSOCIATED GENE 5 (MDA5) 30
1.7 LONG DSRNAS ARE PUTATIVE AGONISTS FOR MDA5 32
1.8 OTHER PUTATIVE AGONISTS FOR MDA5 35
1.9 MDA5 AND RECOGNITION OF CELLULAR RNAS 37
1.10 VIRUSES OF THE *FLAVIVIRIDAE* FAMILY, *FLAVIVIRUS* GENUS 41

CHAPTER 2 **47**

2 MATERIAL AND METHODS **47**
2.1 CELLS 47
2.2 GENERATION OF HUMAN MDA5 (HMDA5) CONSTRUCTS 48
2.3 GENERATION OF HUMAN MDA5 (HMDA5) HYBRIDOMA CELL LINES AND MOUSE ASCITES 49
2.4 GENERATION AND VALIDATION OF THE HEK293.ΔIFIH1 MDA5 KNOCKOUT (KO) CELL LINE 51
2.5 CLONING OF ZIKA VIRUS (ZIKV) PLASMIDS 52
2.6 A549-ZIKV-RNA AND IVT-RNA 55
2.7 BIOASSAYS USING P125-HEK CELL STIMULATION 55
2.8 BIOASSAY USING PRIMARY HUMAN SKIN FIBROBLASTS 56
2.9 ANTIBODIES 57
2.10 WESTERN BLOT (WB) ANALYSIS 58
2.11 RT-QPCR 59
2.12 MICROSCOPY 60
2.13 DATA ANALYSIS AND STATISTICS 62
2.14 INDIVIDUAL NUCLEOTIDE RESOLUTION UV CROSSLINKING AND IMMUNOPRECIPITATION (ICLIP) 63

CHAPTER 3 **76**

3 GENERATION AND VALIDATION OF ANTIBODIES AGAINST HUMAN MDA5 **76**
3.1 GENERATION AND SCREENING OF HUMAN ANTI-MDA5 ANTIBODIES DERIVED FROM HYBRIDOMA CELL LINES AND MOUSE ASCITIC FLUIDS 77
3.2 GENERATION OF A HUMAN CELL LINE KNOCKOUT FOR MDA5 (HEK293.ΔPIFIH1) 82
3.3 VALIDATION OF ANTI-MDA5 ANTIBODIES 87

3.4 DISCUSSION 95

CHAPTER 4 109

4 DEVELOPMENT AND OPTIMISATION OF TECHNIQUES TO IDENTIFY AND CHARACTERISE MDA5 RNA LIGANDS 109

4.1 OPTIMISATION OF INDIVIDUAL-NUCLEOTIDE RESOLUTION UV CROSSLINKING AND IMMUNOPRECIPITATION (iCLIP) FOR HUMAN MDA5 111

4.2 DEVELOPMENT OF CELL-BASED BIOASSAYS TO ASSESS THE IMMUNOSTIMULATORY POTENTIAL OF CELLULAR RNAS 120

4.3 DISCUSSION 126

CHAPTER 5 137

5 ACTIVATION AND INHIBITION OF THE TYPE I INTERFERON RESPONSE BY ZIKA VIRUS 137

5.1 IDENTIFICATION OF RIG-I-LIKE RECEPTOR AGONISTS GENERATED DURING ZIKA VIRUS REPLICATION 138

5.2 GENERATION OF CONSTRUCTS TO EXPRESS ZIKA VIRUS PROTEINS 141

5.3 ZIKA VIRUS (ZIKV) NS5 BLOCKS TYPE I INTERFERON SIGNALLING 144

5.4 DISCUSSION 149

CHAPTER 6 161

6 CONCLUSIONS 161

REFERENCES 167

LIST OF FIGURES

Figure 1 - Pattern recognition receptors sense nucleic acids and induce antiviral interferons. 17

Figure 2 - The RIG-I-like receptor family signalling pathway. 22

Figure 3 - RIG-I-like receptor signalling is regulated by post-translational modifications. 28

Figure 4 – Genome organisation of viruses within the *Picornaviridae* family. 32

Figure 5 - Proteins generated by flaviviruses and vesicle-like replication sites. 43

Figure 6 – Basics of stimulated emission depletion (STED) Super-resolution optical microscopy. 62

Figure 7 - Screening of mouse ascites containing anti-MDA5 antibodies by Western Blot (WB). 79

Figure 8 - Immunostaining of HEK293 cells with mouse ascite 15. 81

Figure 9 - Co-staining of filaments and dsRNAs in HEK293 cells. 83

Figure 10 - Generation of HEK293 cells knockout for MDA5. 84

Figure 11 - Validation of anti-MDA5 antibodies in immunofluorescence (IF) assays. 88

Figure 12 - MDA5 distribution upon viral infection in cell cultures. 91

Figure 13 - Validation of purified monoclonal antibodies (mAbs) against human MDA5 by Western Blot (WB). 93

Figure 14 - Co-immunoprecipitation (co-IP) of RNAs associated with human MDA5. 114

Figure 15 - Essential and further optimisation steps for MDA5 UV-crosslinking and immunoprecipitation (iCLIP) technique. 117

Figure 16 - Effects on interferon (IFN) induction of wild-type (WT) and ATPase mutant MDA5 upon overexpression in 293T-TLA cells. _____ 119
Figure 17 - Transfection of cell and tissue total RNAs into HEK293-IFN-β promoter reporter cells. _____ 123
Figure 18 - Transfection of human tissue total RNA into primary human skin fibroblasts. _____ 125
Figure 19 – Detection of immunostimulatory activity in total RNAs extracted from A549 cells infected with Zika virus (ZIKV). _____ 140
Figure 20 – Cloning and expression of Zika virus (ZIKV) proteins in HEK293 cells. _____ 143
Figure 21 – The effects of Zika virus (ZIKV) protein overexpression in HEK293 cells. _____ 147
Figure 22 – Overexpression of Zika virus (ZIKV) NS5 mutants. _____ 148

LIST OF TABLES

Table 1 – Oligonucleotides to sequence hMDA5 constructs _____ 48

Table 2 – CRISPR oligonucleotides to delete *IFIH1* gene promoter region __ 51

Table 3 – Oligonucleotides to detect human MDA5 by RT-PCR_____ 52

Table 4 - Oligonucleotides used for ZIKV sequences cloning_____ 53

Table 5 - Buffers used on the iCLIP protocol_____ 74

ABBREVIATIONS

293T-TLA: 293T cells clone TLA (stably and constitutively expressing SV40 large antigen)

4SU: 4-thiouridine

5-Aza-CdR: 5-Azacytidine-2-deoxycytidine

ADAR1: Adenosine Deaminases Acting on RNA 1

ADE: antibody-dependent enhancement

AGS: Aicardi-Goutières Syndrome

AP: Alkaline phosphatase

Arboviruses: Arthropod-borne viruses

ATP: Adenosine triphosphate

BP: Base pairs

CARD: caspase activation and recruitment domains

cDNA: Complementar DNA

CDRs: Cytosolic DNA Receptors

cGAMP: cyclic guanosine monophosphate-adenosine monophosphate

cGAS: cGAMP synthase

CKII: Casein kinase II

CLRs: C-type lectin receptors

Co-IP: co-immunoprecipitation

CRISPR (Clustered Regularly Interspaced Short Palindromic Repeats)

CTD: C-terminal domain

CVB3: Coxsackievirus B3

DAMPs: danger-associated molecular patterns

DCs: Dendritic cells

EMCV: Encephalomyocarditis virus

FCS: Fetal calf serum

FRAP: Fluorescence Recovery After Photobleaching

FS: Frame shift

H: High

HCV: Hepatitis C virus

HDAC6: Histone Deacetylase 6

hiCLIP: RNA hybrid iCLIP

hMDA5: Human MDA5

HMW: High molecular weight

IF: Immunofluorescence

IFI16: Interferon-gamma inducible factor 16

IFN: Interferon

IFN-A/D: Comercial name for hybrid recombinant human Interferon α

IFNAR: IFN-α/β-receptors

IKK: IκB kinase complex

IRAlus: inverted repeat Alu structures

IRF3: Interferon regulatory transcription factor 3

ISG: interferon-stimulated genes

ISRE: Interferon-Sensitive Response Element

IVT-RNA: Neo^{1-99} *in vitro* transcribed RNA

JAK: Janus kinase

JEV: Japanese encephalitis virus

KO: Knockout

L: Leader protein

L: Low

LGP2: Laboratory of Genetics and Physiology 2

LMW: Low molecular weight

LPS: lipopolysaccharide

M: Medium

mAb: Monoclonal antibody

MAMs: mitochondrial-associated membranes

MAVS: Mitochondrial antiviral signalling protein

MDA5: Melanoma Differentiation-Associated gene 5

MEF: Mouse embryonic fibroblasts

MeV: Measles virus

MEZ: Merezein

MOI: Multiplicity of infection

MTase: Methyltransferase

Mut: Mutant

MyD88: myeloid differentiation primary response 88

NES: Nuclear export signals

NKs: Natural Killer cells

NLRs: Nucleotide-binding oligomerization domain (NOD)-like receptors

NLS: Nuclear localisation signal

NS: Nonstructural

Nt: nucleotide

ORF: Open Reading Frame

PAMPs: pathogen-associated molecular patterns

PAR-CLIP: Photoactivatable-Ribonucleoside-Enhanced Crosslinking and Immunoprecipitation

PKC: Protein kinase C

PKR: Protein kinase RNA-activated

PNK: T4 polynucleotide kinase

PRRs: pattern recognition receptors

RdRp: RNA-dependent RNA polymerase

RF: Replicative form

RIG-I: (Retinoic acid-inducible gene 1)

RIOK3: RIO kinase 3

RLRs: RIG-I-like receptors

RNF125: Ring finger protein 125

RPM: Rotations per minute

RT-PCR: Reverse Transcription Polymerase Chain Reaction

RT-qPCR: Real Time RT-PCR

RT: Room Temperature

siRNAs: small-interfering RNAs

SNP: Single-nucleotide polymorphisms

ssRNAs: single-stranded RNAs

STAT: Signal transducer and activator of transcription

STED: Stimulated Emission Depletion

STING: Stimulator of interferon genes

SUMO1: Small ubiquitin-like modifier-1

T1D: Type 1 Diabetes

TBEV: Tick-borne encephalitis

TIRAP: TIR-containing adaptor protein

TLRs: Toll-like receptors

TRAM: TRIF-related adaptor molecules

TRIF: TIR domain-containing adaptor-inducing IFN-β

TRIM 25: Tripartite motif-containing protein 25

TSS: Transcription start site

U: Units

UTR: Untranslated region

V-EMCV-RNA: Total RNA extracted from VERO cells infected with EMCV

vGAT: viral glutamine amidotransferase

WB: Western Blot

WT: Wild-type

ZIKV: Zika virus

γHV68: murine gamma herpesvirus 68

CHAPTER 1

1 INTRODUCTION

The immune system contains different types of specialised cells and mechanisms responsible for helping to maintain the human body homoeostasis. Physical barriers, proteins and other chemical molecules act synergistically to prevent and eliminate pathogens and malignant cells. It also contributes to the formation of a sterile environment during development.

There are tentatively two branches of the immune system: innate and adaptive. During an encounter with an infectious agent, the innate system acts as a first line of defence. It triggers different signalling cascades to counteract the invading organisms and contributes to the activation of the adaptive system.

In turn, after several days of exposure to an antigen, the adaptive system generates epitope-specific responses. These responses are mediated by somatic mutations that produce specific memory B and T lymphocytes. Altogether, these mechanisms aim to prevent parasite colonisation that could potentially lead to different diseases.

1.1 INNATE IMMUNE PATTERN RECOGNITION RECEPTORS SENSE PAMPS AND DAMPS

Certain cell types are considered to constitute the innate immune system, such as natural killers (NK), mast cells, eosinophils, basophils, macrophages,

neutrophils, and dendritic cells (DCs). Alongside, all nucleated cells contain innate immune germline-encoded pattern recognition receptors (PRRs). These possess an affinity for a variety of pathogen-associated molecular patterns (PAMPs) and danger-associated molecular patterns (DAMPs) derived from the course of a pathological process (Mogensen, 2009; Brubaker *et al.*, 2015).

Examples of PRRs are Toll-like receptors (TLRs), C-type lectin receptors (CLRs), Retinoic acid-inducible gene I (RIG-I)-like receptors (RLRs), Nucleotide-binding oligomerization domain (NOD)-like receptors (NLRs), and Cytosolic DNA Receptors (CDRs). These become activated by evolutionarily conserved microbe-derived PAMPs and DAMPs - e.g. self-molecules derived from immunogenic cell death - leading to the induction of inflammatory cytokines (Mogensen, 2009; Brubaker *et al.*, 2015; Roers, Hiller and Hornung, 2016).

As an example, gram-negative bacteria lipopolysaccharide (LPS) is a PAMP that binds to the cell surface TLR4. This stimulates transcription factors to produce pro-inflammatory cytokines (Pålsson-McDermott and O'Neill, 2004). Interestingly, cytosolic caspases 4 and 5 (caspase 11 in mice) can also sense LPS. This activates the non-canonical inflammasome pathway to induce IL-1β, IL-18, and pyroptosis (Shi *et al.*, 2014).

NLRP3 is a canonical component of the inflammasome pathway. Its activation requires two main steps: a) activation of TLR signalling by a microbial PAMP (signal 1, priming) – this upregulates the expression of pro-IL-1β and NLRP3; b) activation of NLRP3 induced by, for example, adenosine triphosphate (ATP) (signal 2). Finally, caspase 1 cleaves pro-IL-1β to its mature form, IL-1β (Mariathasan *et al.*, 2006; Franchi, Muñoz-Planillo and Núñez, 2012).

Therefore, there are many types of PAMPs and DAMPs, such as LPS, flagellin, peptidoglycans, glycolipids, ATP, fibronectin, heparan sulphate, etc., that can trigger PRRs (Brubaker *et al.*, 2015).

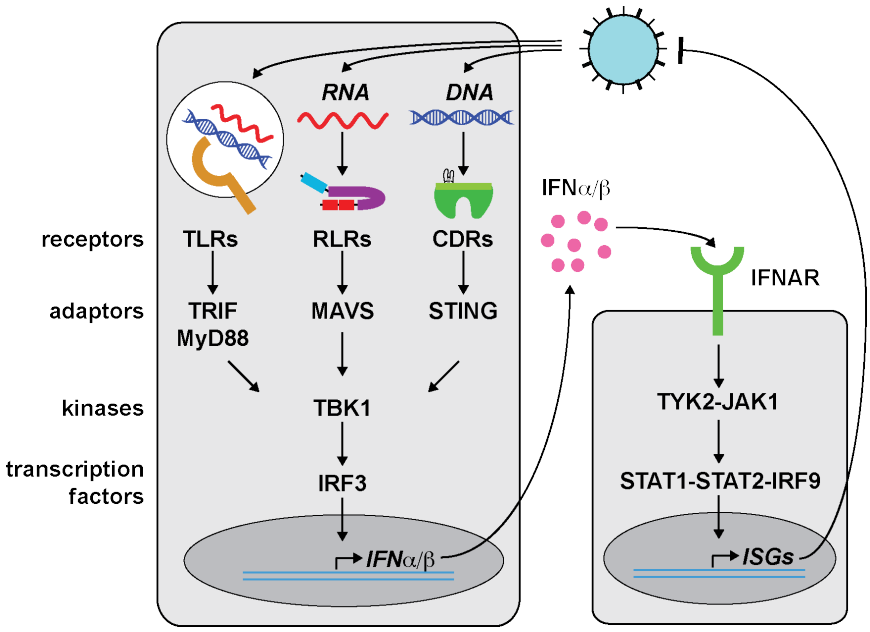


Figure 1 - Pattern recognition receptors sense nucleic acids and induce antiviral interferons. RNA or DNA can be sensed by endosomal Toll-like receptors (TLRs) and cytosolic RIG-I-like receptors (RLRs) and DNA receptors (CDRs). Each of these receptors triggers different adaptors: TRIF/MyD88 (TIR domain-containing adaptor-inducing IFN-β /myeloid differentiation primary response 88); MAVS (Mitochondrial Antiviral Signalling Protein); and STING (Stimulator of interferon genes). IRF3 (Interferon regulatory transcription factor 3) is then phosphorylated, dimerized and translocated to the nucleus. Type I interferons (IFNs) are produced and secreted. They act on the same or different cells containing the IFN I receptor (IFNAR). IFNAR activation leads to the activation of the JAK/STAT (Janus kinase/Signal transducer and activator of transcription) pathway and transcription of IFN-stimulated genes. Figure provided by Prof. Dr. Jan Rehwinkel.

Additionally, TLR-3/7/8/9, RLRs and CDRs can sense nucleic acids (RNA or DNA) derived from microbes (Figure 1) or the host. The latter is of particular interest in the context of immunogenic cell death, gain/loss-of-function mutations, mislocalization and aberrant accumulation of nucleic acids in autoimmune and

autoinflammatory diseases (Roers, Hiller and Hornung, 2016; Schlee and Hartmann, 2016).

James Chen's group ground-breaking discovery in 2013 revealed the sensor that detects cytosolic DNA. cGAS (cGAMP synthase) binds to DNA and generates cGAMP (cyclic guanosine monophosphate-adenosine monophosphate), a di-nucleotide with the ability to bind and activate STING (Stimulator of Interferon Genes) (Li *et al.*, 2013; Sun *et al.*, 2013).

cGAS has been shown to survey the cytosol and recognises DNAs of viral and cellular origins (e.g. mitochondrial DNAs) (Li *et al.*, 2013; West *et al.*, 2015). This concept has guided several studies aiming to explore its role during viral infections, autoimmune/autoinflammatory diseases, cancer pathogenesis and treatment, and cell senescence (Gao *et al.*, 2015; Chen *et al.*, 2016; T. Li *et al.*, 2016; Wang *et al.*, 2017; Yang *et al.*, 2017).

Interestingly, cGAMP has been shown to activate STING in bystander cells through GAP-junctions (Ablasser *et al.*, 2013). Additionally, enveloped viruses were demonstrated to incorporate cGAMP produced in infected cells (Bridgeman *et al.*, 2015; Gentili *et al.*, 2015). These mechanisms could potentially facilitate the transcription of ISGs (Interferon-Stimulated Genes) in neighbouring uninfected or newly infected cells, respectively.

IFI16 (interferon-gamma inducible factor 16) is another CDR and is localised mainly in the nucleus, but detects exogenous and viral DNA in the cytosol. It is believed to support cGAMP/cGAS signalling and thus to contribute to STING activation (Almine *et al.*, 2017; Jønsson *et al.*, 2017).

1.2 THE TYPE I AND III INTERFERON SYSTEMS INDUCE INTERFERON-STIMULATED GENES

Figure 1 depicts the signalling pathways of different nucleic acid sensors. In brief, TLRs use TIRAP/MyD88 (TIR-containing adaptor protein/myeloid differentiation primary response 88) and TRIF/TRAM (TIR domain-containing adaptor-inducing IFN-β/TRIF-related adaptor molecules) as adaptor molecules. RLRs use MAVS (Mitochondrial Antiviral Signalling Protein) as an adaptor, while CDRs – cGAS/cGAMP - use STING (Roers, Hiller and Hornung, 2016; Schlee and Hartmann, 2016).

Despite these PRRs use different adaptors, their signalling cascades converge to similar ends: activation of transcription factors (e.g. Interferon regulatory transcription factor 3, IRF3) followed by the transcription and secretion of cytokines, such as type I and III Interferons (IFN) (Brubaker *et al.*, 2015; Roers, Hiller and Hornung, 2016; Schlee and Hartmann, 2016).

IFN I comprise 13 subtypes of IFN-α (IFNA1, 2, 4, 5, 6, 7, 8, 10, 13, 14, 16, 17, and 21) and one IFN-β subtype (mainly expressed by fibroblasts). Three subtypes of IFN-λ represent IFN III in humans: IFN-λ1 (IL-29), IFN-λ2, and IFN-λ3 (IL28A/B). IFN I and III induce the expression of similar sets of genes and thus possess antiviral, antiproliferative, antitumour activities as well as contribute towards the activation of the adaptive immune system (Z. Zhou *et al.*, 2007; de Weerd and Nguyen, 2012).

IFN I and III act in autocrine and paracrine manners by binding different cell surface receptors (Figure 1). IFN I binds to IFN-α/β-receptors (IFNAR1 and 2 subunits) expressed in all cell types. IFN III requires a widely distributed receptor, IL10RB, and a cell type-specific high-affinity receptor, IFNLR1. IFNLR1

expression is mostly restricted to cells of epithelial origin (de Weerd and Nguyen, 2012).

The activation of these receptors triggers the JAK/STAT (Janus kinase/Signal transducer and activator of transcription) signalling pathway (Figure 1). Ultimately, ISGs are transcribed and some of which contain direct antiviral activity (de Weerd and Nguyen, 2012).

ISGs act at different levels to block viral replication. For example, PKR (Protein kinase RNA-activated) has an affinity for double-stranded RNAs (dsRNAs), and its autophosphorylation causes host protein translational shut-off (Williams, 1999). PKR was also shown to control the stability of IFN-β mRNAs during viral infection (Schulz *et al.*, 2010).

OAS1 (2'-5' oligoadenylate synthetase 1) is another example of an ISG that detects dsRNAs. It synthesises 2',5'-oligoadenylates that activate RNase L, which is responsible for the degradation of host and viral RNAs (Hornung *et al.*, 2014).

1.3 THE RIG-I-LIKE RECEPTOR FAMILY

RIG-I is the founding member of the RLR family. Initially, RIG-I was described to respond to retinoic acid treatment of gastric cancer cells (Huang *et al.*, 2000). Later, Takashi Fujita's group reported RIG-I was able to trigger IRF-3 and IFN-β promoters upon transfection of poly (I:C) dsRNAs into cell cultures. They also found it to be an ISG due to upregulation upon IFN-β treatment (Yoneyama *et al.*, 2004).

The RLR family comprises RIG-I, melanoma differentiation-associated gene 5 (MDA5), and laboratory of genetic and physiology 2 (LGP2) (Wu and Chen, 2014).

Figure 2 illustrates RIG-I/MDA-5/LGP2 protein domains and the RIG-I/MDA5 downstream signalling pathway, which is activated upon RNA recognition. RLRs share a DExD/H box RNA helicase domain and a C-terminal domain (CTD), both of which mediate RNA binding. RIG-I and MDA5, but not LGP2, also comprise two N-terminal caspase activation and recruitment domains (CARDs) known to be required for downstream signalling (Rehwinkel and Reis e Sousa, 2013).

In the case of RIG-I, the CARDs are in close interaction with the helicase domain and are only exposed/released upon conformational changes induced by RNA binding (Figure 2) (Jiang *et al.*, 2011; Kowalinski *et al.*, 2011a).

RIG-I has been characterised to bind to the ends of RNA molecules, while MDA5 recognises long dsRNA stems (Figure 2) (Wu *et al.*, 2013). Following their activation by an appropriate RNA molecule, RIG-I and MDA5 interact with MAVS through their CARD domains. In turn, MAVS forms prion-like oligomers and induces IFN I and III production through IRF-3, IRF-7, and nuclear factor κB (NF-κB) (Rehwinkel and Reis e Sousa, 2010; Wu *et al.*, 2014; Xu *et al.*, 2014).

MAVS was first described to localise in the outer mitochondrial membrane (Figure 2) (Seth *et al.*, 2005). Later it was shown that MAVS also localises to peroxisomes (Dixit *et al.*, 2010) and endoplasmic reticulum mitochondrial-associated membranes (MAMs) (Horner *et al.*, 2011).

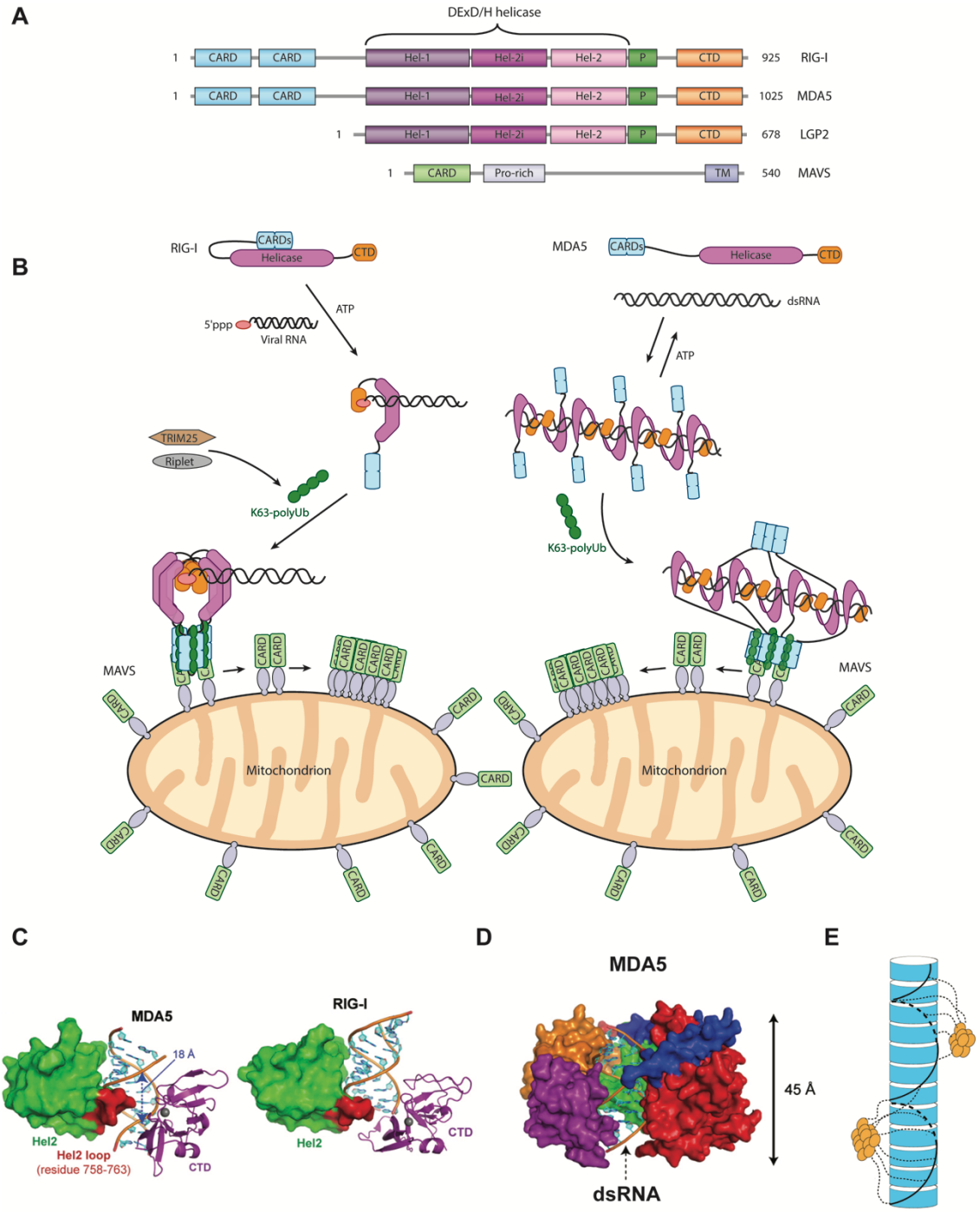


Figure 2 - The RIG-I-like receptor family signalling pathway. A) RIG-I (Retinoic acid-inducible gene 1), MDA5 (melanoma differentiation-associated gene 5) and LGP2 (laboratory of genetic and physiology 2) contain a helicase (Hel) and a C-terminal domain (CTD) that bind to RNAs. RIG-I and MDA5 also have two CARD (Caspase activation and recruitment domain) domains responsible for signalling. B) RIG-I binds to the ends of 5'-triphosphates-containing dsRNAs while MDA5 forms filaments on long dsRNAs. RLR (RIG-I-like receptor) oligomerization is stabilised by CARD K63-polyubiquitination leading to binding mitochondria-localised MAVS CARD domain. This binding creates a template for MAVS prion-like aggregation essential for activation of the downstream signalling pathway. C-D) Structural data show RIG-I affinity for ends of dsRNAs and MDA5 binding to the stems of dsRNAs. E) Model for MDA5 oligomerization onto long dsRNAs Sources: A and B) Wu and Chen, 2014; C-E) Wu *et al.*, 2013.

MAVS localisation was suggested to define which type of IFN is induced: IFN III is preferentially induced by peroxisomal-localised MAVS, while mitochondrial and MAMs-localised MAVS can induce both IFN I and III (Odendall *et al.*, 2014). Another report agrees with the later point of view but suggests peroxisomal MAVS can also induce both IFN I and III (Bender *et al.*, 2015). More studies are needed to clarify this issue and to understand the role of MAVS in different signalling platforms.

LGP2 does not contain CARD domains and thus is not expected to interact with MAVS. Instead, by interacting with dsRNAs, LGP2 is believed to act as a negative of RIG-I and positive regulator of MDA5 signalling pathways (Uchikawa *et al.*, 2016). This is because LGP2 has a CTD domain related to RIG-I and a helicase domain closely related to MDA5. Therefore, it is possible that LGP2 affinity for 5' ends of RNAs may block the preferential binding site of RIG-I, while it contributes to nucleate MDA5 filament formation (Uchikawa *et al.*, 2016).

1.4 THE AGONISTS FOR RIG-I

Although RIG-I and MDA5 are structurally related and trigger a similar signalling cascade, they recognise different types of RNAs. They respond to infection with different viruses or distinct products derived from the same viral infection (Wu and Chen, 2014). A non-exhaustive list of reported RIG-I agonists is presented below. (MDA5 putative ligands will be discussed in a different section.)

RIG-I senses a diverse group of viruses (e.g. paramyxoviruses, Sendai virus, influenza virus, and Japanese encephalitis virus - JEV). These viruses do

not accumulate – or protect by vesicle-like membranes – high levels of long dsRNAs in the cytosol of infected cells (Kato *et al.*, 2006; Weber *et al.*, 2006; Uchida *et al.*, 2014).

This feature is relevant as MDA5 and RIG-I are believed to distinguish the length of dsRNAs. Long poly (I:C) dsRNA favours MDA5 activation. However, partial digestion of these synthetic RNAs with type III RNase transforms MDA5 into RIG-I ligands (Kato *et al.*, 2008). Additionally, activation of RNase L by 2',5'-oligoadenylates generates cleavage products from self-RNAs that might trigger RIG-I (Malathi *et al.*, 2007). This suggests RIG-I has a preference for short rather than long dsRNAs.

RIG-I, but not MDA5, has a high affinity for 5'-triphosphates (V. Hornung *et al.*, 2006) present, for example, in influenza virus genomic RNAs (Pichlmair *et al.*, 2006; Rehwinkel *et al.*, 2010a). RIG-I can also become activated by 5'-diphosphates such as those found in reoviruses genome (Goubau *et al.*, 2015). Structural data support the affinity of RIG-I to 5'-end phosphates (Kolakofsky, Kowalinski and Cusack, 2012).

Other studies have suggested different ligands for RIG-I. Polyuridine motifs (Poly U/UC) found in the genome of Hepatitis C virus (HCV: *Flaviviridae*, *Hepacivirus*) were required for RIG-I activation. Deletion of these motifs failed to trigger IFN I even in the presence of 5'-triphosphates (Saito *et al.*, 2008a; Uzri and Gehrke, 2009). This suggests a possible additional mechanism for RIG-I activation that is sequence-dependent.

RIG-I also seems to have the potential to sense DNA transcription products. RNA polymerase III can transcribe AT-rich dsDNAs (e.g. poly dA-dT)

into 5'-triphosphate-containing dsRNAs that serve as agonists for RIG-I (Ablasser *et al.*, 2009; Chiu, MacMillan and Chen, 2009).

Cellular messenger RNAs (mRNAs) are 5'-triphosphorylated and co-transcriptionally 5'capped before transported from the nucleus to the cytoplasm. A CAP0 structure (guanosine methylated on the position 7: ^{m7}GpppNN) is essential for mRNA translation. An additional methylation (N_1-2'O-Methylation: ^{m7}GpppNmN) added to CAP0 RNAs forms a CAP1 structure.

CAP1 has been reported to prevent RIG-I recognition (Schuberth-Wagner *et al.*, 2015; Devarkar *et al.*, 2016). The authors yet identified the conserved residue H830 that prevents RIG-I activation by CAP1 cellular mRNAs (Schuberth-Wagner *et al.*, 2015; Devarkar *et al.*, 2016). This mechanism is proposed to prevent self-RNA recognition.

The murine gammaherpesvirus 68 (γHV68) expresses vGAT (viral glutamine amidotransferase). This is a pseudoenzyme that dimerizes with the host protein PFAS (phosphoribosylformylglycinamidine synthase) to promote RIG-I deamidation. This process renders RIG-I unable to bind to RNA PAMPs despite RIG-I becoming active due to conformational changes. Furthermore, vGAT prevents IRF3 activation. Both actions are required to block the induction of antiviral cytokines by γHV68 (He *et al.*, 2015).

During Hepatitis B virus (HBV: *Hepadnaviridae*, *Orthohepadnavirus*) infection in hepatocytes, RIG-I was found to produce IFN III, but not IFN I. Interestingly, in the same settings, RIG-I can also act as a direct antiviral effector by binding to HBV genomic RNA. Hence, RIG-I mechanically blocked HBV P protein (viral polymerase), and thus inhibited its activity (Sato *et al.*, 2015).

1.5 ACTIVATION AND CONTROL OF RIG-I-LIKE RECEPTOR SIGNALLING PATHWAY

As previously mentioned, RIG-I CARDs are in close interaction with the helicase domain in its inactive state. The CARDs are released upon RNA binding to allow interaction with MAVS (Figure 3). On the other hand, it is less clear which conformation MDA5 adopts in its inactive state. Post-translational modifications, however, have been described to play important roles in both activation and de-activation of the RLR signalling pathway (Figure 3).

In its resting state, RIG-I and MDA5 are phosphorylated. Protein kinase C-α (PKC α) and PCK-β phosphorylate RIG-I CARD domains at S8 and T170 residues (Gack *et al.*, 2010; Nistal-Villán *et al.*, 2010; Maharaj *et al.*, 2012). Furthermore, casein kinase II (CKII) phosphorylates T770 and S854-855 residues of RIG-I CTD domains. Mutations of either of these phosphorylation sites render RIG-I constitutively active (Sun *et al.*, 2011).

The MDA5 S88 residue (CARD1 domain) is phosphorylated by an unknown kinase (Wies *et al.*, 2013). Additionally, RIO kinase 3 (RIOK3) phosphorylates the S828 residue (CTD domain) preventing MDA5 oligomerisation. RIOK3 ablation or over-expression led to MDA5 activation or inhibition, respectively (Takashima *et al.*, 2015).

In contrast to RIG-I and MDA5, MAVS requires phosphorylation to activate the downstream signalling pathway. MAVS becomes phosphorylated by TBK1 (TANK-binding kinase 1) and IKK (IκB kinase complex), forming a platform to phosphorylate and activate IRF3 (Liu *et al.*, 2015).

As phosphorylation is required for both RIG-I and MDA5 inactivation, it is assumed dephosphorylation might take place to activate these receptors.

Indeed, both RIG-I and MDA5 CARD domains were found to be targeted by PP1 (protein phosphatase 1), isoforms PP1-α and PP1-γ (Wies *et al.*, 2013). PP1-α and PP1-γ interact with RIG-I and MDA5 during viral infection and not in uninfected cells. This interaction is necessary for their dephosphorylation and IFN signalling (Wies *et al.*, 2013).

RLR activation was also suggested to rely on sumoylation by SUMO1 chains (small ubiquitin-like modifier-1) (Fu *et al.*, 2011; Hu *et al.*, 2017). TRIM38, a SUMO E3 ligase, was shown to sumoylate RIG-I (K96 and K888) and MDA5 (K43 and K865) at early stages of virus infection. This was relevant to facilitate PP1 phosphatase activity. Additionally, sumoylation prevented K48-polyubiquitination and thus avoided degradation of both sensors (Hu *et al.*, 2017).

Phosphorylation is also expected to prevent RIG-I polyubiquitination-mediated activation. TRIM25 (Tripartite motif-containing protein 25) is an E3 ubiquitin ligase found to bind to RIG-I CARD1 and add K63-polyubiquitins to RIG-I CARD2 (Gack *et al.*, 2007). TRIM25 ubiquitination of RIG-I K172 residue is prevented by both S8 and T170 phosphorylations (Gack *et al.*, 2007; Maharaj *et al.*, 2012). Finally, TRIM25-mediated K63-polyubiquitination is necessary for RIG-I oligomerization, interaction with MAVS and thereby activation of the downstream signalling pathway (Gack *et al.*, 2007; Jiang *et al.*, 2012a).

It is less clear whether TRIM25-mediated K63-polyubiquitination of MDA5 happens in living cells and is required for MDA5 activation (Gack *et al.*, 2007; Chiang and Gack, 2017).

James Chen's group proposed based on data from an *in vitro* reconstitution assay that unanchored K63-polyubiquitins (i.e., 4 or more K63-

linked ubiquitin monomers unattached to any protein) can bind and activate RIG-I and MDA5 (Zeng *et al.*, 2010; Jiang *et al.*, 2012a).

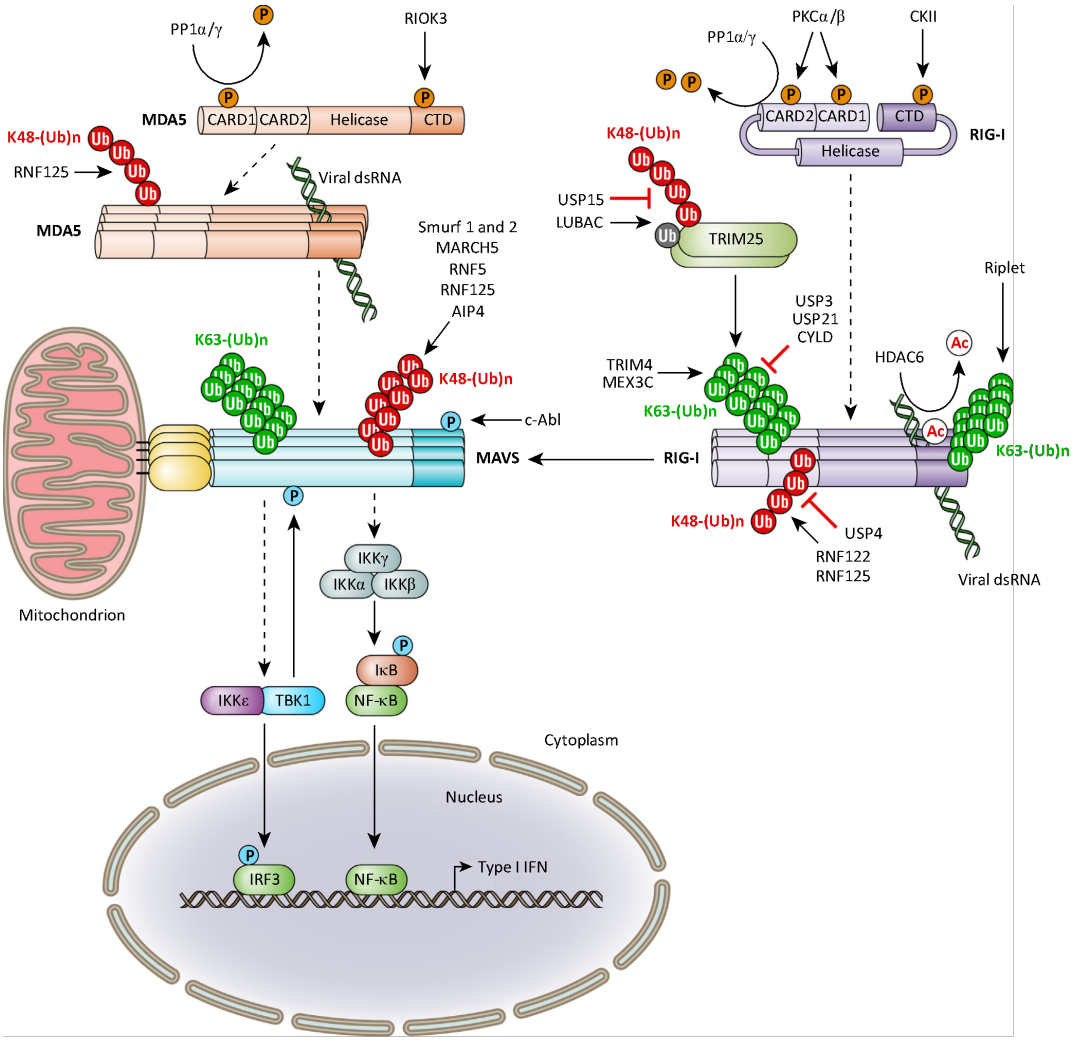


Figure 3 - RIG-I-like receptor signalling is regulated by post-translational modifications. RIG-I (Retinoic acid-inducible gene I) and MDA5 (Melanoma differentiation-associated gene 5) are phosphorylated (p) in their inactive state. In this case, RIG-I is also in a "closed conformation". Upon RNA ligand binding, RIG-I undergoes conformational changes, and both receptors become dephosphorylated by phosphatases (PP1α/γ). RIG-I and MDA5 are expected to form oligomers which are stabilised by K63-polyubiquitination (K63-Ub). MAVS (Mitochondria antiviral signalling protein) and IRF3 (Interferon regulatory transcription factor 3) are also phosphorylated to become activated. To target proteins for the proteasomal degradation, they can become K48-polyubiquitinated (K48-Ub). Source: (Chiang and Gack, 2017).

These reports thereby suggest a model where RIG-I and MDA5 CARDs are receptors for unanchored K63-polyubiquitin chains (Zeng *et al.*, 2010; Jiang *et al.*, 2012a). Because most of these studies were performed *in vitro* or in cell-

free systems, further investigation is required to define MDA5 K63-polyubiquitination and the enzymes responsible for this mechanism. On that note, TRIM65 was recently suggested to target specifically MDA5 for K63-ubiquitination at its K743 residue (Lang *et al.*, 2016; Meng *et al.*, 2017).

Cell-free systems have shown MDA5 forms filaments on dsRNAs in a head-to-tail manner (Wu *et al.*, 2013). The stems of dsRNAs are bound by the helicase and CTD domains of MDA5, while the CARD domains are expected to oligomerize (CARDs of up to eleven MDA5 monomers were modelled to oligomerize) (Wu *et al.*, 2013).

Given the above, further studies are still required to reveal a model that could explain how MDA5 signalling can become activated by K63-polyubiquitination, filament formation, and CARDs oligomerization. It also remains to be demonstrated how these events above would form a template capable of triggering MAVS oligomerization.

RIG-I monomers were suggested as the minimum units able to trigger its signalling (Louber *et al.*, 2014). In contrast, RIG-I has been shown to form K63-polyubiquitinated tetramers that bind MAVS (Zeng *et al.*, 2010; Patel *et al.*, 2013).

Structural data suggested K63-ubiquitin binding stabilises RIG-I tetramers (Peisley *et al.*, 2014). The authors termed this mechanism as a “lock-washer model”, where these tetramers form a template for MAVS prion-like filament formation (Hou *et al.*, 2011; Wu *et al.*, 2014; Xu *et al.*, 2014).

Another level of RIG-I activation is dependent on its acetylation status. HDAC6 (histone deacetylase 6) deacetylates RIG-I K858 and K909 residues (CTD domain) and this allows homo-oligomerization required for downstream signalling (Liu *et al*., 2016). Depletion of HDAC6 led to an inefficient response

against to Vesicular Stomatitis Virus (VSV) and Influenza virus possibly due to a lowered ability to sense PAMPs by acetylated RIG-I (Choi *et al.*, 2016).

Finally, RLR signalling pathway needs to be inhibited to avoid chronical IFN activation. RNF125 (Ring finger protein 125) is a ubiquitin E3 ligase encoded by an ISG and is responsible for adding K48-polyubiquitin chains to RIG-I, MDA5, and MAVS (Arimoto *et al.*, 2007; Hao *et al.*, 2015). RNF125 and other enzymes have been linked to promoting proteasomal degradation of proteins in the RLR signalling pathway (Chiang and Gack, 2017). Hence, K48-polyubiquitination-mediated degradation is an important mechanism to control the induction of IFN by RLRs.

MAVS prion-like filaments also must be degraded to prevent further induction of IFNs. MARCH 5 (Membrane Associated RING-GC protein 5) was identified as an E3 ubiquitin ligase residing in mitochondria and required for K48-polyubiquitination of MAVS aggregates (Yoo *et al.*, 2015).

MAVS K7 and K500 residues are needed for ubiquitination, and MARCH5-deficient mice are more resistant to viral infection and prone to induce higher levels of IFN (Yoo *et al.*, 2015). It remains to be elucidated how MARCH5 can recognise and target protein aggregates to proteasomal degradation.

1.6 THE DISCOVERY OF MELANOMA DIFFERENTIATION-ASSOCIATED GENE 5 (MDA5)

MDA5 was described in 2002 by two independent groups (Kang *et al.*, 2002; Kovacsovics *et al.*, 2002). Tschopp's group reported it as a murine protein termed HELICARD with 84% homology to its human orthologue (Kovacsovics *et*

al., 2002). They observed ATPase activity in response to RNA and, at a lower extent, to DNA (Kovacsovics *et al.*, 2002).

Using an antibody against the CARD domains, they observed expression of two proteins of about 140kDa and 45kDa detectable in mouse tissues and upon ectopic expression in 293T cells. Further bands - cleavage products - were detected by stimulating cells with Fas ligand to induce apoptosis (Kovacsovics *et al.*, 2002).

Full-length HELICARD showed a cytoplasmic localisation. Upon cleavage, two main products were found to localise to the cytoplasm (CARD-containing fragment, 1-278) and the nucleus (Helicase-containing fragment, 252-1025). The nuclear localisation of the helicase cleavage product influenced DNA fragmentation during apoptosis (Kovacsovics *et al.*, 2002).

In humans, MDA5 was found to be increasingly induced by TNF-α, IFN-β, and IFN-β + Merezein (MEZ) in HO-1 human melanoma cell cultures. The authors treated HO-1 cells with a combination of IFN-β + MEZ and observed melanoma growth restriction. They hypothesised MDA5 was a key molecule responsible for this phenotype as its ectopic expression alone led to similar results (Kang *et al.*, 2002).

Furthermore, they recognised MDA5 had a cytoplasmic localisation and an RNA-dependent ATPase activity induced by dsRNAs. Their unpublished results also suggested human MDA5 *in vitro* translation could lead to several small alternative translational products. Nothern blot analysis revealed MDA5 expression can be detected in several tissues, but lower in the brain, testis, and lungs (Kang *et al.*, 2002).

1.7 LONG dsRNAs ARE PUTATIVE AGONISTS FOR MDA5

Experiments *in vivo* demonstrated MDA5 recognises viruses within the *Picornaviridae* family, which comprises several genera including *Cardiovirus*, *Enterovirus*, and *Rhinovirus*. Figure 4 depicts representative viruses within each genus and genome organisation. Encephalomyocarditis virus (EMCV: *Picornaviridae*, *Cardiovirus*) virions contain a capsid and lack an envelope. Its genome consists of a positive sense single-stranded RNA of about 7-8.8kb. A single open reading frame (ORF) is flanked by 5' and 3' untranslated regions (UTRs) (Figure 4). The 5'-end is covalently linked to a viral protein, Vpg, and contains an internal ribosome entry site (IRES).

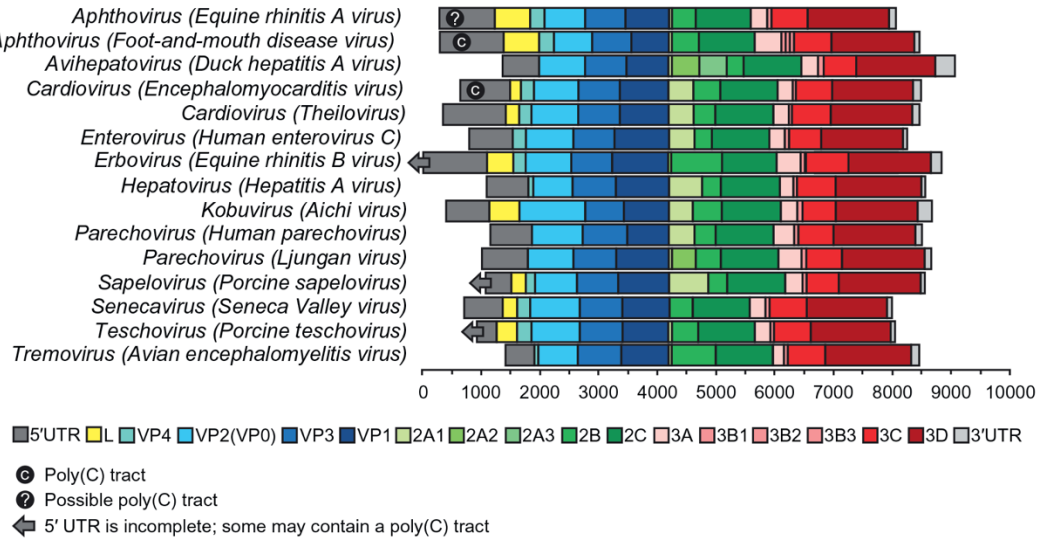


Figure 4 – Genome organisation of viruses within the *Picornaviridae* family. *Picornaviridae* family comprise 12 genera of viruses. Representative viruses are highlighted for each genus. 5' and 3' untranslated regions (UTR) are depicted in dark and light grey, respectively. Viral proteins (VP) are represented in coloured bars as indicated. Source: King *et al*., 2012.

JEV (*Flaviviridae*, *Flavivirus*) is also a positive sense single-stranded RNA genome and can accumulate dsRNAs. However, mice survival and cytokine

induction during EMCV and JEV infection are dependent on MDA5 and RIG-I, respectively (Kato *et al.*, 2006). Other flaviviruses, such as Dengue virus (DENV) and West Nile Virus (WNV), were found to engage both MDA5 and RIG-I (Fredericksen *et al.*, 2008; Y.-M. Loo *et al.*, 2008). It is not clear why EMCV, DENV and WNV generate MDA5 agonists, but not JEV.

All these cytoplasmic viruses replicate within vesicle-like membranes (Figure 5B) (King *et al*., 2012). This method of replication might protect or delay RNA detection by RLRs. In addition, different replication dynamics and cell types may explain the activation of distinct RLRs (Kato *et al.*, 2006; Espada-Murao and Morita, 2011; Uchida *et al.*, 2014; Takamatsu, Uchida and Morita, 2015).

EMCV, but not Influenza virus or Sendai virus, triggers MDA5 and accumulates high levels of dsRNAs in infected cells (Pichlmair *et al.*, 2006; Weber *et al.*, 2006). The correlation between MDA5 activation with the presence of long dsRNAs is also observed in experiments using long synthetic poly (I:C) (Kato *et al.*, 2008).

In addition, transfection of mouse embryonic fibroblasts (MEFs) with total RNA of cells infected with EMCV triggers an MDA5-mediated IFN response. On the other hand, total RNA from uninfected cells did not trigger cytokines (Pichlmair *et al.*, 2009; Jiang *et al.*, 2011).

Infection and replication of Coxsackievirus B3 (CVB3: *Picornaviridae*, *Cardiovirus*) or mengo virus (a strain of EMCV) generate a long dsRNA replicative form (RF). Purification of this RNA species and transfection into MEFs led to IFN I induction that was dependent on MDA5. In support of this, recombinant MDA5 directly bound to purified picornavirus RF which induced

MDA5's ATPase activity. Additionally, the authors demonstrated MDA5 induced IFN I preferentially to dsRNAs longer than 2kb (Feng *et al.*, 2012).

By mixing recombinant MDA5 and nucleic acids in cell-free systems, MDA5 was found to bind to dsRNAs, ssRNAs (single-stranded RNAs), and DNA (Peisley *et al.*, 2011). However, only dsRNAs induced ATP hydrolysis activity (Peisley *et al.*, 2011, 2012; Berke *et al.*, 2012). MDA5 head-to-tail cooperative oligomerization leads to filament formation of different sizes according to the length of dsRNA stems (Peisley *et al.*, 2011; Wu *et al.*, 2013). It is believed MDA5 filament formation is initiated from several nucleation points.

In this regard, longer filaments are likely formed by the junction of two or more shorter filaments. In this model, short dsRNA stems alone are less likely to form stable filaments (Peisley *et al.*, 2012). ATP hydrolysis promotes MDA5 dissociation from dsRNAs by coordinating the disassembly of the filaments. Interestingly, longer filaments have a lower ATP hydrolysis rate leading to the formation of more stable complexes than shorter filaments (Peisley *et al.*, 2011).

Those findings in cell-free systems suggest a model where MDA5 is more stable when bound to longer than shorter dsRNAs. Therefore, they provide the molecular basis to understand how MDA5 could distinguish cellular RNAs (that do not generate long dsRNAs) from viral RNAs (Peisley *et al.*, 2011, 2012). Furthermore, similar studies demonstrated MDA5 does not recognise specific sequences. Crystal structures of MDA5:dsRNA complexes have shown MDA5 binds to the phosphate backbones along synthetic dsRNAs where it oligomerizes (Wu *et al.*, 2013).

Interestingly, MDA5 and RIG-I might also have direct antiviral effector-like functions that are dependent on their ATPase activities and independent of the

IFN signalling pathway. Full-length or truncated proteins (without the CARD domains) were shown to displace viral proteins pre-bound to dsRNAs. Removal of viral proteins from viral dsRNAs by MDA5 and RIG-I also facilitated the binding and activity of other host dsRNA-binding proteins, such as PKR (Yao *et al.*, 2015).

Animal experimentation has reinforced the hypothesis that LGP2 is a positive regulator of MDA5 signalling, while it antagonises RIG-I. As an example, LGP2 KO (knockout) mice were resistant to lethal injection with VSV (recognised by RIG-I) but failed to mount a response against EMCV (recognised by MDA5) (Venkataraman *et al.*, 2007). The mechanisms by which LGP2 contributes to MDA5 activation are still under investigation.

To help to elucidate this issue, Bruns *et al*. (2014) demonstrated in cell-free systems that MDA5:LGP2:dsRNA complexes led to the formation of several short rather than long MDA5 filaments. Transfection of these complexes into 293T cells activated the IFN-β promoter equally or more efficiently than long filaments formed by MDA5:dsRNAs complexes (Bruns *et al.*, 2014). Additionally, it has been proposed that the LGP2 helicase domain resembles the MDA5 helicase domain and thus would have the ability to nucleate MDA5 filament formation (Uchikawa *et al.*, 2016).

1.8 OTHER PUTATIVE AGONISTS FOR MDA5

The evidence presented above suggests LGP2 acts as a positive regulator of MDA5 and could potentially bind to similar types of RNAs. Caetano Reis & Sousa's group developed a native co-IP (co-immunoprecipitation) assay for

LGP2 in cells infected with EMCV. They found LGP2 binds to RNA species that can trigger MDA5, but not RIG-I, signalling (Deddouche *et al.*, 2014).

Surprisingly, RNAs bound by LGP2 were short ssRNAs of about 170bp. These RNA species matched a region of the EMCV antigenome corresponding to the L (leader) protein (Deddouche *et al.*, 2014). Complete deletion of EMCV L from the virus genome generated a virus with lower ability to produce MDA5 ligands (Deddouche *et al.*, 2014).

Pichlmair *et al*. (2009) also performed co-IP assays in cells infected with EMCV. In this case, they used an antibody against dsRNAs, J2 mAb (monoclonal antibody), and were able to precipitate RNAs with the ability to trigger MDA5 (Pichlmair *et al.*, 2009).

Also, they purified different RNA species derived from VERO cells infected with EMCV (V-EMCV-RNA): ssRNAs, dsRNAs, and high-ordered high molecular weight RNAs (HMW: a mix of ssRNAs and dsRNAs). They transfected these RNA species in cell cultures and treated the cells with ribavirin to prevent virus replication. They observed MDA5 was activated after transfection with high-ordered HMW RNAs, but not with the other RNA species (Pichlmair *et al.*, 2009).

The most direct way to identify MDA5 ligands is through MDA5 co-IP assay. However, this has not been considered a trivial experiment. To date, only one attempt has been published.

The authors employed an adapted protocol of PAR-CLIP (Photoactivatable-Ribonucleoside-Enhanced Crosslinking and Immunoprecipitation) by incubating virus-infected cells with 4SU (4-thiouridine) followed by UV (Ultraviolet) crosslinking at 365nm (Runge *et al.*, 2014).

Cells were infected with Measles virus (MeV: *Paramyxoviridae*, *Morbillivirus*), a negative polarity ssRNA virus. Deep sequencing revealed MDA5 binds to the antigenome (positive polarity strand) with a high preference for a region within the L, large protein, gene. (This gene is not comparable to EMCV L gene.) In these settings, evidence for dsRNA binding was missing (Runge *et al.*, 2014).

Furthermore, no particular RNA motif was identified, except for enrichment of AU-containing sequences. Further experiments revealed AU-rich sequences favoured MDA5 binding by reducing ATP hydrolysis (Runge *et al.*, 2014).

1.9 MDA5 AND RECOGNITION OF CELLULAR RNAS

Cellular RNAs are not expected to generate long (>2kb) dsRNAs. Yet, accumulating evidence suggests that MDA5 also binds self-RNAs. This seems to be the case during cancer treatment with DNA demethylating agents, autoinflammatory diseases (e.g. Aicardi-Goutières syndrome, AGS), and perhaps autoimmune diseases (e.g. Type 1 diabetes, T1D).

Two independent groups have explored the mechanisms by which treatment of colorectal and ovarian cancer cells with DNA demethylating agents (e.g. 5-Aza-CdR: 5-Azacytidine-2-deoxycytidine) led to cancer growth inhibition (Chiappinelli *et al.*, 2015; Roulois *et al.*, 2015). These agents inhibit DNA methyltransferases and can result in the overexpression of endogenous retroviruses (ERVs) (Chiappinelli *et al.*, 2015).

Upregulation of ERVs was associated with the induction of type I IFNs and inhibition of cancer initiating cells (Roulois *et al.*, 2015). This phenomenon

required MDA5 (Roulois *et al.*, 2015) and the downstream adaptor MAVS (Chiappinelli *et al.*, 2015; Roulois *et al.*, 2015). In accordance with an MDA5-mediated role, transfection of dsRNAs into these cells was sufficient to mimic the effects of 5-AZA-CdR treatment (Roulois *et al.*, 2015). However, the origin and type of RNA agonists, possibly derived from ERVs, were not addressed.

In the context of autoinflammatory diseases, AGS is a neurological syndrome where patients present with basal ganglia calcification associated with a type I IFN signature. Some patients also develop microcephaly and other severe neurological symptoms (Crow and Manel, 2015).

Mutations in at least seven genes related to nucleic acid sensing pathways have been correlated with AGS: *TREX1*, *RNASEH2A*, *RNASEH2B*, *RNASEH2C*, *SAMHD1*, *ADAR1*, and *IFIH1* (Crow and Manel, 2015). Two of these genes are associated with RNA sensing pathways: *ADAR1* encoding for Adenosine Deaminases Acting on RNA 1 (ADAR1) and *IFIH1* encoding for MDA5 (Crow and Manel, 2015).

ADAR1 has two isoforms, ADAR1p150 and ADAR1p110. The p150 isoform is IFN-inducible. Both isoforms edit dsRNAs by converting adenosine into inosine (A-to-I editing) thus affecting structure and stability of these RNAs. Additionally, this might introduce mutations into proteins as the translational machinery reads “I” as guanosine bases (Nishikura, 2015).

AGS-related *ADAR1* mutations are mostly situated in its catalytic domain at the interface that interacts with RNA. Tests *in vitro* - using constructs mimicking the p110 isoform mutants - identified one of the mutants, G1007R, had a lowered ability to execute A-to-I editing (Rice *et al.*, 2012).

It is believed that deficiency in A-to-I editing might lead to the accumulation of immunoreactive dsRNA species. Indeed, patients with *ADAR1* mutations had an IFN signature, which was even higher in a patient containing the G1007R mutation (Rice *et al.*, 2012).

The correlation between *ADAR1* deficiency and IFN spontaneous induction is supported by studies in young and adult mice (Hartner *et al.*, 2009; XuFeng *et al.*, 2009; Qiu *et al.*, 2013). Pestal *et al*. (2015) demonstrated *ADAR1* KO mice led to multi-organ development defects and embryonic lethality. In this study, the expression of ISGs was associated with the MDA5-MAVS axis and reliant on the p150 isoform (Pestal *et al.*, 2015).

In another study, ADAR1 editing was impaired in a knock-in mouse model. This also resulted in embryonic lethality associated with an IFN signature that was dependent on MDA5 (Liddicoat *et al.*, 2015). The authors suggested cytosolic Alu elements present in the 3'UTRs (untranslated regions) of mRNAs are potential ligands for MDA5 (Liddicoat *et al.*, 2015).

Alu elements constitute a significant part of the human genome and are about 300bp long. They are well-known substrates for ADAR1 which, in turn, can reduce their immunostimulatory potential (Liddicoat *et al.*, 2015; Chen and Yang, 2017). Hence, Alu elements have been proposed as endogenous ligands for MDA5 in the context of AGS patients containing *ADAR1* loss-of-function and, perhaps, *IFIH1* gain-of-function mutations (Rice *et al.*, 2012; Liddicoat *et al.*, 2015).

As mentioned above, some AGS patients were found to contain mutations in the *IFIH1* (MDA5) gene resulting in an IFN I signature. These were described as gain-of-function mutations as demonstrated by functional assays (Oda *et al.*,

2014; Rice *et al.*, 2014). Indeed, overexpression of MDA5 mutant constructs in HEK293T cells induced higher levels of IFN-β than the WT (wild-type) protein. This induction was enhanced after transfection of dsRNAs such as poly (I:C) for all constructs (Rice *et al.*, 2014).

In agreement with this, another group overexpressed WT MDA5 and mutant constructs in a human hepatoma cell line (Huh7). The mutant constructs induced higher levels of IFN-β (Oda *et al.*, 2014).

In contradiction to the other report (Rice *et al.*, 2014), the authors suggested MDA5 activation was not ligand-specific (Oda *et al.*, 2014). In a different experiment, they rescued MDA5 expression in MDA5 KO MEFs by using WT or AGS-related mutant constructs. Upon infection of these MEFs with EMCV, they only found WT MDA5 to be responsive, but not the mutants (Oda *et al.*, 2014).

Single nucleotide polymorphisms (SNPs) in the *IFIH1* gene have been found in patients with the autoimmune diseases, including T1D (Smyth *et al.*, 2006; Nejentsev *et al.*, 2009). The rs1990760 (A946T) polymorphism is the most studied *IFIH1* SNP found in autoimmune diseases (Smyth *et al.*, 2006). It is located in the MDA5 CTD domain in a region (940-959) expected to affect ATPase activity and filament stabilisation. It is suggested to reduce ATPase activity and, therefore, increase stability for RNA binding.

Yet, T1D can be induced in an MDA5 homo- or heterozygous, but not in KO, non-obese diabetes mouse model upon infection with Coxsackievirus B4 (*Picornaviridae*, *Enterovirus*) (Lincez, Shanina and Horwitz, 2015). This finding provides a link between genetic mutation and an environmental factor in triggering T1D. However, it remains to be elucidated which types of RNAs

(cellular and/or viral) are sensed by MDA5 in the context of T1D and whether the viral infection is indeed required.

In support of cellular RNA sensing by MDA5, it has been shown in a knock-in mouse model that *Ifih1* T946 is likely a partial gain-of-function mutation. The mice presented a phenotype consistent with higher induction of IFN I expression. Additionally, these animals were more prompted to develop autoimmune diseases (Gorman *et al.*, 2017).

1.10 VIRUSES OF THE *FLAVIVIRIDAE* FAMILY, *FLAVIVIRUS* GENUS

The *Flaviviridae* family contains three genera: *Hepacivirus*, *Flavivirus*, and *Pestivirus*. It comprises spherical enveloped viruses of 40-50nm in diameter. The genome is a ssRNA of positive polarity and is about 11kb long. They all lack a 3'UTR poly (A) tract (King *et al.*, 2012).

HCV is an important hepacivirus that causes chronic infection in humans and is considered carcinogenic (Thrift, El-Serag and Kanwal, 2016). It is well known for its ability to block RLR signalling by cleaving MAVS with the viral protease NS3/4A (Li *et al.*, 2005; Horner *et al.*, 2011; Bender *et al.*, 2015).

While pestiviruses could pose a problem for animals, flaviviruses are known to cause diseases in humans – e.g. DENV and WNV -, and formed mostly by arthropod-borne viruses (arboviruses) (King *et al.*, 2012).

The genome of flaviviruses is formed by a single ORF (Open Reading Frame) flanked by 5' and 3'UTRs. The 5'UTR contains a CAP1 structure while the 3'UTR finishes on a conserved 3'CU dinucleotide (King *et al.*, 2012).

The ORF generates a single polyprotein that is co-translationally cleaved by viral and host proteases (Figure 5). Cleavage products give rise to three structural (capsid, pre-membrane, and envelope) and seven NS (nonstructural) proteins (NS1, NS2A, NS2B, NS3, NS4A, NS4B, and NS5). NS2B-NS3 (NS2B3) forms the viral protease complex. NS3 also has triphosphatase and helicase activities, and NS5 contains capping (methyltransferase domain) and RNA-dependent RNA polymerase (RdRp domain) activities (King *et al.*, 2012).

Briefly, DENV will be taken as an example of a pathogenic flavivirus relevant to public health. This virus has been extensively studied for the past decades due to the high rate of infections in tropical and subtropical countries (Katzelnick, Coloma and Harris, 2017). DENV is a species containing four viruses (classically referred as “serotypes”): DENV1-4 (King *et al.*, 2012).

Most of the DENV cases are asymptomatic, but also classical fever and severe forms of the disease can be found. One of the reasons for its severe clinical presentation has been associated with the antibody-dependent enhancement (ADE) phenomenon: exposure to one DENV serotype leads to life-long protection with the generation of neutralising antibodies to that particular serotype. Some of these antibodies can bind with low affinity to the other DENV serotypes in a future secondary exposure and enhance virus infection. This can trigger a “cytokine storm” that is relevant to the pathophysiology of the severe form of the disease (Balsitis *et al.*, 2010; Halstead, 2014; Katzelnick, Coloma and Harris, 2017).

DENV has been reported to block RLR, CDR and JAK/STAT signalling pathways through multiple mechanisms involving its viral proteins. One example

is NS3 that prevents RIG-I translocation from the cytosol to organelle-localised MAVS (Chan and Gack, 2016).

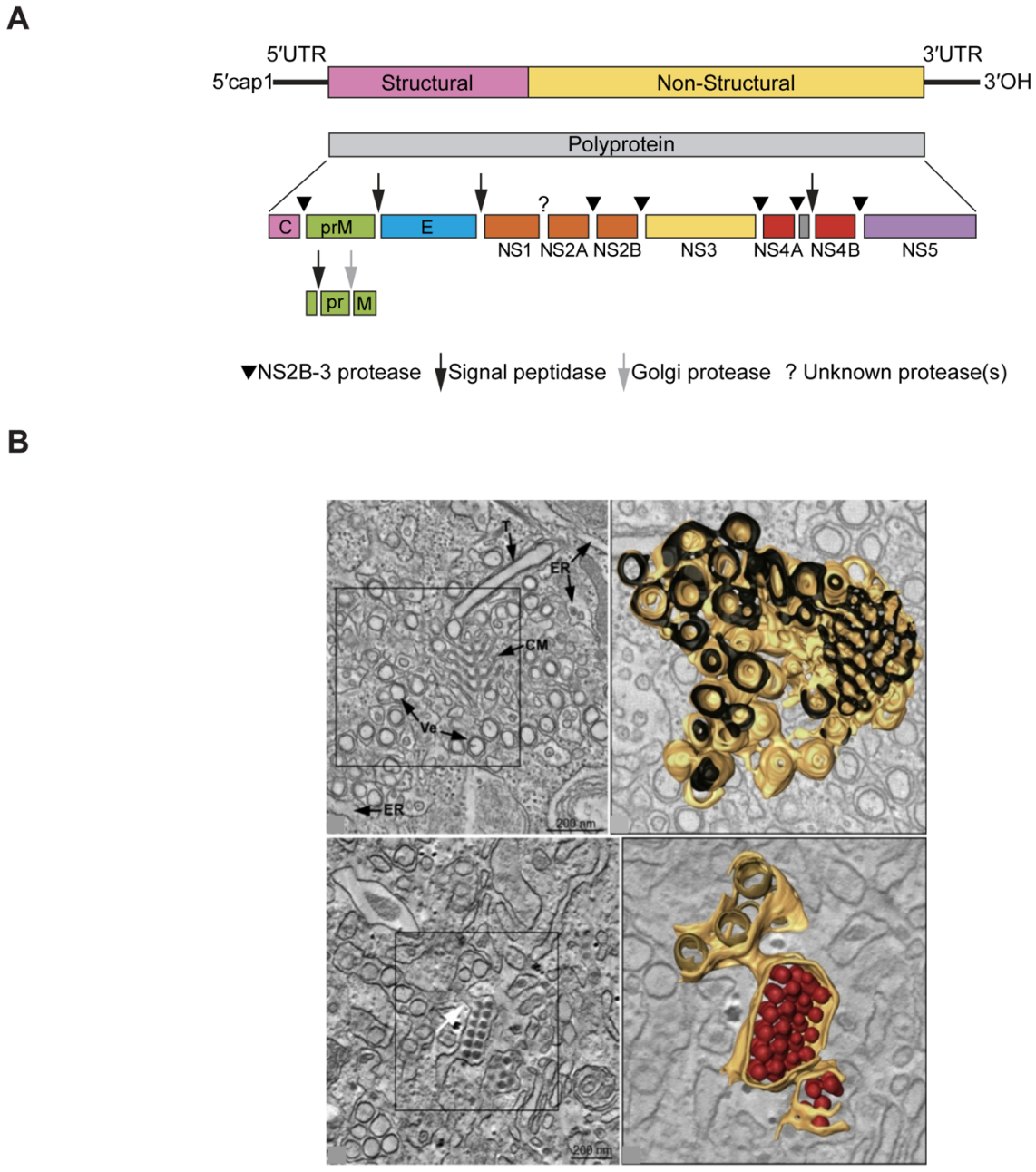


Figure 5 - Proteins generated by flaviviruses and vesicle-like replication sites. A) Flaviviruses contain 5'- and 3' UTRs (Untranslated regions) flanking a single ORF (Open Reading Frame). A single polyprotein is co-translationally cleaved by host and viral proteases generating structural and non-structural proteins (NS): capsid (C), pre-Membrane (prM), Envelope (E), NS1, NS2A, NS2B, NS3, NS4A, NS4B, and NS5. During virion maturation, prM is further cleaved producing the pr peptide and the M protein. B) Flaviviruses replicate within vesicle-like (Ve) structures derived from ER (endoplasmic reticulum) membranes. Convoluted membranes (CM) and tubes (T) can also be identified. Sources: A) adapted from King *et al.*, 2012; B) Welsch *et al.*, 2009.

Another line of evidence suggests that the DENV protease complex NS2B3 has the potential to cleave cGAS and its adaptor STING (Aguirre *et al.*, 2012, 2017; Yu *et al.*, 2012). This mechanism has been suggested to inhibit the sensing of DNA leaked from damaged mitochondria during DENV replication (Aguirre *et al.*, 2017).

DENV NS5 protein was shown to block the JAK/STAT signalling pathway by degrading human but not mouse STAT2 (Ashour *et al.*, 2009, 2010). This degradation is mediated by NS5's interaction with the E3 ubiquitin ligase UBR4 (Morrison *et al.*, 2013).

Flaviviruses are thus capable of causing infection in humans and block the antiviral type I/III IFN responses. More recently, Zika virus (ZIKV) has been another flavivirus added to this list of pathogens causing a significant impact on public health.

ZIKV was discovered in 1947 in the Zika Forest in Uganda (Africa) but had never been associated with major epidemics in humans until 2007. From both genotypes, African and Asian, the Asian genotype is more closely related to the strains of the recent outbreak, including the current one in the Americas. ZIKV seems to have entered in the Americas through Brazil around 2013 and was soon associated with increasing numbers of cases of microcephaly in newborn babies and Guillain-Barré syndrome in adults (Faria *et al.*, 2016).

A full ZIKV genome was rescued from the brain of an aborted foetus presenting with microcephaly (Mlakar *et al.*, 2016). Furthermore, immunodeficient mouse models were generated and demonstrated that ZIKV can cross the placental barrier and infect the brain of the developing foetus (C. Li *et al.*, 2016; Cugola *et al.*, 2016; Miner *et al.*, 2016).

Sustained cases of ZIKV infection are occurring in regions of the globe containing *Aedes* mosquitoes and naïve populations (Weaver, 2017). However, clinical observation and animal experimentation have also raised concerns related to sexual transmission (Moreira *et al.*, 2016; Yockey *et al.*, 2016; Uraki *et al.*, 2017).

ZIKV has been shown to replicate in mouse testis (Govero *et al.*, 2016), vaginal tissues (Yockey *et al.*, 2016) and can be transmitted by sexual contact (Tang *et al.*, 2016). Viral replication in these tissues led to infection of the foetus and replication in foetal brain, resulting in intrauterine growth restriction and embryonic death (Yockey *et al.*, 2016).

Interestingly, ADE seems to go beyond the ability to enhance DENV infection only. Non-neutralising cross-reactive antibodies from previous flavivirus (e.g., DENV and WNV) infections can also enhance ZIKV infection (Dejnirattisai *et al.*, 2016; Paul *et al.*, 2016; Priyamvada *et al.*, 2016; Bardina *et al.*, 2017). These findings potentially pose another level of difficulty in generating an efficacious and safe vaccine for flaviviruses.

ZIKV replication is sensitive to the antiviral effects of IFN I. Viral replication is prevented in cellular cultures treated with IFN I prior to infection (Hamel *et al.*, 2015; Kumar *et al.*, 2016). For infection *in vivo*, the virus better infects immunodeficient mice (e.g., IFNAR or STAT2 KO) (Govero *et al.*, 2016; Lazear *et al.*, 2016; Miner *et al.*, 2016; Yockey *et al.*, 2016).

In line with this, ZIKV has been found to target human STAT2 for degradation in order to block the IFN signalling pathway (Grant *et al.*, 2016; Kumar *et al.*, 2016; Chaudhary *et al.*, 2017).

1.1.1. Aims of the thesis

The goals of my DPhil project are (i) to generate and validate MDA5 specific antibodies and to use them to explore MDA5's biology; (ii) to develop a bioassay to assess whether MDA5 senses cellular RNAs and to optimise a stringent co-IP method to identify MDA5-associated RNAs; (iii) to investigate whether ZIKV infection generates RLR agonists and blocks the IFN signalling pathway.

The generation and validation of MDA5 specific antibodies can be useful to unravel fundamental aspects of the activation, regulation and dynamics of the MDA5 signalling axis. Insights into these questions will not only be relevant to virus-host interaction studies, but will also help to understand the contribution of MDA5 to cancer treatment, AGS, and T1D. In this context, it is also important to be able to demonstrate that MDA5 senses cellular RNAs in addition to viral RNAs. The long-term goal is to identify and characterise nucleic acids directly bound by MDA5 and to understand the molecular basis of self/non-self discrimination by MDA5. Finally, it is fundamental to comprehend how human pathogens can be recognised by and fight against the immune system. This can contribute to clarify the pathophysiology of viral diseases and, perhaps, lead to an intelligent design of vaccines and/or treatments.

CHAPTER 2

2 MATERIAL AND METHODS

2.1 CELLS

Cells were maintained in DMEM (Sigma Aldrich) supplemented with 10% fetal calf serum (FCS) (Sigma Aldrich) and 2mM L-Glutamine (Gibco) at 37°C and 5% CO_2. Throughout the study, we used A549, HEK293, 293T-TLA (293T cells clone TLA - stably and constitutively expressing the SV40 large antigen), and human skin fibroblast cultures. HEK293-derived cell lines were also used and are described below.

HEK293 cells stably transduced with an ISRE-Luciferase (Luc) reporter construct (3C11) were previously generated by our laboratory (Bridgeman *et al.*, 2015). This cell line was generated by Dr. Jonathan Maelfait.

Our laboratory also generated HEK293 cells stably expressing the human *IFNβ* promoter-Luc region and GFP (p125-HEK293 cells). These cells were rendered KO for MDA5, RIG-I, or MAVS using specific CRISPR (Clustered Regularly Interspaced Short Palindromic Repeats) guides. All these cells were generated by Dr. Alice Mayer (Dias Junior *et al*., submitted).

Primary human skin fibroblasts were a kind gift from Professor Dr. Yanick Crow (University of Manchester, UK). We obtained seven different cellular cultures: two from healthy donors (WT fibroblast); two from AGS patients each containing different mutations in *ADAR1* gene (R892H or I872T); two from AGS patients each containing different mutations in *IFIH1* (MDA5) gene (R779H or

D393V); one from an AGS patient containing a mutation in *SAMHD1* gene (Q149X). These cultures were maintained as above, but using 3% O_2.

2.2 GENERATION OF HUMAN MDA5 (hMDA5) CONSTRUCTS

HEK293 cells were treated with IFN-A/D (a hybrid human recombinant IFN-α - Sigma) and cDNAs were used to clone hMDA5, 3XFLAG-hMDA5. A kozak sequence was added followed by 3XFLAG peptide sequence with the following primer:

gccgccATGGACTACAAAGACCATGACGGTGATTATAAAGATCATGACATCG ATTACAAGGATGACGATGACAAGTCGAATGGGTATTCCACAGACG. The reverse primer containing a stop codon contained the following sequence: CTAATCCTCATCACTAAATAAACAGCATTCTG.

hMDA5 was then cloned into pCDNA3.1/V5-His-TOPO (Invitrogen) as recommended by the manufacturers. The 3XFLAG-hMDA5 construct was used as a template to generate hMDA5 K335A mutant (3XFLAG-hMDA5-K335A). For such, a mutagenesis PCR kit® (Agilent) was used according to the manufacturer's instructions. The following primers were used for mutagenesis PCR: gcctccctacagggagtggagccaccagagtggctgttta and taaacagccactctggtggctccactccctgtagggaggc. The sequences of all constructs were confirmed using the primers described in Table 1.

Table 1 – Oligonucleotides to sequence hMDA5 constructs

Oligonucleotide	Sequence (5' to 3')
hMDA5_F_302	ACTTGCCCTCTCCATCGTTTG
hMDA5_F_694	AATCTGGAGAAGGAGGTCTGG

hMDA5_F_1117	TTCCGCAAGGAGTTCCAACC
hMDA5_F_1494	GCAAGCCAAAGCTGAAGAACAC
hMDA5_F_1926	AGATGATAGTGATGAGGGTGGTG
hMDA5_F_2274	ACACAGCAGTGAGTTCAAACC
hMDA5_F_2676	TGCCAAGCATTACAAGAATAACCC
hMDA5_R_2804	AATTCTGGGGTCATATTGACGTG
hMDA5_R_2393	ATATCCAGACCTTCTTCTGCCAC
hMDA5_R_1958	TACTCATCATCACCACCCTCATC
hMDA5_R_1609	TGCATGGCTCCTGTATTTGG
hMDA5_R_1300	ATTGAACACCAGCATCTTCTCC
hMDA5_R_850	AATCACTGCCCATGTTGCTG
hMDA5_R_421	CCTCCATGCACTTATCCAAGAC

2.3 GENERATION OF HUMAN MDA5 (hMDA5) HYBRIDOMA CELL LINES AND MOUSE ASCITES

To generate MDA5 recombinant proteins, we cloned 3X-FLAG-hMDA5 into a pBacPAK-His3-GST vector (pBacPAK-His3-GST-3xFLAG-hMDA5). MDA5 was cloned into XhoI and NotI restriction sites using the primers XhoI-3xFLAG(1-23)_Fwd (aCTCGAGttATGGACTACAAAGACCATGACGG) and NotI-hMDA5-R (TTgcggccgcCTAATCCTCATCACTAAATAAACAGCATTCTG). Recombinant 3xFLAG-hMDA5 was expressed in SF9 or HIGH5 insect cells. These cells were infected with baculoviruses for 3 days at 28°C at different multiplicities of infection (MOIs). The recombinant protein was purified by affinity chromatography using glutathione-sepharose matrix (GE Healthcare, Little Chalfont, UK). The protein was successfully cleaved overnight at 4°C with GST-C3-protease. Further

purification was achieved after gel filtration using Superdex 200 10/300 GL column (GE Healthcare). Protein purity was verified by acrylamide gel electrophoresis, and protein yield was quantified using a Nanodrop apparatus (ThermoScientific, Waltham, MA) (not shown). All recombinant protein expression and purification were performed by the Protein Purification Facility (Cancer Research UK).

We shipped our hMDA5 recombinant protein to Professor Dr Jin Boquan's group (Department of Immunology, Fourth Military Medical University, China). His group generated 29 hybridoma cell lines expressing hMDA5 mAbs after mice immunization. In addition, 29 mouse ascetic fluids were generated by injecting the individual hybridoma lines in the mouse peritoneal cavities. Therefore, we received in our laboratory 29 mouse ascites and 03 hybridoma cell lines to test for the expression of hMDA5 mAbs.

The hybridoma cells were cultured in RPMI 1640 containing 5-10% FCS, 2mM L-Glutamine, and recombinant mouse IL-6 (20-50IU/ml) (Invitrogen). These cells were cultivated in CELLine Bioreactors (Wheaton® CELLine™ Bioreactors, WCL0350-5) according to manufacturer's instructions. Supernatants containing antibodies were filtered and frozen at -80°C freezer until use. The mAbs were purified and concentrated by using Mouse TCS Purification System (Abcam). Antibodies were quantified using Nanodrop.

Purified mAbs 15, 16, and 17 were found to be mouse IgG1 isotype according to the Ig Isotyping Mouse Instant ELISA™ kit (Thermo Fisher).

2.4 GENERATION AND VALIDATION OF THE HEK293.ΔIFIH1 MDA5 KNOCKOUT (KO) CELL LINE

The CRISPR guides targeting *IFIH1* (MDA5) gene were designed by Dr. Joey Riepsaame (previous affiliation: MRC Weatherall Institute of Molecular Medicine, University of Oxford). In brief, the CRISPR oligos were designed using an online tool (crispr.mit.edu). Four pairs of CRISPR primers were designed as below.

Table 2 – CRISPR oligonucleotides to delete IFIH1 gene promoter region

Oligonucleotide	Sequence (5' to 3')
F1	CACCGCCTTTGGTTAAGGACACCGC
R1	AAACGCGGTGTCCTTAACCAAAGGC
F2	CACCGCTTCACCCGCCCCGACCAAA
R2	AAACTTTGGTCGGGGCGGGTGAAGC
F3	CACCGATAGCGGAAATTCTCGTCTG
R3	AAACCAGACGAGAATTTCCGCTATC
F4	CACCGCAGGGTGAAAATGTACATCC
R4	AAACGGATGTACATTTTCACCCTGC

We used the CRISPR vector pX335-U6-Chimeric_BB-CBh-hSpCas9n(D10A) (Cong *et al.*, 2013) in our experiments. The vector was a gift from Professor Dr Feng Zhang (Broad Institute MIT and Harvard, USA).

Each pair of primers were cloned into individual vectors as described elsewhere (Pyzocha *et al.*, 2014). In such a way, four plasmids were generated targeting to delete about 603 nucleotides from the *IFIH1* gene. This region covered 521 nucleotides from MDA5 5'UTR (including the annotated Transcription Start Site) and 82 nucleotides from the canonical ATG start codon.

We co-transfected all four constructs into HEK293 cells and followed all steps recommended by Zheng's lab to generate KO cell lines (Pyzocha *et al.*, 2014). KO cell clones were investigated by Western Blot (WB), Immunofluorescence (IF) (see Chapter 3), and sequencing of the target genomic DNA (not shown). RT-PCR was used to detect mRNAs in WT and KO cell lines (Table 3).

Table 3 – Oligonucleotides to detect human MDA5 by RT-PCR

Oligonucleotide	Sequence (5' to 3')
Forward 1	ATGTCGAATGGGTATTCCACAGAC
Forward 2	CGGGAACATGCAGGCAGTTG
Reverse A	CTAATCCTCATCACTAAATAAACAGCATT
Reverse B	AATCACTGCCCATGTTGCTG

2.5 CLONING OF ZIKA VIRUS (ZIKV) PLASMIDS

A DNA sequence of the single ZIKV open reading frame encoding for all structural and non-structural proteins was derived from a sequenced ZIKV complete genome (GenBank accession KU527068) recovered from the brain of a microcephalic aborted foetus (Mlakar *et al.*, 2016). The genome was annotated for sequence segments encoding individual proteins using sequence alignment with an annotated reference genome (GenBank accession NC_012532.1) (Kuno and Chang, 2007). DNA fragments encoding for the Capsid, Envelope, and pr-Membrane proteins as well as the non-structural proteins NS2A, NS2B, NS3, NS4A-2K, and NS4B were obtained by gene synthesis (GeneArt String linear DNA fragments; Thermo Fischer Scientific) after addition of a start codon (AUG)

to the 5' end of DNA sequences. Fragments were cloned into the pCR8/GW/TOPO Gateway entry vector (Invitrogen). After sequence integrity was verified *via* sequencing, inserts were Gateway-cloned into the pcDNA3.2/V5-DEST vector (Invitrogen) using the Gateway LR Clonase II Plus Enzyme Mix (Invitrogen). Fragments encoding the non-structural proteins NS1 and NS5 were generated by gene synthesis into the pDONR221 Gateway donor vector (GeneArt Gene, Thermo Fischer Scientific) and Gateway-cloned into the pcDNA3.2/V5-DEST vector. DNA constructs encoding the other ZIKV proteins utilised in this project (NS4A, 2K-NS4B, NS4A-2K-NS4B, NS2B-NS3, NS5-eYFP) were created by (Overlap)-PCR from existing ZIKV protein encoding plasmids using Phusion High Fidelity DNA Polymerase (New England Biolabs) (Table 4). NS5 mutants were created by mutagenesis PCR and confirmed by sequencing.

Table 4 - Oligonucleotides used for ZIKV sequences cloning

Oligonucleotide	Purpose	Sequence (5' to 3')
751_2K-NS4B_f	Cloning of 2K-NS4B	AGGAGGACAGCTATGTCTCCCCAGGACAACCAAATGGCAATCATCATCATGGTAGCAGTAGGTCTTCTGGGCTTGATTACCGCCAATGAACTCGGATGGTTGGAG
734_2K-NS4B_r	Cloning of 2K-NS4B	ACGTCTCTTGACCAAGCCAG
749_NS4A_f	Cloning of NS4A	AGGAGGACAGCTATGGGAGCGGCTTTTGGAGTG
750_NS4A_r	Cloning of NS4A	TCTTTGCTTTTCTGGCTCAGG
753_NS4A-2K-NS4B_f	Cloning of NS4A-2K-NS4B (overlap PCR)	GGCGGTAATCAAGCCCAGAAG
754_NS4A-2K-NS4B_f2	Cloning of NS4A-2K-NS4B (overlap PCR)	GGCAATCATCATCATGGTAGCAGTAGGTCTTCTGGGCTTGATTACCGCCAATGAACTCGGATGGTTGGAGAG
779_NS2B-NS3_r1	Cloning of NS2B-NS3 (overlap PCR)	CAGGCACATCCCATAGAGCACCACTCCTTTTTCCAGTCTTCACGTATACGTA
780_NS2B-NS3_f2	Cloning of NS2B-NS3 (overlap PCR)	CGTGGTACGTATACGTGAAGACTGGAAAAAGGAGTGGTGCTCTATGGGATGTGCCTG

781_NS2B-NS3_r2	Cloning of NS2B-NS3 (overlap PCR)	TCTTTTCCCAGCGGCAAACTCCTTG
797_NS2B-NS3_f1	Cloning of NS2B-NS3 (overlap PCR)	AGGAGGACAGCTATGAGCTGGCC
783_NS5-eYFP_r1	Cloning of NS5-eYFP (overlap PCR)	GCGGCCGCCACTGTGCTGGATATCAA CCACTTTGTACAAGAAAGCTGGGTCG AATTCGCCCTCAGCACTCCAGGTGTA GACCCTTCTTC
784_NS5-eYFP_f2	Cloning of NS5-eYFP (overlap PCR)	TTCTTGTACAAAGTGGTTGATATCCAG CACAGTGGCGGCCGCTCGAGTCTAG AGGGGCCGCGGTTCGAAGTGAGCAA GGGCGAGGAGCTG
785_NS5-eYFP_r2	Cloning of NS5-eYFP (overlap PCR)	CAGCTCGTCCATGCCGAGAGTG
786_NS5-eYFP_f1	Cloning of NS5-eYFP (overlap PCR)	AGGAGGACAGCTATGGGGGGTG
aNLS mutant – Cluster 1 (KHK to AA) Fwd	NS5 NLS mutagenesis PCR	cctggttgtggaaagagctaggcgcagccgcacggc cacgagtctgtaccaaag
aNLS mutant – Cluster 1 (KHK to AA) Rev	NS5 NLS mutagenesis PCR	ctttggtacagactcgtggccgtgcggctgcgcctagct ctttccacaaccagg
aNLS mutant – Cluster 2 (RQ to AA) Fwd	NS5 NLS mutagenesis PCR	ccagacccccaagaaggcactgctgcggttatgagc atggtc
aNLS mutant – Cluster 2 (RQ to AA) Rev	NS5 NLS mutagenesis PCR	gaccatgctcataaccgcagcagtgccttcttgggggt ctgg
2-O'methyltransferase mutant - Fwd	NS5 E218A cap1 mutagenesis PCR	ccgcaactctacacatgcgatgtactgggtctctg
2-O'methyltransferase mutant - Rev	NS5 E218A cap1 mutagenesis PCR	cagagacccagtacatcgcatgtgtagagttgcgg
NS5 M2634V F	Cloning of NS5 "African mutant"	atagctttgcaccaacatgggttcttcatgaccag
NS5 M2634V R	Cloning of NS5 "African mutant"	ctggtcatgaagaacccatgttggtgcaaagctat
NS5 M3392V F	Cloning of NS5 "African mutant"	cacctatgatcctgcgcatcatgttgactgtgttttta
NS5 M3392V R	Cloning of NS5 "African mutant"	taaaaacacagtcaacatgatgcgcaggatcataggt g

2.6 A549-ZIKV-RNA AND IVT-RNA

A549-ZIKV-RNA was generated by infection of A549 cells (obtained from R. E. Randall, University of St Andrews) with ZIKV (isolate ZIKV/H.sapiens/Brazil/PE243/2015, GenBank accession KX197192.1) at an MOI of 5. 20 hours later, cells were lysed in TRIzol (Invitrogen) and total RNA was extracted according to manufacturer's instructions. Neo^{1-99} *in vitro* transcribed RNA was generated as previously described (Rehwinkel *et al.*, 2010b). Purified RNAs were incubated with alkaline phosphatase (AP) (Roche) using 2 units of enzyme per µg of RNA. Samples were incubated at 50°C for 1 hour and RNAs were purified by phenol-chloroform extraction. Negative control reactions were performed in parallel by omitting the enzyme.

2.7 BIOASSAYS USING P125-HEK CELL STIMULATION

p125-HEK293 (clone 17 – stably expressing *IFNβ* promoter-Luc region and GFP) were used in the bioassay to detect whether total RNA transfection could elicit IFN I responses (Chapter 4). At least 30,000 cells per well were seeded in a 96-well plate. On the day after, cells were pre-treated or not with different concentrations of recombinant IFN-A/D (Sigma-Aldrich or R&D Systems). In most of the experiments, 30U/ml of IFN-A/D was used and cells were allowed to incubate for one day. The cells were washed and fresh medium was added. Cells were transfected with 100ng of total RNAs from cell cultures or commercially available human tissues (Takara Clontech and Ambion). Cells were transfected with Lipofectamine 2000 (Invitrogen) as recommended by the manufacturer. Total RNAs from cell cultures were extracted using TRIzol (Invitrogen) and DNAse (Ambion) treated prior to transfections. Activation of the *IFNβ* promoter was measured in the following day using OneGlo luciferase assay (Promega).

For experiments designated for ZIKV in Chapter 5, cells were seeded at 50,000 cells per well in a 96-well plate. On the following day, cells were transfected with different doses of IVT-RNA or A549-ZIKV-RNA complexed with 0.2 µl of Lipofectamine per well. (For experiments aiming to detect MDA5 stimulation, cells were pre-treated with 3 or 30U/ml of IFN-A/D as above.) After one day incubation, luciferase activity was also measured using OneGlo assay. In some experiments, cells were seeded at 200,000 cells per well in a 24-well plate one day before transfection with graded doses of IVT-RNA complexed with 1µl of Lipofectamine. On the next day, cells were trypsinised, resuspended in FACS buffer (PBS, 1% FCS, 2mM EDTA, 0,02% sodium azide) containing 1µg/ml of DAPI and GFP expression was analysed by flow cytometry.

To validate that MAVS-KO p125-HEK cells can still activate the *IFNβ* promoter, WT and MAVS-KO p125-HEK cells were seeded at 20,000 cells per well in a 96-well plate. On the next day, cells were treated with 200U/ml IFNα. After 24 hours, cells were transfected with 100ng of pcDNA3-MAVS. Luciferase activity was measured one day later.

2.8 BIOASSAY USING PRIMARY HUMAN SKIN FIBROBLASTS

Human skin fibroblasts (presented above) were seeded at a density of 10,000 cells/well in a 96-wells plate. On the following day, cells media were removed and replaced with 40µl media containing total RNAs complexed in Lipofectamine 2000. In this experiment, only total RNA from human tissues (25 – 100ng/well) (Takara Clontech and Ambion) were used. The transfection mixture was allowed to incubate for 4-6 hours at 37°C. Cell monolayers were then washed twice with 200µl of fresh media and incubated with 100µl medium/well for 24h. After this

incubation period, cell supernatants were either transferred to 3C11 (HEK293 cells stably expressing the ISRE-Luc promoter and GFP) or frozen at -80°C freezer for future use.

For the bioassay, 3C11 cells (HEK293 cells stably expressing ISRE reporter) were seeded in 96-wells plate at a density of 40,000 cells/well. On the following day, media were replaced for the human skin fibroblasts supernatants described above. Cells were incubated for a further 24h and luciferase activity was measured using the OneGlo (Promega) assay.

2.9 ANTIBODIES

Primary antibodies utilised for immunoblotting were STAT1 (clone 42H3, Cell Signaling, 1:1000), pSTAT1(Y701) (clone D4A7, Cell Signaling, 1:1000), STAT2 (clone D9J7L, Cell Signaling, 1:1000), RIG-I (clone Alme-1, AdipoGen, 1:1000), MAVS (Enzo Life Sciences #ALX-210-929-C100, 1:500) and MDA5 (clone 17, mouse mAb raised in-house, 1:1000 or 1:500), V5-HRP (Invitrogen, 1:5000), beta-actin-HRP (clone AC-15, Sigma Aldrich, 1:10000), GAPDH-HRP (Proteintech, 1:10000). HRP-coupled secondary antibodies include sheep-anti-mouse and donkey-anti-rabbit (both GE Healthcare, 1:3000).

For immunofluorescence (IF) assays MAVS antibody (1:400) above was also used; IRF-3 (D6I4C, Cell Signalling, 1:400); dsRNAs J2 mAb (SCICONS English & Scientific Consulting Kft., 1:200), MDA5 (mAb15 and 16 raised in-house, 1:100), and nuclei using NucBlue® Live ReadyProbes® Reagent (Thermo Fisher). Fluorescent Alexa Fluor (488nm, 568nm, and/or 647nm) goat-anti-mouse or goat-anti-rabbit secondary antibodies (Thermo Fisher) were used at

1:500. Secondary antibodies able to detect total IgGs, IgG1, and/or IgG2 were used in some experiments.

2.10 WESTERN BLOT (WB) ANALYSIS

WB for MDA5 iCLIP experiments (Chapter 4) are described in another section (section 2.1). Here, the following protocol is described for experiments with ZIKV (Chapter 5), but represents a standard protocol for most of WB experiments in this study. HEK293 or HEK293T cells were seeded at a density of $8x10^5$ or $1x10^6$ cells/well, respectively, in 6-well plates. 24 hours later, cells were transfected with 1500ng of ZIKV or control plasmids using Lipofectamine 2000 (Invitrogen). On day three of the experiment, cells were treated with recombinant human IFN-A/D. After an additional 24 hours incubation period, cells were lysed in lysis buffer (50mM TRIS-HCl pH 7.4, 150mM NaCl, 1% Triton X-100, 0.1% SDS, 0.5% sodium deoxycholate) containing 1:100 Protease Inhibitor Cocktail (Cell signalling Technology). Phosphatase Inhibitor Cocktail 3 (Sigma-Aldrich) was added for analysis of STAT protein phosphorylation. Supernatants were removed by centrifugation and precipitates were sonicated using the Bioruptor sonicator (Diagenode). Protein concentrations were determined using Pierce BCA Protein Assay Kit (Thermo Scientific) and equalized by dilution of samples with lysis buffer. Subsequently, 5x Laemmli sample buffer (312.5mM TRIS-HCl, 10% SDS, 25% beta-mercaptoethanol, 50% glycerol, 0.01% bromophenol blue, pH 6.8) was added and samples were incubated at 95°C for 10 minutes. Samples were run on NuPAGE Novex 4-12% Bis-TRIS gels (Invitrogen) using NuPage MOPS-SDS running buffer (Invitrogen). Proteins were subsequently blotted onto PROTRAN Pure nitrocellulose membrane (PerkinElmer). Membranes were blocked with 5%

skim milk powder (Sigma-Aldrich) in TBS 0.1% Tween-20 (5% milk TBS-T) for 1 hour at room temperature and were then incubated with primary antibodies in 5% milk TBS-T overnight at 4°C. Primary antibodies that bind to phosphorylated residues were diluted in 5% BSA in TBS-T.

Membranes were washed thrice with TBS-T and incubated with HRP-coupled secondary antibodies in 5% milk TBS-T for 1 hour at room temperature. After three further washes with TBS-T, proteins were detected using Western LightningPlus-ECL (PerkinElmer) and Amersham Hyperfilm MP (GE Healthcare). If needed, antibodies were stripped from the membrane with stripping buffer (200 mM glycine, 0.1% SDS, 1% Tween-20, pH 2.2) for 20 minutes at room temperature. Membranes were washed with TBS-T, blocked as previously and re-probed.

2.11 RT-qPCR

Experiments designated to detect MDA5 RNAs were performed in HEK293, HEK293.ΔIFIH1, and 293T-TLA cells. Cells were seeded at a density of $1.5x10^5$ cells/well in 24-well plates. 24 hours later, cells were pre-treated or not with IFN-A/D (100 U/ml) for 24 hours prior to RNA purification.

After an additional 24 hours incubation period, RNA was extracted from cells using the QIAshredder (Qiagen) and RNeasy Mini Kit (Qiagen) according to manufacturer's instructions.

RNA concentration was measured with a Nanodrop system (Thermo Fischer Scientific). RNA was reverse transcribed into cDNA using SuperScript II Reverse Transcriptase (Invitrogen). The PCR reaction containing TaqMan Universal PCR Master Mix (Applied Biosystems) and TaqMan Primer/Probes

(see below) was run on 7500 Fast Real time PCR System (Applied Biosystems) or QuantStudio 7 Flex Real-Time PCR System (Thermo Fischer Scientific) with the following cycle conditions: 10 minutes 95°C, and 40 cycles of 15 seconds 95°C followed by 1 minute 60°C. Gene expression was analysed with the Ct method using *GAPDH* expression for normalization.

TaqMan primer probes used include *GAPDH* (Assay ID: Hs02758991_g1), *IFIH1* (exons 1-2 junction, Assay ID: hs00223420_m1), and *IFIH1* (exons 8-9 junction, Assay ID: hs01070332_m1).

2.12 MICROSCOPY

For experiments using fixed samples, low cell densities were seeded in glass coverslips coated with poly-L-lysine (Sigma). On the following day, cells were infected with viruses or transfected with RNAs using Lipofectamine 2000.

After 24h incubation, cells were washed three times with PBS (Invitrogen) and fixed at RT with 4% methanol-free formaldehyde (Thermo Fisher) diluted in PBS for 15min. Cells were washed several times with PBS for 30sec, 60sec, 5min., 10min., and 15min. Membrane permeabilisation was performed with 0.1% Triton X-100 (Sigma) diluted in PBS and incubated at RT for 10min. Cells were washed with PBS for 30sec and twice 5min. each and then incubated in blocking buffer (PBS, 3%Bovine Serum Albumin – Sigma-, 2.0% Normal Goat Serum - Sigma) for 30min. at RT.

Primary antibodies were diluted in blocking buffer and incubated overnight at 4°C. After three washes with PBS for 5min. each, secondary antibodies were also diluted in blocking buffer and incubated 1h at RT. This step was followed by three further washes with PBS for 5min. each. Nuclei staining (NucBlue® Live

ReadyProbes® Reagent, Thermo Fisher) was diluted one drop per ml of PBS and incubated during the first PBS wash. Slides were mounted using SlowFade® Diamond Antifade Mountant (Thermo Fisher).

Alternatively, a modified microscopy protocol for fixed samples was used. That involved mainly cells fixation at 4°C using a cytoskeleton stabilizing buffer (CSB). Prior to fixation, cells were washed two times with 37ºC pre-warmed DMEM 0% FCS (D0). 500µL of D0 was added and cells incubated for 30min. at 37ºC.

Half the volume of D0 medium was removed and replaced with 2X CSB containing 8% methanol-free formaldehyde. 1X CSB formulation is: 100mM NaCl (Sigma), 10mM PIPES, pH6.8 (Sigma), 3mM $MgCl_2$, 1mM EGTA (Sigma), 300mM Sucrose (Sigma), diluted in water and filtered. Cells were fixed on ice for 15min. All the other steps were similar to the protocol described above.

293T-TLA cells were transfected with ZIKV NS5-eYFP. One day post-transfection, cells were excited with a 488 nm laser and the emission was collected between 520-570 nm.

For visualisation of cellular localisation of NS5 NLS mutants in living cells, nuclei were co-stained with the membrane permeable NucBlue® Live ReadyProbes® Reagent (Thermo Fisher).

A Zeiss 880 confocal microscope was used in most of experiments. For experiments using STED (Stimulated emission depletion) super-resolution microscopy, an in-house made microscope was used (Figure 6). This microscope design has been described elsewhere (Clausen *et al.*, 2013).

STED microscopy improves the spatial resolution of optical microscopy from conventionally 200nm down to the nanoscale (e.g., <80nm). This

technology is able to determine the precise localisation of molecular assemblies in cells down to the level of single molecules (Schermelleh, Heintzmann and Leonhardt, 2010; Eggeling, Willig and Barrantes, 2013), an achievement that has recently been awarded by the Nobel Prize in Chemistry 2014. The basic principles of STED is illustrated in Figure 6. We expected the molecular re-arrangements during the immune responses to virus infection to be on small spatial scales, that is why we anticipated the use of super- resolution fluorescence microscopy methods.

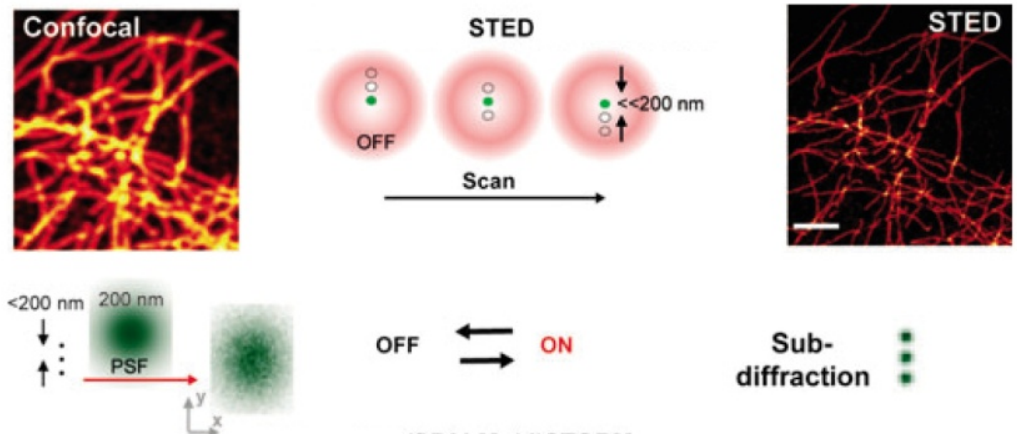


Figure 6 – Basics of stimulated emission depletion (STED) Super-resolution optical microscopy. Conventional microscopy (such as confocal microscopy) produces blurred images of structures at scales lower than 200nm due its limited spatial resolution. In STED, two laser beams are overlaid: one for fluorescence excitation while another one featuring a local intensity zero switches fluorescence off, generating effective observation spots << 200nm. Source: Eggeling, Willig and Barrantes, 2013.

2.13 DATA ANALYSIS AND STATISTICS

Primary data were analysed using Office Excel 2016 (Microsoft) and GraphPad Prism v7.00 (GraphPad Software). SnapGene (GSL Biotech) and ApE (M. Wayne Davis, The University of Utah) were utilised to assist cloning.

Graphs and figures were created using GraphPad Prism v7.00 and Adobe Illustrator (Adobe Systems). Statistical analysis was performed in GraphPad Prism v7.00. as detailed in the figure legends.

2.14 INDIVIDUAL NUCLEOTIDE RESOLUTION UV CROSSLINKING AND IMMUNOPRECIPITATION (ICLIP)

The protocol described here is an adaptation and combination of three previously published protocols (Huppertz *et al.*, 2014; Van Nostrand *et al.*, 2016; Zarnegar *et al.*, 2016). Figures 12A and 13C summarise the method and were adapted from Huppertz *et al*. (2014).

We used iCLIP as the core protocol, including by the use of the Urea Cracking Buffer high stringent step as wells as its described primers and adaptors (Huppertz *et al.*, 2014).

For adaptor ligation, we employed the suggestions from the enhanced CLIP (eCLIP) method (Van Nostrand *et al.*, 2016). From the eCLIP method, we also used the protocol to generate the INPUT samples (Van Nostrand *et al.*, 2016). The RT steps were derived from the infrared CLIP (irCLIP) method (Zarnegar *et al.*, 2016).

Below, I describe the protocol we have been optimising to co-IP RNAs associated to MDA5. Table 5 displays all buffer recipes mentioned below. Primer and adaptor sequences are found in the original articles mentioned above, especially Huppertz *et al*. (2014).

Preparation of cell pellets and beads-antibody conjugates

293T-TLA cells were seeded at density of $1x10^7$ cells per dish. Next day, cells were transfected with 5μg of 3XFLAG-hMDA5, 3XFLAG-hMDA5 (K335A

mutant), or HA-hMDA5 plasmids using 5μg of Lipofectamine 2000 (Invitrogen). All these constructs were previously cloned into a pCDNA3.1 mammalian expression vector (Invitrogen).

Transfection reagents were washed away in the following day and cells were mock- or infected with EMCV at MOI 0.1. Cells were further incubated for 16-24h until signs of cell detachment.

Cell monolayers were washed in cold PBS and UV-crosslinked with 100mJ/cm^2 using 254nm Spectralinker. Samples without UV crosslinking were used as negative controls. Cells were scraped in PBS, centrifuged 2,000 rotations per minute (RPM) for 5min, and snap frozen in dry ice after removal of supernatants containing PBS and cell debris. Cell pellets were then transferred to -80°C freezers until use.

Monoclonal (mAb) M2 α-FLAG (Sigma) antibodies were covalently linked to magnetic beads. To assist the handling of magnetic beads, magnetic stands (Invitrogen) were used in all washing steps. Bead-mAb conjugation was performed according to Dynabeads Antibody Coupling kit (Invitrogen) manufacturer's instructions.

I used 30μg of mAb per mg of beads as recommended by Huppertz *et al*. (2014). I used 100ul of the beads for each immunoprecipitation experiment. Prior to use, Bead-mAb conjugates were washed once in 100ul of High-Salt Buffer and once in RIPA buffer. Samples were resuspended in 100ul RIPA buffer.

Pellets from 2-6 dishes were used per IP experiment. More than 6 dishes were used for experiments aiming the optimisation of the sequencing steps.

Cell lysate preparation and first round of co-immunoprecipitation (co-IP)

Frozen pellets were lysed in RIPA buffer containing EDTA-free protease cocktail inhibitors (Roche). Samples were sonicated using Bioruptor plus for five cycles with alternating 30s on/30s off at low intensity. 20 units (U) of Turbo DNase (Ambion) was added and incubated at 37°C 1000 RPM for 5 min.

Samples were transferred to ice and 2U RNAse A (MB grade Affimetrix) was added. Different amounts of RNAse A were used in experiments aiming titration of its concentration. Lysates were further incubated at 37°C 1000 RPM for 5 min. Samples were transferred to ice for at least 3min.

In the meantime, RNAsin (Promega) was added (0.5U/ml final concentration) to block the activity of RNAse A. Lysates were spun 15min at 13,000 RPM at 4ºC and supernatants were transferred to a new 2ml tube. This latter step was repeated once more.

For INPUT samples, an aliquot of the supernatants was taken for WB and RT-PCR. INPUT samples were processed in a different manner than the co-IP bound fraction (beads) samples. The latter is described below, while the INPUT samples preparation has been detailed in Van Nostrand *et al.* (2016).

The cleared lysates were incubated with the bead-mAb conjugates previously prepared. These were rotated for 2h at 4ºC. After this incubation, the supernatants were discarded and beads were washed twice with High-Salt Buffer and once with PNK buffer. Samples remained on ice and in PNK buffer until the beads for the second co-IP round were ready to use.

Preparation of non-covalent Bead-mAb conjugates (Antibody-beads II) and second round of co-immunoprecipitation (co-IP)

100ul of Protein G dynabeads (Invitrogen) per sample were washed twice with RIPA buffer (without protease inhibitor). All washing steps were made with 900ul of the respective buffer. The beads were re-suspended in 100ul RIPA buffer containing 20ug M2 FLAG antibody per sample.

This mixture was incubated for 30-60min. at room temperature (RT). These conjugates were washed once with RIPA buffer; twice with T-20 IP buffer; and re-suspended in 100ul T-20 IP buffer per sample. The PNK buffer was removed from the co-IPed samples from "first co-IP round step". 100ul of Urea Cracking Buffer were added to these samples. This mixture was incubated at 65ºC 1100 RPM for 3min. The samples were transferred to ice, spun down, and supernatants transferred to 1.5mL Eppendorf tubes containing 1mL TP-20 IP Buffer with RNAsin and protease cocktail inhibitors.

The Antibody-Beads II conjugates were then added to this mixture. The second co-IP was then processed by rotating these samples at 4ºC for 2h. After this incubation time, the supernatants were discarded and beads were washed twice with High-Salt Buffer and twice with PNK buffer.

RNA 3'-ends de-phosphorylation and radioactive labelling

After washing steps above, the beads were treated with T4 polynucleotide kinase (PNK) enzyme to remove 3'-end phosphates.

The samples were re-suspended in a 300ul reaction volume as follows:

224ul Water

60ul 5X PNK pH6.5 buffer (Table 5)

3ul 0.1M DTT (Invitrogen)

5ul RNase inhibitor (Promega)

1ul Turbo DNase (Ambion)

7ul T4 PNK enzyme (NEB)

The samples were incubated at 37ºC 1200 RPM for 20min. The beads were then washed twice with PNK buffer; twice with High Salt Buffer; twice with PNK buffer; three times with RNA ligase (no DTT) buffer.

Radioactive labelling was performed at this stage for most of the experiments. Alternatively, this step was conducted after adaptor ligation step described below in few experiments. All of the sample content or only 10% of the samples were used for RNA radiolabelling using ϒ-32p-ATP (PerkinElmer) with the following reaction.

Samples were re-suspended in a 20ul reaction volume followed by incubation at 37ºC 1000RPM for 5min.:

2ul 10X PNK-buffer (NEB)

2ul T4 PNK (NEB)

2ul (10uCi) ϒ-32p-ATP (PerkinElmer)

14ul Water

The beads were then washed in 900ul PNK-buffer and used for WB (gel purification) as described below.

L3 RNA adaptor ligation and WB gel purification

Most of the samples were ligated with the L3 RNA adaptor (Huppertz *et al.*, 2014) prior to radioactive labelling (esp. samples designated for sequencing).

After the washes, the samples were re-suspended in 28.5ul reaction volume and allowed to incubate at 25ºC 200RPM for 120min.

9.8ul water

3ul 10x RNA ligase buffer (no DTT) (Table 5)

0.8ul 100% DMSO (NEB: PCR grade)

12ul 50% PEG 8000 (20% final. NEB)

0.4ul RNase inhibitor (Promega)

2.5ul RNA ligase high concentration (NEB)

then individually add,

1.5ul 20uM rApp L3-adaptor (Huppert *et al*., 2014)

After the incubation, the beads were washed once with PNK buffer and transferred to a new tube. This transfer followed one more wash in PNK buffer; twice in High-Salt Buffer; and three times in PNK-buffer.

After the washes, samples were gel purified similarly to a WB protocol. Beads were resuspended in 20ul loading buffer:

5μl 4x Sample Buffer (Table 5)

1μl 1M DTT (20x); 50mM final concentration

14μl Water

Samples were frozen at this stage overnight at -20ºC to be processed on the following day. The samples were then incubated 10min at 70ºC 1,200 RPM; spun and left on ice for 2min. Eluates were separated from the beads using a magnet stand and 20ul of sample was loaded per lane on a 4-12% gradient Bis-Tris gel. In some experiments, 8% gels were used instead.

The gels were left to run at 180V for 2h in NuPage MOPS-SDS running buffer (Invitrogen). Proteins were subsequently transferred onto PROTRAN Pure nitrocellulose membrane (PerkinElmer) using NuPage Transfer Buffer (Invitrogen). Transfer was allowed to proceed for 90min. at 100V.

Proteinase K treatment and RNA purification

For the radioactively labelled samples, the radioactive membranes were exposed to radiofilms overnight (or longer) within WB cassettes in -80ºC freezers. RNAs were then possible to be visualised.

MDA5-RNA complexes were removed from the nitrocellulose membranes by excising the gel membranes above 160kDa until lower than 260kDa. Radioactive films were used to assess this step in order to spot the precise positions of the complexes. The excised membranes were cut into small slices to fit the bottom of a 2mL Eppendorf tube.

To release the RNAs from MDA5, the excised membranes were incubated with 200ul of PK Buffer containing Proteinase K (Roche) at 1mg/ml final concentration. Reactions were incubated at 50ºC for 60min. 1000 RPM.

RNAs were then purified with a Phenol:Chloroform (neutral pH, Sigma) protocol. Membrane slices were discarded and the supernatants were mixed with

200ul Phenol:chloroform. This mixture was transferred to a Phase-Lock tube (VWR) and incubated 10min. at 37ºC 1400 RPM. Samples were centrifuged 12,000 RPM for 2min. at RT. To further clean-up phenol contamination, 800ul of chloroform was added and mixed by inverting the tube for around 10 times. Samples were again centrifuged 12,000 RPM for 2min. at RT. The aqueous layer was transferred to a new 2ml Eppendorf tube. To precipitate the RNAs overnight on a -20ºC freezes, the aqueous layer was further mixed with 10ul 5M NaCl (NaCl avoids SDS precipitation present in the PK buffer), 1ul glycoblue (Thermo Fisher Scientific), and 800ul cold 100% ethanol (Sigma). (In all future Phenol:Chloroform purification steps, 40ul Sodium Acetate pH 5.5 was used instead of NaCl.)

In the following day, RNAs were pelleted after centrifugation at top speed (13,000 RPM) for 30min. at 4ºC. RNAs were washed with cold 80% ethanol and spun 5min. 13,000 RPM for 5min. RNAs were resuspended in 10.75μl Water.

Reverse Transcription (RT) using TIGRT-III enzyme

Eluted RNA samples were mixed with 2ul of 0.5uM RT primers (described in Huppert *et al*., 2014) per sample. This mix was denaturated at 70°C for 5min. and immediately placed on ice. The following items were then added:

4ul 5 x TGIRT buffer (Table 5)

1ul 100mM DTT (Invitrogen)

0.25ul RNasin Plus (Promega)

1ul TGIRT (Ingex)

The reactions were incubated at 25ºC for 30min. After this incubation time, 1ul of 10mM dNTPs (Invitrogen) were added and mixed well. RT step was then allowed to process with the following incubation times in a thermocycler: 5min at 25ºC, 20min at 42ºC, and 40min at 60ºC.

To degrade RNAs and dissociate the TGRT-III enzyme from its complexes, 1ul 5M NaOH was added to the mixes. Samples were heated 3min. 95ºC, then quickly transferred to ice. The pH was restored by adding 1ul 5M HCl.

Complementary DNAs (cDNAs) were precipitated overnight at -20ºC by adding 380ul TE-buffer (Ambion), 1ul glycoblue, and 40ul Sodium Acetate pH 5.5.

In the next day, the pellets were formed after centrifugation at 4ºC at 13,000 RPM for 30min. Pellets were washed with 80% EtOH, and spun 5min. at 13,000 RPM. Pellets were re-suspended in 8ul water.

Gel size fractionation, purification and circularisation of cDNAs

To remove the excess of non-ligated adaptors and improve PCR amplification of products of different sizes, the cDNAs were size fractionated in a denaturaning TBE-Urea gel. The fragments were: H: High 120-200bp; M: Medium 80-120bp; L: low 70-80 (Huppertz *et al.*, 2014).

To the cDNA pellets previously re-suspended, 8ul of 2X TBE-Urea loading buffer (Invitrogen) were added. Pellets were heated at 80ºC for 5min., quickly transferred to ice, and loaded onto a 6% TBE-Urea gel (Invitrogen).

The samples were allowed to run for 40min. at 180V in TBE buffer (Invitrogen). After this time period, H, M, and L gel bands were excised using a

DNA marker (Invitrogen) as reference. The gel fragments were transferred to 2ml Eppendorf tubes and mixed with 400ul of TE buffer (Invitrogen). The gel pieces were crushed with a 1ml syringe plunger and incubated at 37ºC for 1h at 1250 RPM. Samples were placed on dry ice for 3min. and further at 37ºC for 1h at 1250 RPM. The liquid phase was transferred to a Costar SpinX column containing 2 glass filters (VWR) and centrifuged 13,000 RPM for 1min. The filtered fraction was collected and cDNAs were purified and precipitated following Phenol:Chloroform as described above. After overnight precipitation, cDNAs were re-suspended in the following ssDNA circularisation reaction:

6.3ul Water

0.8ul Circligase II buffer (Epicentre/Illumina)

0.4ul $MnCl_2$ (Epicentre/Illumina)

0.5ul Circligase II (Epicentre/Illumina)

The reactions were transferred to PCR tubes and incubated 1.5h at 60ºC. The next steps were meant to re-linearize the cDNAs products while creating Forward and Reverse sites for PCR primers. In order to do this, circularised cDNAs were cleaved with BAMHI restriction enzyme. To achieve this, circularised ssDNAs were first allowed to generate a small dsDNA site at a region containing BAMHI sequence using a cut oligo (Huppertz *et al*., 2014) with 30ul of the following reaction:

4ul Fastdigest buffer (Fermentas)

1ul 10uM cut oligo (Huppertz *et al*., 2014)

25ul Water

To anneal the cut oligo to the specific site within the circularised ssDNA, the following thermal annealing programme was used in a thermocycler:

95ºC 2min

95-25ºC 20sec (Successive cycles of 1ºC decrease for 20sec each temperature)

25ºC Infinite

After cut oligo annealing, 2ul BamHI was added to this reaction and incubated 30min at 37ºC followed by its inactivation at 80ºC for 5min. The mixtures were topped up to 400ul with TE buffer and proceed to overnight cDNA clean-up and precipitation as previously described. The linear cDNA pellets were then re-suspended in 21ul water.

Polymerase Chain Reaction (PCR) using Phusion polymerase

For PCR, 1ul cDNA was used for each reaction as follows:

1ul cDNA

0.25ul 10uM P5 primer (Huppertz *et al*., 2014)

0.25ul 10uM P3 primer (Huppertz *et al*., 2014)

5ul HF-Phusion-mix [NEB, M0531S]

3.5ul Water

The cycling conditions were: 98ºC for 2min; 13-23 cycles of 98ºC for 15sec/65ºC for 30sec/72ºC for 30sec; then final elongation at 72ºC for 3min. PCR products were mixed with 2ul 5x Novex Hi-Density TBE Sample Buffer (Thermo

Fisher) and loaded onto a 6%TBE gel (Invitrogen). Samples were allowed to run at 180V for 30min. and cDNAs were visualised with SYBR Gold (Thermo Fisher).

For sequencing using MiSeq 50 cycles (Illumina), PCR products were purified from 6%TBE gels and eluted in water or TE buffer. Quality control was performed to confirm cDNA concentrations and sizes.

Usually, a mixture of H and M bands were sent to sequencing. Further developments on this protocol are still required and, as such, are not here described.

Table 5 - Buffers used on the iCLIP protocol

Buffer	Final Concentration/Formulation
RIPA	50mM Tris.HCl pH 7.4 (Ambion) 150mM NaCl (Ambion) 1% NP-40/Nonidet (Sigma) 0.1% SDS (Sodium Dodecyl Sulfate. Sigma) 0.5% Sodium Deoxycholate (Sigma) Nuclease-free Water (Invitrogen)
High-Salt	50mM Tris.HCl pH 7.4 1M NaCl 1% NP-40 0.1% SDS 0.5% Sodium Deoxycholate Nuclease-free Water
Urea Cracking Buffer (Freshly prepared)	50mM Tris-HCl, pH7.4 6M Urea (Sigma) 1% SDS 25% PBS (Invitrogen) Nuclease-free Water
T20-IP	50mM Tris-HCl, pH7.4

	150mM NaCl 0.5% Tween (Sigma) 0.1mM EDTA (Ambion) Nuclease-free Water
PNK buffer (Wash buffer)	20mM Tris.HCl pH 7.4 10mM $MgCl_2$ (Ambion) 0.2% Tween Nuclease-free Water
PK (Proteinase K) buffer	100mM Tris.HCl pH 7.5 50mM NaCl 1mM EDTA 0.2% SDS Nuclease-free Water
5X PNK Buffer pH 6.5	350mM Tris pH 6.5 (Sigma) 50Mm $MgCl_2$ Nuclease-free Water
5X PNK Buffer pH 6.5 (Low DTT)	350mM Tris.HCl pH 6.5 50mM MgCl2 5mM DTT (Invitrogen) Nuclease-free Water
10X RNA Ligase Buffer	500mM Tris-HCl pH 7.5 100Mm $MgCl_2$ Nuclease-free Water
5X TGIRT buffer	100mM Tris.HCl pH 7.5 2.25M NaCl 50mM MgCl2 Nuclease-free Water

CHAPTER 3

3 GENERATION AND VALIDATION OF ANTIBODIES AGAINST HUMAN MDA5

Most studies have addressed MDA5 signalling in cell-free systems or using tagged proteins ectopically expressed in cell cultures. As an example of the former case, MDA5 has been shown to form filaments on long dsRNAs (Peisley *et al.*, 2011, 2012; Berke *et al.*, 2012; Wu *et al.*, 2013; Bruns *et al.*, 2014). MDA5 filament formation is thought to induce type I/III IFNs (Wu *et al.*, 2013; Bruns *et al.*, 2014) and to disrupt binding of viral proteins pre-attached to dsRNAs (Yao *et al.*, 2015).

Currently, these studies in the test tube form the basis of our understanding of how MDA5 responds to dsRNAs and induces the expression of antiviral cytokines. However, none of them addressed these questions in living cells. For example, MDA5 filaments have never been visualised in cells or purified from cell cultures, either endogenously or upon ectopic expression.

Hence, several questions remain open to confirmation and validation. Some of these issues are: i) What is the physiological ligand for MDA5?; ii) Does MDA5 form filaments in living cells?; iii) If so, what is the role of such filaments?; iv) Are they capable of triggering cytokines and/or act as direct antiviral effectors?; v) How would they interact with MAVS?; vi) How are they degraded?; vii) If not filaments, what is the MDA5 signalling platform and how is it controlled?

These questions have been open for several years and proved difficult to address. Validated and specific antibodies against human MDA5 are needed to explore these issues. Commercial antibodies are available but have not received much attention from the scientific community due to low specificity and affinity.

Here, we aimed at generating and validating a panel of antibodies against human MDA5. I have tested them for their specificity in techniques such as IF, WB, and IP.

3.1 GENERATION AND SCREENING OF HUMAN ANTI-MDA5 ANTIBODIES DERIVED FROM HYBRIDOMA CELL LINES AND MOUSE ASCITIC FLUIDS

As MDA5 is encoded by an ISG (Kang *et al.*, 2002), we pre-treated HEK293 cells with recombinant IFN-A/D to upregulate its expression. We used this system to clone human MDA5 from cDNA into a mammalian expression vector (pCDNA3.1). A 3XFLAG tag was added to its N-terminus and the plasmid was sequenced. Interestingly, we found this construct contained two common T1D-associated SNPs, rs3747517/R843H and rs1990760/T946A (Nejentsev *et al.*, 2009).

We also cloned human MDA5 from cDNA into a baculovirus system and transduced SF9 insect cells to generate recombinant protein for purification. We sent the purified proteins to our collaborator Dr. Jin Boquan (Department of Immunology, Fourth Military Medical University, China). Dr. Boquan's group immunised mice with the recombinant human MDA5 and generated 29 antibody-secreting hybridoma cell lines. Additionally, they injected these hybridoma cell lines in separate mice and produced mouse ascitic fluids (hereafter named "ascites") collected from the animals' peritoneal cavities.

In turn, I screened these 29 mouse ascites for their ability to recognise ectopically expressed 3XFLAG-hMDA5 in HEK293 cells (Figure 7). Figure 7 shows most of the mouse ascites detected MDA5 protein by WB, except for ascite 27. Ascite 20 presented a weak signal. Specially ascites 09, 15, 16 and 21 detected a single band close to the expected size (about 135 kDa) of MDA5.

As a control, I probed a membrane with an anti-FLAG antibody (α-FLAG) and detected MDA5 as a smeared band of long size range (Figure 7). This smear was absent from untransfected lysates demonstrating the specificity of the commercial FLAG monoclonal antibody. A similar pattern was observed by most of the remaining ascites (Figure 7).

Considering most of the ascites were detecting the expression of 3XFLAG-MDA5, a central band of about 160 kDa was observed (Figure 7). This is probably the size that canonical MDA5 runs at the settings used for this experiment. Further products (“smeared bands”) slower and faster migrating than 160 kDa were seen by using most of the ascites and α-FLAG.

Some of these ascites potentially detected endogenous levels of MDA5 as a single 160 kDa band was observed in untransfected cells (Figure 7), but these findings were not consistent for all of them.

Furthermore, I transfected HA-tag containing MDA5 (HA-MDA5) to screen which ascites are specific for MDA5 and not for the FLAG peptide (not shown). Amid the most likely specific candidates, I shortlisted ascites 15, 16, and 17 for further experiments. Ascites 15 and 16 presented similar results in all techniques and were mainly chosen for IF assays as shown below.

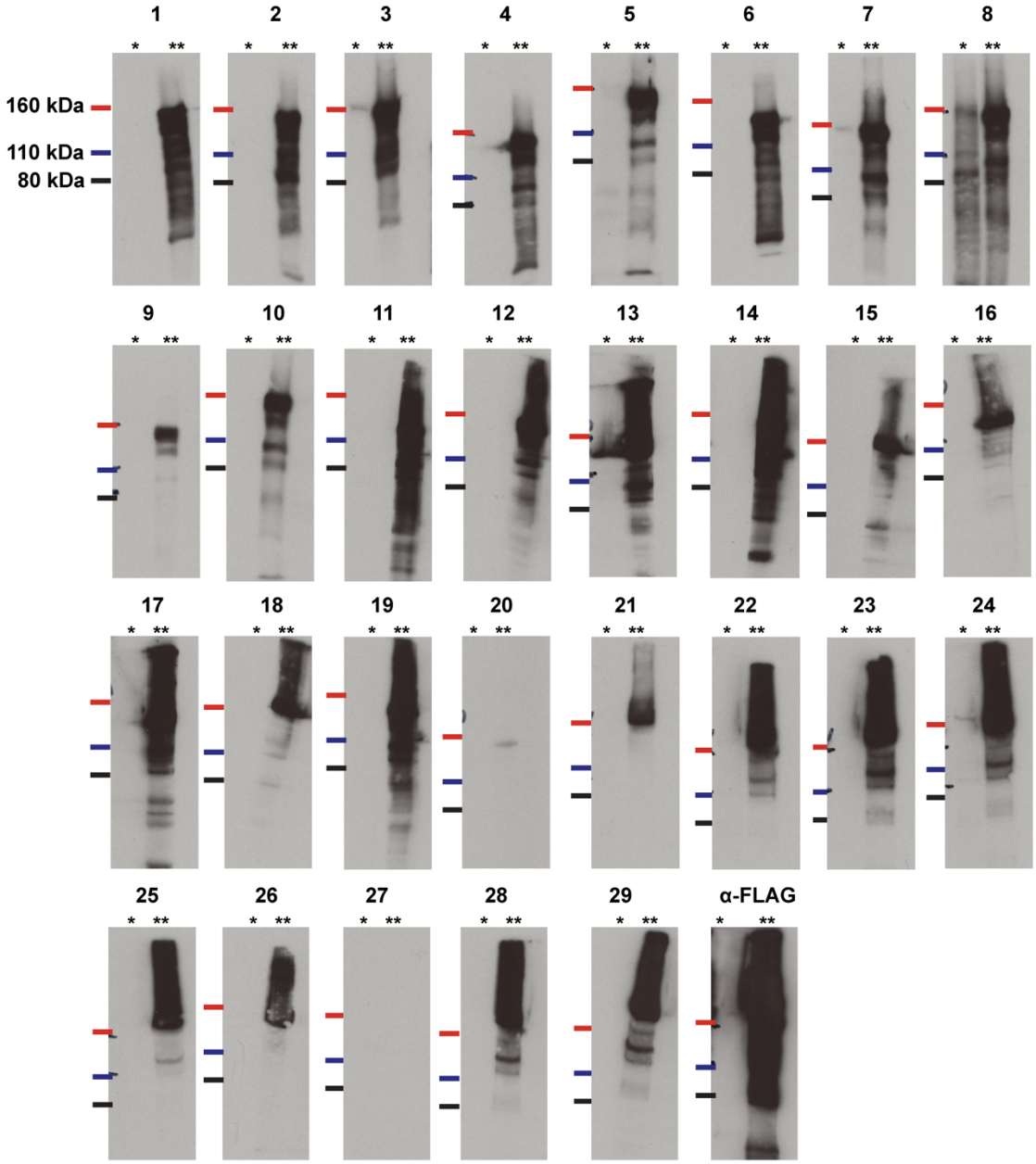


Figure 7 - Screening of mouse ascites containing anti-MDA5 antibodies by Western Blot (WB). 293T-TLA cells were left untransfected (*) or transfected with 3XFLAG-human MDA5 (**). Cell lysates were used for WB and probed with anti-FLAG antibody (α-FLAG) or mouse ascites (1-29). The mouse ascites were derived from mice injected with monoclonal antibody-secreting hybridoma cell lines. Protein markers are represented in coloured bars: red (160 kDa), blue (110 kDa), and black (80 kDa). The whole screening was performed with one biological replicate. Some ascites were tested multiple times.

For IF assays, I stained HEK293 cells to analyse the distribution of MDA5 in unstimulated cells and in cells transfected with V-EMCV-RNA (Figure 8A). I chose V-EMCV-RNA transfection as it induced higher levels of IFN I than EMCV infection (not shown).

Ascite 15 staining in unstimulated cells demonstrated a diffuse staining throughout the cytoplasm (Figure 8A). Nuclear staining was also observed suggesting this antibody possibly produced a certain degree of background in these cells.

Interestingly, cells transfected with V-EMCV-RNA for 24h revealed a structured staining in addition to a weaker diffuse background (Figure 8A). The structures were bright foci resembling punctae and long filaments. These structures were not seen in cells transfected with HMW poly (I:C) or the RIG-I agonists IVT RNA (see Figure 11A for an example).

To further assess the nature of these filaments, we used STED (stimulated emission depletion) super-resolution microscopy. In comparison to conventional confocal microscopy, images acquired with STED increased the resolution of those structures (Figure 8B). These observations supported the finding that V-EMCV-RNA transfection in HEK293 cells led to the appearance of filamentous structures detected by ascite 15 (Figure 8B).

In a separate experiment, I co-transfected V-EMCV-RNA and 3XFLAG-hMDA5 and co-stained the cells with mouse ascite 15 and α-FLAG antibody. I analysed cells presenting both structured staining patterns (punctae and filaments) – revealed by ascite 15 - and 3XFLAG-hMDA5 staining. In this case, α-FLAG only demonstrated a diffuse, but not structured, MDA5 distribution.

These experiments suggested ectopically expressed MDA5 does not form filamentous structures.

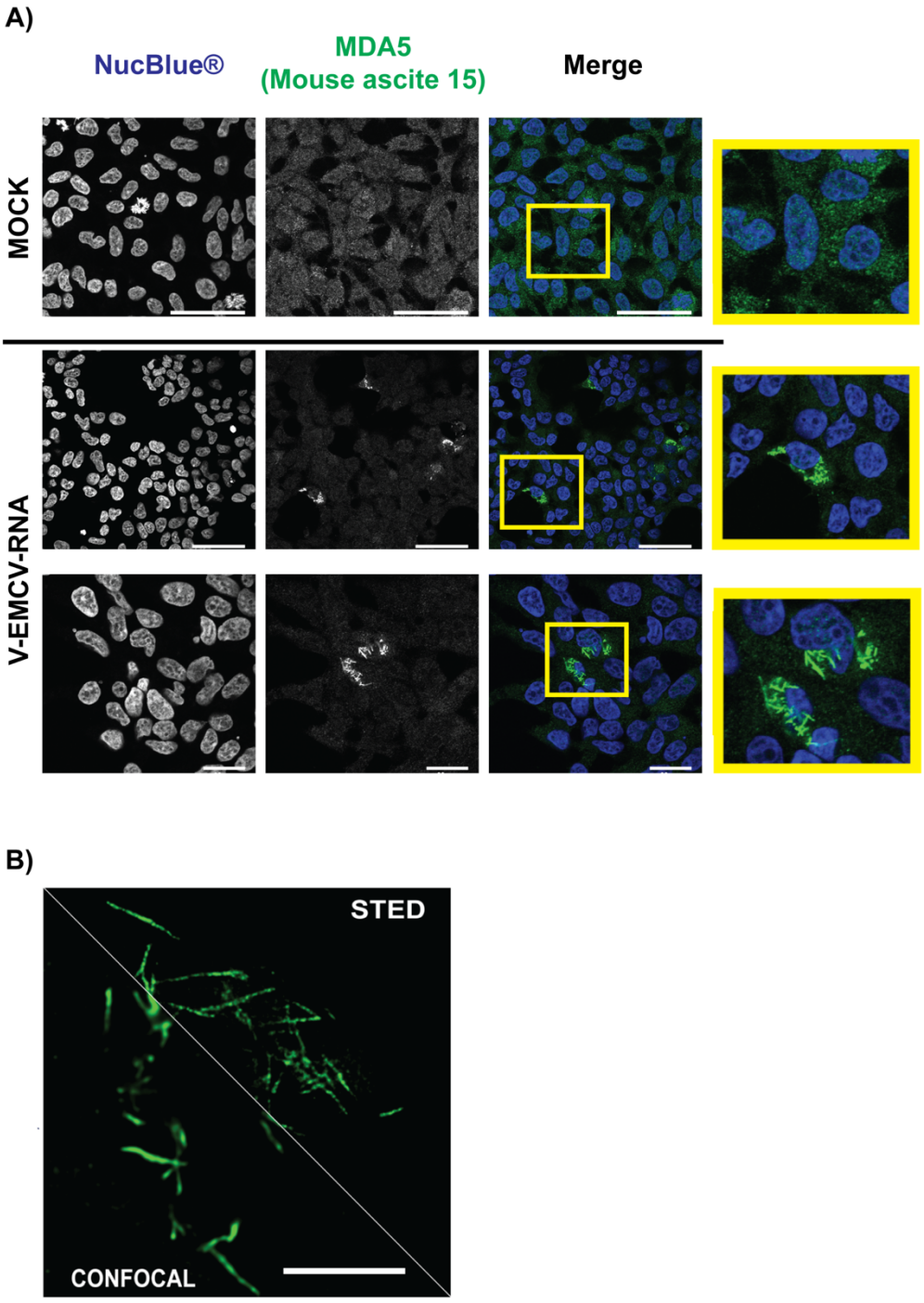


Figure 8 - Immunostaining of HEK293 cells with mouse ascite 15. HEK293 cells were mock-treated or transfected with total RNA from VERO cells infected with EMCV (V-EMCV-RNA). Cells were fixed and stained with mouse ascite to detect MDA5 distribution. A) Punctae and filaments were observed in cells transfected with V-EMCV-RNA, but not in untransfected (mock) cells. B) Super-resolution STED (Stimulated Emission Depletion) microscopy improved confocal resolution and confirmed the presence of long filaments. Bars in "A": 50µm (Top and Middle rows) and 20µm (Bottom row). Bar in "B": 5µm. The images are representative of at least 3 biological replicates.

To assess the possibility these filaments could be formed along dsRNAs, I transfected cells with V-EMCV-RNA and, after fixation, co-stained with ascite 15 and J2 (dsRNA) mAb (Figure 9). Indeed, all cells presenting punctae and filamentous structures also co-stained for dsRNAs (example in Figure 9A). Furthermore, I selected individual cells co-staining for filaments and dsRNAs and acquired a Z-stack (Figure 9B). dsRNAs and filaments were present throughout the whole cell (Figure 9B). Yet co-localisation was not clearly observed. Altogether, these experiments suggest dsRNA bound by MDA5 is not accessible to J2 mAb staining. Another possibility is that these filaments might be bound to different RNA species, if any.

3.2 GENERATION OF A HUMAN CELL LINE KNOCKOUT FOR MDA5 (HEK293.ΔpIFIH1)

To verify the specificity of the antibodies we generated against human MDA5, we developed two human MDA5 KO cell lines using CRISPR technique in HEK293 cells.

First, we aimed at removing the annotated *IFIH1* (MDA5) promoter plus approximately the first 80 nucleotides (nt) after the canonical ATG start codon (HEK293.ΔpIFIH1). This leads to a deletion of more than 600 nucleotides (Figure 10A).

Another MDA5 KO cell line (HEK293.FS) was generated by Dr. Alice Mayer in our laboratory. A point mutation was introduced in MDA5's first CARD domain. In this case, a single nucleotide was inserted leading to a frame shift (FS) within the coding region (Figure 10A).

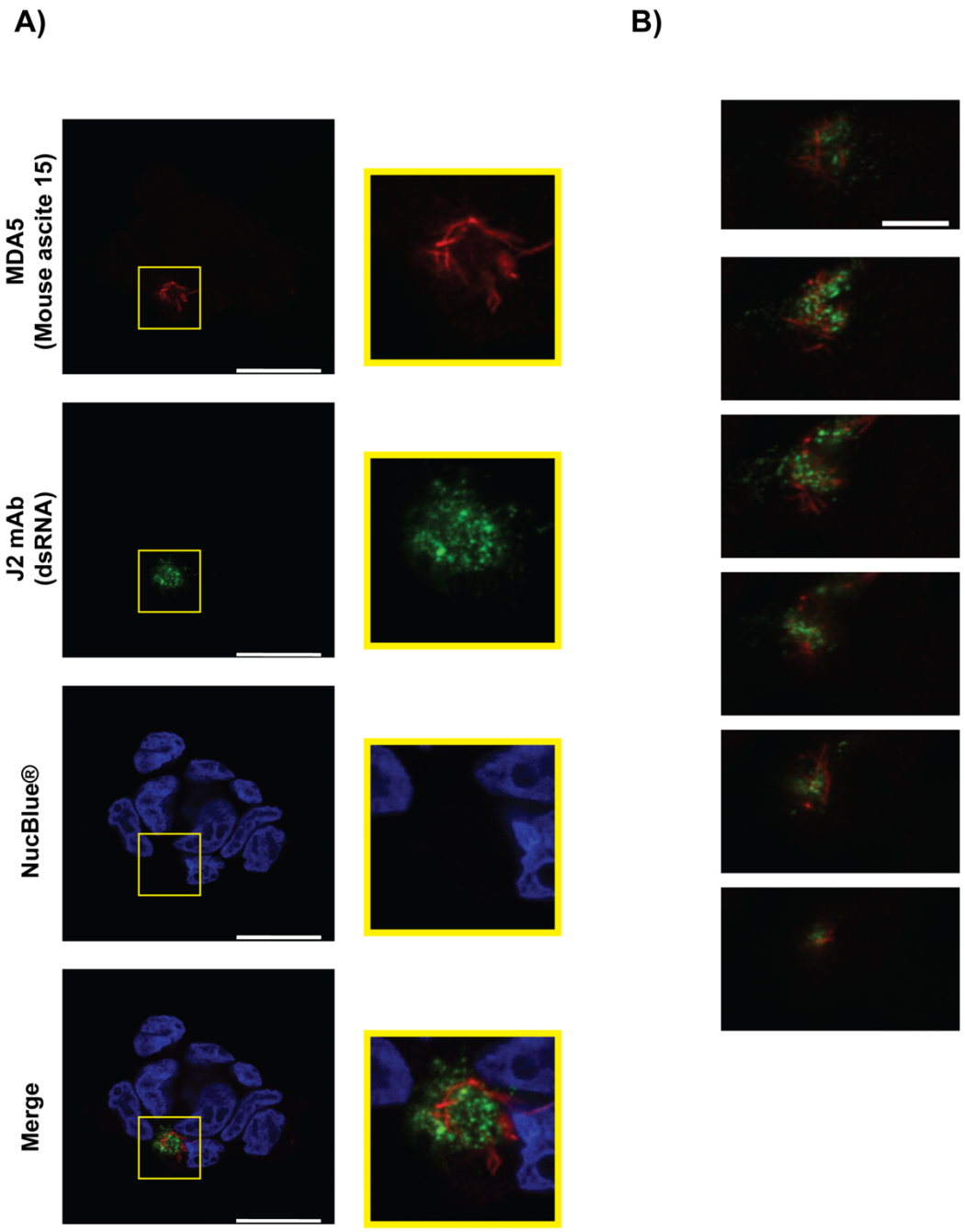


Figure 9 - Co-staining of filaments and dsRNAs in HEK293 cells. A) HEK293 cells were transfected with total RNA from VERO cells infected with EMCV (V-EMCV-RNA) for 24h. Upon fixation, the cells were co-stained with ascite 15 (MDA5) and J2 (dsRNA) monoclonal antibody (mAb). B) Z-stack images throughout a single cell staining for MDA5 and dsRNAs. Bars in “A”: 20µm. Bar in “B”: 5µm. Nuclei are stained in blue. The images are representative of two biological replicates.

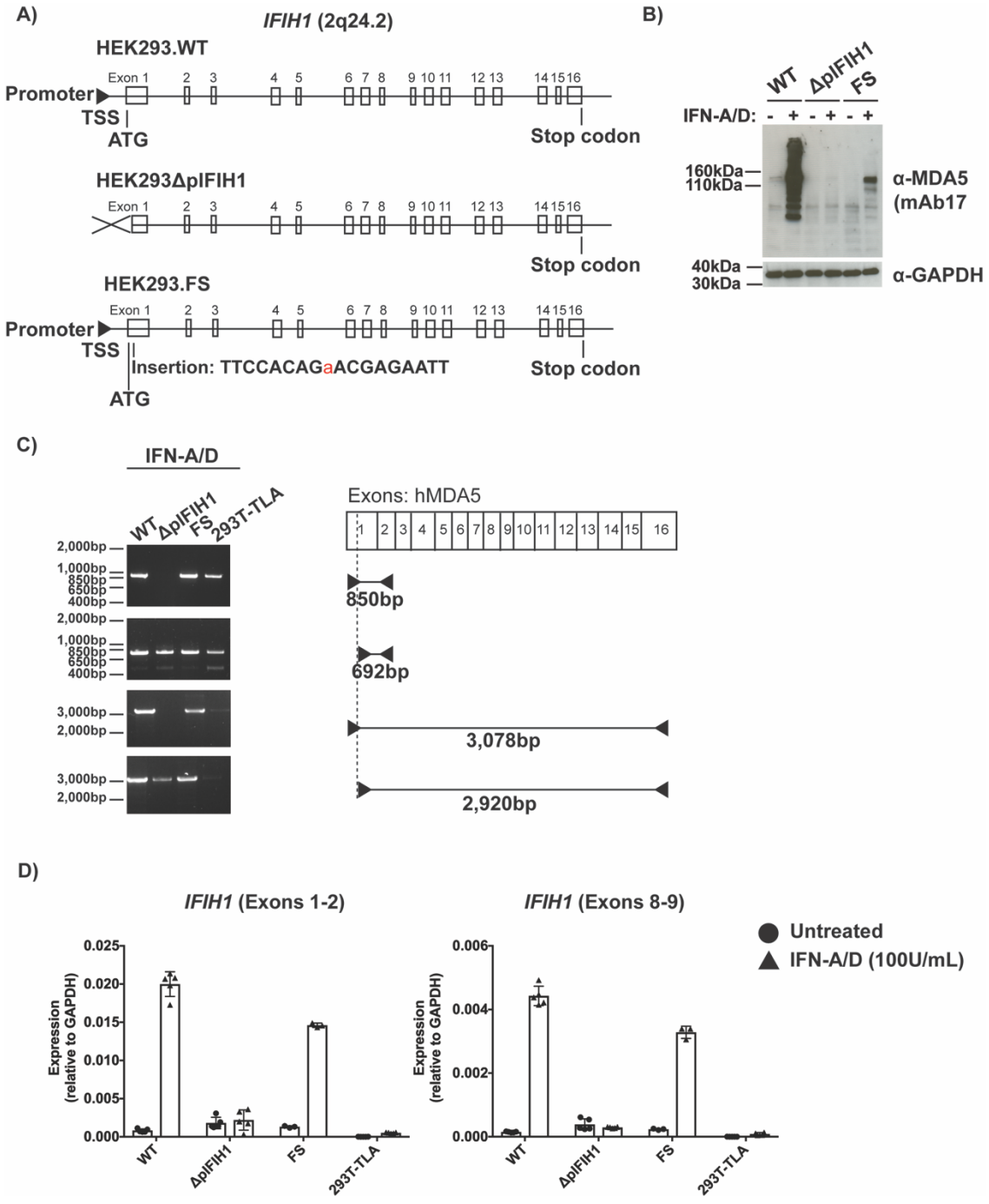


Figure 10 - Generation of HEK293 cells knockout for MDA5. A) HEK293.ΔpIFIH1 MDA5 knockout cell line was generated by deleting the *IFIH1* (MDA5) promoter, including the transcription start site (TSS). Additionally, the first 80 nucleotides downstream to the start codon (ATG) were removed. HEK293.FS cell line was generated by Dr. Alice Mayer by creating a frame shift (FS) due to a nucleotide insertion in the MDA5 coding sequence. B) Western blot for endogenous MDA5 in HEK293 cell lines treated or not with recombinant IFN-A/D. Membranes were probed with a purified MDA5-specific monoclonal antibody, mAb17. C) RT-PCR to detect MDA5 mRNA expression in HEK293 and 293T cell lines treated with recombinant IFN-A/D. Dotted vertical line shows the 3'end of the region deleted in HEK293.ΔpIFIH1. D) RT-qPCR to detect MDA5 mRNA in cells treated or not with recombinant IFN-A/D. qPCR primers were used to detect the junctions of Exons 1-2 or Exons 8-9. Experiments were performed in biological duplicates (B and D) or triplicates (C). Bars in D represent standard deviations (SD) and technical replicates (circle and triangles) are shown. Exceptionally, FS samples (D) represent a biological simplicate with technical triplicate.

I cultured three different hybridoma cell lines and purified MDA5-specific monoclonal antibodies (mAb) from their supernatants. These purified antibodies are here denominated mAb15, 16, and 17 to differentiate them from the non-purified mouse ascites 15, 16, and 17. The purified mAbs and ascites correspond to the same hybridoma cells.

I chose mAb17 to check whether MDA5 expression was abrogated in our KO cell lines by WB (Figure 10B). In WT HEK293 cells, mAb17 detected endogenous levels of MDA5, especially after treatment with recombinant IFN-A/D. This also led to the detection of a smeared band where the primary product runs close to 160kDa (Figure 10B).

As expected, regardless of IFN treatment, an MDA5 band was absent in HEK293.ΔpIFIH1 cell lysates. This suggested MDA5 expression was abrogated in these cells (Figure 10B).

In contrast to this, a band corresponding to MDA5's predicted molecular weight was observed in HEK293.FS cells treated with IFN. This signal was, however, much weaker than in WT cells (Figure 10B). Other two products were detected in both KO systems by mAb17. These bands were unaffected by IFN treatment (Figure 10B).

By deleting the *IFIH1* promoter, we also expected to abrogate expression of MDA5 mRNA. To test this, I treated all cells with IFN-A/D to upregulate MDA5 expression and extracted total RNAs to perform RT-PCR (Reverse Transcription Polymerase Chain Reaction). First, I used primers designed to amplify 850bp spanning the canonical start codon (ATG) located in exon 1 until a random location in exon 2 (Figure 10C).

Total RNAs from WT HEK293 and HEK293.FS amplified a cDNA product, but not HEK293.ΔpIFIH1. This was expected as the canonical start codon was deleted from HEK293.ΔpIFIH1 cells. I then designed a different forward primer to a region not targeted by CRISPR and repeated the RT-PCR. Surprisingly, all samples generated a band of the expected size (692bp) (Figure 10C). These experiments suggested a truncated mRNA for MDA5 might still be expressed in HEK293.ΔpIFIH1 cells.

I repeated the same strategy as described above, but with a new reverse primer designed to target the mRNA stop codon. A similar result was observed: the forward primer located at the canonical start codon amplified a full-length mRNA product in all samples (3,078bp), except in HEK293.ΔpIFIH1. And again, the forward primer designed to a downstream region of the CRISPR deletion also amplified specific cDNA sizes in all samples (2,920bp) (Figure 10C).

I used total RNAs from 293T-TLAs as controls and cDNAs were amplified in all conditions. However, the bands were weaker than for the other cell lines, particularly for the long amplicons (Figure 10C). This suggests MDA5 expression is lower in 293T-TLAs and this was also confirmed by WB (not shown) and quantitative real time PCR (RT-qPCR) (Figure 10D).

I used RT-qPCR as a second strategy to detect MDA5 mRNA in samples treated or not with IFN. These primers were designed to amplify cDNAs from exon junction sites. I used two different pairs of primers (Exons 1-2 and Exons 8-9), which target regions downstream to the CRISPR deleted region.

MDA5 mRNA expression was detected in all samples, including in HEK293.ΔpIFIH1 cells. The expression was enhanced upon IFN treatment in WT and HEK293.FS cells, but not in HEK293.ΔpIFIH1 cells (Figure 10D). In addition,

mRNA levels were reduced if samples were pre-treated with siRNAs (small-interfering RNAs) targeting *IFIH1* in all samples (not shown). The data above suggested two possibilities: a) MDA5 has an alternative promoter; and/or b) possibly an alternative truncated mRNA.

I performed two preliminary experiments to address the second possibility. First, I detected by 5'RACE (Rapid Amplification of cDNA Ends) and sequenced a truncated MDA5 mRNA that is likely 5'capped. I found this product in WT HEK293, HEK293.ΔpIFIH1, and primary human skin fibroblasts cultures (not shown). Second, I designed primers to amplify putative MDA5 truncated mRNAs by primer extension technique. cDNAs were radiolabelled, and a truncated product was readily detectable in all samples tested (not shown).

3.3 VALIDATION OF ANTI-MDA5 ANTIBODIES

As MDA5 was not detected by WB in HEK293.ΔpIFIH1 cells, I used this cell line as a KO system to validate the ascites and purified mAbs we generated.

I tested whether the staining by ascite 15 in IF assays was specific. Mock-transfected cells presented a diffuse staining irrespective of the cell line genotype. I also transfected the synthetic RIG-I ligand, IVT-RNA, to see whether MDA5's distribution would be affected. WT HEK293 cells showed a stronger diffuse signal for MDA5 expression than HEK293.ΔpIFIH1 cells and mock-transfected cells (Figure 11A). This is probably indicative of MDA5 overexpression in WT HEK293 cells upon transfection of IVT-RNA.

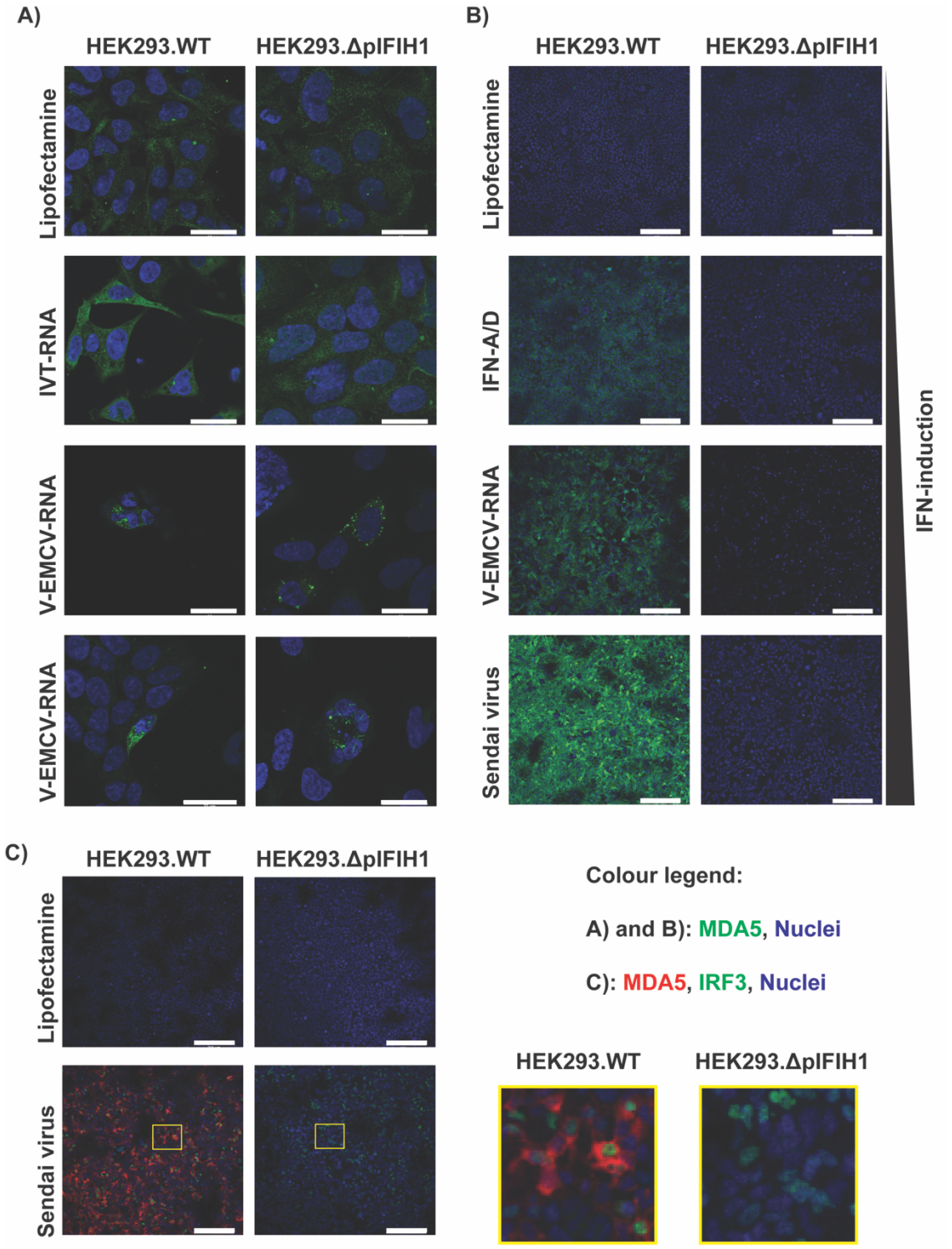


Figure 11 - Validation of anti-MDA5 antibodies in immunofluorescence (IF) assays. MDA5 was stained in wild-type (WT) and knockout (KO: HEK293.ΔpIFIH1) HEK293 cells by IF. Using ascite 15 (A) or purified monoclonal antibody 15 (mAb15) (green in B; red in C). In "C", MDA5 (mAb15) was co-stained with an antibody against IRF3 (green). Right panels show magnifications of the highlighted fields (yellow rectangles). A, B, & C) Cells were treated with different stimuli as indicated: Lipofectamine only, 100U/ml of recombinant IFN-A/D, transfection of *in vitro*-transcribed RNA (IVT) and total RNA of VERO cells infected with EMCV (V-EMCV-RNA), or infection with Sendai virus (moi 1). Images are representative of at least two biological replicates. Bars correspond to 30µm (A) and 200µm (B and C). Nuclei are shown in blue, MDA5 in green (A and B) and red (C), and IRF3 in green (C).

Importantly, transfection of V-EMCV-RNA revealed punctae and filamentous structures in both WT and KO cells (Figure 11A). This suggested non-specificity of ascite 15 (and 16) in IF assays, and thus these structures may not be MDA5 (see discussion below).

I next tested the specificity of the purified mAbs 15, 16, and 17 in IF assays. The mAb17 was not specific as it detected a positive signal in both WT and KO cell lines, which was not enhanced by IFN treatment (not shown).

Results for mAb15 are shown and are similar to mAb16 (not shown). I treated WT and KO cell lines with lipofectamine only or different stimuli to upregulate expression of MDA5 (Figure 11B).

Staining with mAb15 did not detect MDA5 in untreated (lipofectamine) cells. MDA5 was increasingly induced upon treatment with IFN-A/D, transfection of V-EMCV-RNA, and infection with Sendai virus (RIG-I stimulus). In all cases, MDA5 expression was only detected in WT but not in KO cells (Figure 11B). The staining was diffuse in the cytoplasm and did not reveal filaments or punctate structures.

To confirm HEK293.ΔpIFIH1 cells can induce IFN upon RIG-I stimulation (e.g. Sendai virus infection), I co-stained MDA5 (mAb15) and IRF-3 to visualise the induction of the IFN system. Here, I also used a different secondary antibody to detect MDA5 signal to exclude non-specific signal related to possible secondary antibody non-specific binding (Figure 11C).

As previously seen, lipofectamine treatment did not induce MDA5 expression in both cell types. IRF-3 was also not detected. Upon Sendai virus infection, nuclear IRF-3 staining was observed in both WT and KO cell lines. In the same cells, cytoplasmic MDA5 was only seen in WT cells (Figure 11C). This

reveals HEK293.ΔpIFIH1 cells can trigger IRF-3 nuclear accumulation but do not induce MDA5 expression.

Although direct EMCV infection is a weak inducer of IFN I in comparison to transfection of V-EMCV-RNA, I looked into the distribution of MDA5, MAVS, and dsRNAs in cells infected with EMCV or Sendai virus (Figure 12). For these experiments, I also used a modified IF protocol (see methods).

In cells infected with EMCV, MAVS presented a punctate staining and MDA5 showed formation of aggregates. dsRNAs were readily detectable in those cells. In some cells, MDA5, MAVS, and dsRNAs co-stained in the cytoplasm of the same cell (Figure 12A).

Sendai virus infection revealed an expected mitochondrial-like staining for MAVS. MDA5 was diffuse throughout the cytoplasm while dsRNAs were not detected (Figure 12A).

Infection of primary human skin fibroblasts with EMCV or Sendai virus or transfection with V-EMCV-RNA demonstrated a similar pattern as seen in HEK293 cells (Figure 12B). In this case, I only stained for MDA5.

In comparison to lipofectamine-treated cells, Sendai virus infection induced MDA5 expression with diffuse staining throughout the cytoplasm (Figure 12B). Transfection of V-EMCV-RNA mildly upregulated MDA5 and enhanced the presence of aggregated structures. EMCV infection mostly revealed the presence of aggregates. A closer inspection showed punctate structures in EMCV-infected samples. These observations suggested MDA5 localisation is altered in the presence of EMCV RNA.

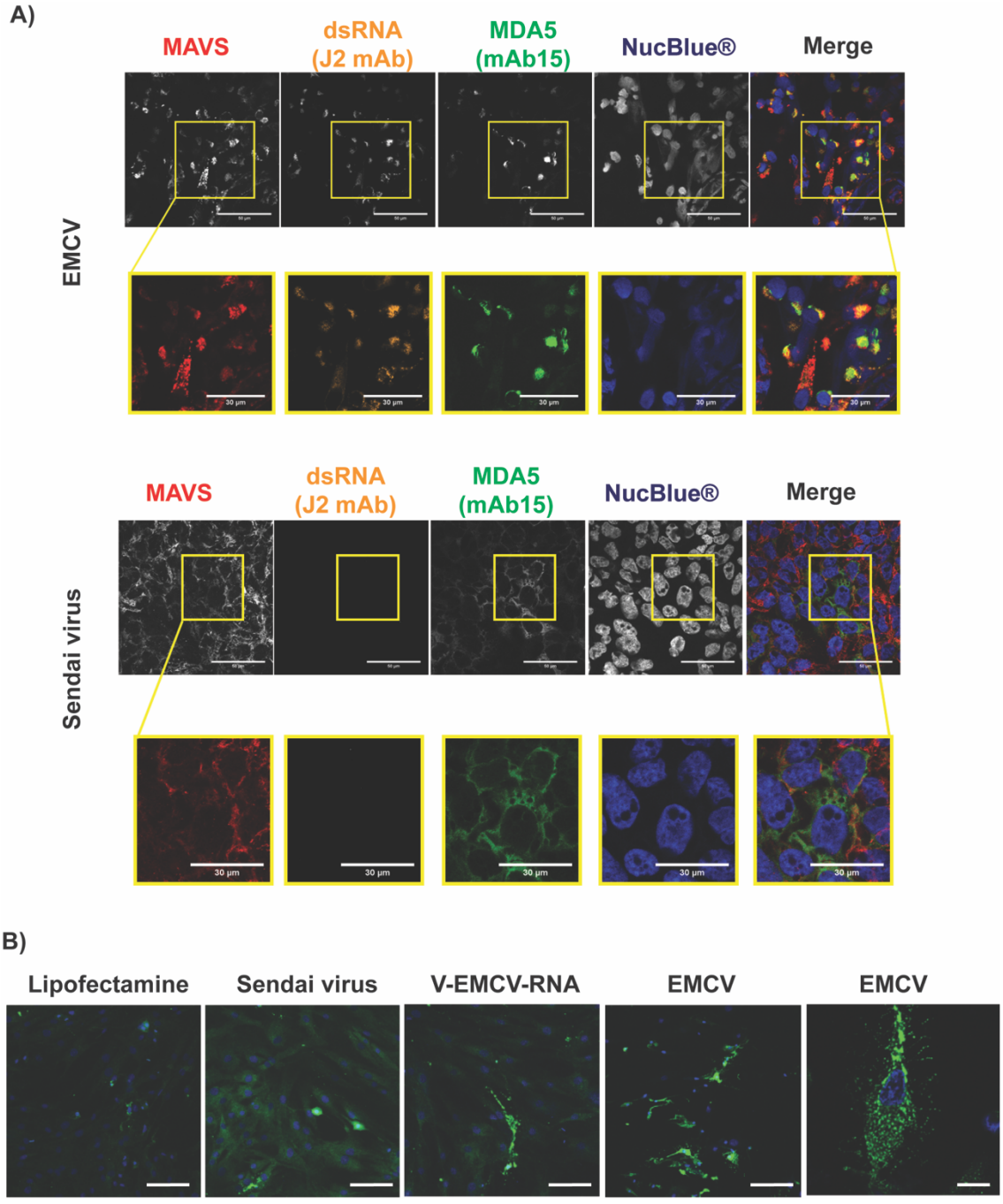


Figure 12 - MDA5 distribution upon viral infection in cell cultures. HEK293 (A) and primary human skin fibroblasts (B) were infected with Sendai virus (moi1) or EMCV (moi1) for 16-24h. Additionally, fibroblasts were transfected with total RNA from VERO cells infected with EMCV (B). Cells were co-stained for MDA5 (mAb15) (A & B), MAVS, dsRNAs, and nuclei (A). Nuclei are shown in blue. Images are representative of two biological replicates. Bars in "A" are 50µm and 30µm (for the magnified images). Bars in "B" are 200µm and 20µm (for the last magnified image).

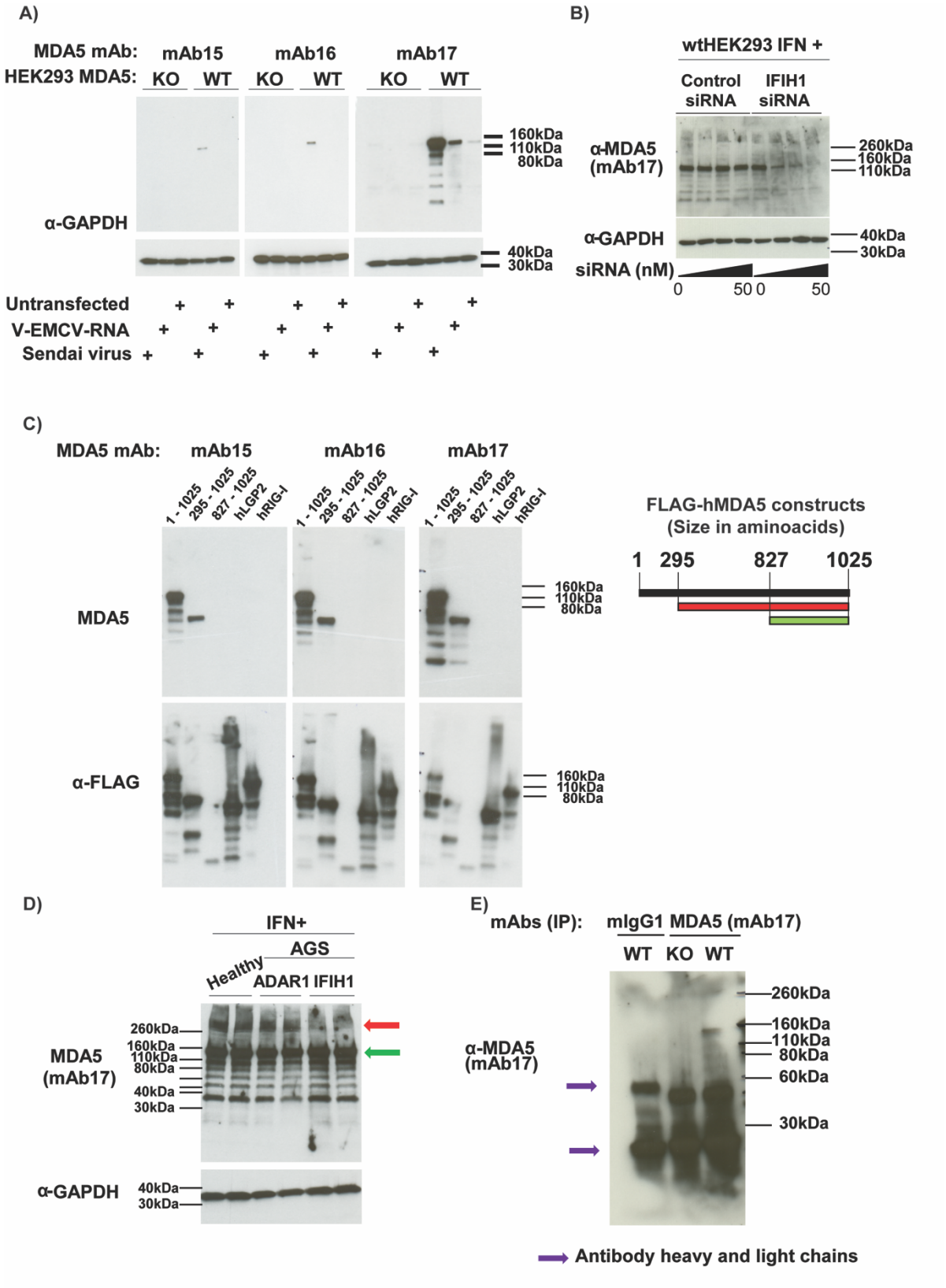

A)
MDA5 mAb:
mAb15
mAb16
mAb17
HEK293 MDA5:
KO
WT
KO
WT
KO
WT
160kDa
110kDa
80kDa
α-GAPDH
40kDa
30kDa
Untransfected
V-EMCV-RNA
Sendai virus
B)
wtHEK293 IFN +
Control siRNA
IFIH1 siRNA
α-MDA5 (mAb17)
260kDa
160kDa
110kDa
α-GAPDH
40kDa
30kDa
siRNA (nM)
0
50
0
50
C)
MDA5 mAb:
mAb15
mAb16
mAb17
1 - 1025
295 - 1025
827 - 1025
hLGP2
hRIG-I
MDA5
α-FLAG
160kDa
110kDa
80kDa
FLAG-hMDA5 constructs
(Size in aminoacids)
1
295
827
1025
D)
IFN+
AGS
Healthy
ADAR1
IFIH1
MDA5 (mAb17)
260kDa
160kDa
110kDa
80kDa
40kDa
30kDa
α-GAPDH
40kDa
30kDa
E)
mAbs (IP):
mIgG1
MDA5 (mAb17)
WT
KO
WT
α-MDA5 (mAb17)
260kDa
160kDa
110kDa
80kDa
60kDa
30kDa
Antibody heavy and light chains

Figure 13 - Validation of purified monoclonal antibodies (mAbs) against human MDA5 by Western Blot (WB). A) HEK293 cells (wild-type, WT, or MDA5 knockout, KO: HEK293.ΔpIFIH1) were left untreated or were transfected with total RNA from VERO cells infected with EMCV (V-EMCV-RNA) or were infected with Sendai virus. Blots were probed with mAbs 15, 16, and 17. B) HEK293 WT cells were treated with small-interfering RNAs (siRNAs) against *IFIH1* (MDA5) or non-target control siRNAs. Membranes were probed with mAb17. C) WT HEK293 cells were transfected with several 3XFLAG-containing constructs: full-length-hMDA5 (1-1025 amino acids, aa), ΔCARD hMDA5 (295-1025aa), CTD MDA5 (827-1025), full-length-hLGP2, and full-length-hRIG-I. Membranes were probed with mAbs 15, 16, 17, and α-FLAG. D) Human skin fibroblasts from two different healthy donors or from patients with Aicardi-Goutieres Syndrome (AGS) were pre-treated with 100 U/ml of IFN-A/D prior to cell lysis. AGS patients contained mutations in *ADAR1* (R892H and I872T) and *IFIH1* (R779H and D393V) genes. Membranes were probed with mAb17. The red arrow indicates a putative post-translationally modified MDA5 protein. The green arrow indicates canonical MDA5. The purple arrows indicate mAb17 heavy and light chains. GAPDH protein was probed as loading control where indicated. A-C experiments were performed in biological triplicates. D and E were performed in biological duplicate.

Next, I validated the specificities of mAbs 15, 16, and 17 by WB (Figure 13). I used cell lysates from WT and KO cell lines that were untreated, transfected with V-EMCV-RNA, or infected with Sendai virus (Figure 13A).

All antibodies showed specificity for MDA5. MAb17 was the most sensitive by also detecting low amounts of MDA5 in non-transfected and non-infected cells. Particularly in cells infected with Sendai virus, several smaller products were observed (Figure 13A). This banding pattern was similar to the one previously seen with several mouse ascites and α-FLAG upon ectopic expression of 3XFLAG-hMDA5 (Figure 7).

The other two mAbs (15 and 16) only detected MDA5 upon Sendai virus infection, probably due to a higher expression of IFN I. They did not detect any proteins in lysates from the KO cell line. mAb17 detected very weak bands approximately to 160kDa and lower to 80kDa in lysates from KO cells (Figure 13A).

To further explore the specificity of mAb17, I transfected increasing amounts of siRNAs against *IFIH1* (MDA5) in WT cells (Figure 13B). The MDA5 signal was much reduced in samples transfected with the highest quantities of

specific siRNAs. A non-specific band - lower than 80kDa - could still be visualised in those blots (Figure 13B).

We generated constructs coding for truncated forms of 3XFLAG-hMDA5 (Figure 13C) and tested which ones could be recognised by these mAbs. I overexpressed these constructs in HEK293 cells and found they were all expressed as detected by the α-FLAG antibody.

All three mAbs detected the full-length (1-1025aa) and the ΔCARD (295-1025aa) MDA5 constructs, but a construct including only the CTD (827-1025aa) was not detected. Interestingly, mAb15 and 16 also detected proteins that migrated faster. These bands may correspond to fragments of MDA5 generated upon overexpression of these constructs. Importantly, none of the mAbs detected full-length 3XFLAG-hLGP2 or 3XFLAG-hRIG-I (Figure 13C).

To test if similar phenotype could be seen in primary cells, I treated primary human skin fibroblasts with recombinant IFN-A/D. I used fibroblasts from healthy donors and from patients with AGS containing different mutations in *ADAR1* or *IFIH1* genes (Figure 13D). As previously observed (Figures 5 and 11A-C), mAb17 detected several other bands migrating faster or slower compared to the canonical MDA5 band (Figure 13D).

I tested these antibodies for their ability to IP MDA5 from HEK293 cells (WT and MDA5 KO) (Figure 13E) and primary human skin fibroblasts in native conditions. All mAbs were able to precipitate MDA5 (see an example for mAb17, Figure 13E).

3.4 DISCUSSION

In this study, we generated a panel of mouse ascites containing anti-human MDA5 antibodies and three purified mAbs (15, 16, and 17) from hybridoma cell lines. Most of them detect ectopically expressed MDA5 by WB, and some antibodies also detect endogenous MDA5, particularly after IFN treatment.

The majority of these antibodies also recognised several alternative products (HMW and low molecular weight, LMW, bands) in a specific manner. Similar findings were found during expression of 3XFLAG-hMDA5 and detection with α-FLAG mAb. These results suggest MDA5 is regulated by post-translational modifications and other mechanisms (e.g. cleavage, alternative translational sites and/or alternative mRNAs).

HMW bands likely correspond to post-translational modifications of MDA5. These were better observed after ectopic expression in HEK293 cells or endogenously in human skin fibroblasts upon Sendai virus infection or IFN-A/D treatment. This suggests that post-translational modification of MDA5 does not necessarily require the introduction of exogenous RNAs in the cell cytosol (e.g. RNA transfection or infection with specific viruses).

Sendai virus infection is not expected to be sensed by MDA5. Therefore, HMW bands found in Sendai virus-infected cells are also likely due to induction of type I IFNs.

In support to this, ectopic expression of MDA5 or IFN-A/D-induced upregulation of the endogenous protein alone were each sufficient to induce the putative post-translational modifications. It is also important to note that ectopic

expression of MDA5 is also known to induce IFN I (for an example, see Figure 16A – Chapter 4).

Given the above, it is interesting to investigate to which extent some of these modifications are dependent on other ISGs and/or RNA ligands (e.g. cytosolic RNAs). A preliminary experiment could involve transfection of 3XFLAG-hMDA5 and blocking of the IFNAR receptor to prevent induction of ISGs.

The protocols used for WB in this study were not optimised to detect post-translational modifications (not aim of this study). This lack of protocol optimisation and the proteome differences between HEK293 and human skin fibroblasts cell cultures could account for the fact HMW bands were more readily detectable in skin fibroblasts.

Using protein lysates from these fibroblasts treated with IFN-A/D, it was possible to co-IP HMW MDA5 proteins containing SUMO1 and ubiquitin chains (not shown).

This is in line with observations from two independent groups showing MDA5 can become sumoylated with SUMO1 chains (Fu *et al.*, 2011; Hu *et al.*, 2017). Both groups suggest this is required for activation of the MDA5 signalling pathway.

In one study, TRIM38 was found to be responsible for MDA5 sumoylation at two different sites (K43 and K865), but not for its polyubiquitination (Hu *et al.*, 2017). Instead, TRIM38 inhibited the ability of MDA5 to become polyubiquitinated. Sumoylation contributed to MDA5 activation by supporting its dephosphorylation and preventing proteasome-mediated degradation (Hu *et al.*, 2017).

The other study suggested that PIAS2β is the E3 ligase responsible for MDA5 sumoylation at one site within its CTD domain. The authors suggested this event is unlikely to affect MDA5 K-48-polyubiquitination and thus might not interfere in MDA5 proteasome-mediated degradation (Fu *et al.*, 2011).

Altogether, more than one E3 ligase has been linked to MDA5 sumoylation. In both cases, sumoylation was required for agonist-mediated responses (Fu *et al.*, 2011; Hu *et al.*, 2017). It is not known, however, whether they act cooperatively and whether they have different outcomes for protein function in different cell types.

Both studies (Fu *et al.*, 2011; Hu *et al.*, 2017) used constructs overexpressing MDA5 in most of their experiments. When detected endogenously, sumoylated MDA5 was co-IPed by indirect means, e.g. TRIM38 endogenous co-IP (Hu *et al.*, 2017). Therefore, the use of antibodies against endogenous MDA5 would be an interesting experiment to further validate these findings.

To this end, the antibodies we generated in the present study also led us to suggest that SUMO1 chains might be attached to MDA5. Therefore, our mAbs could be used to validate MDA5 sumoylation and probably to help to identify, for example, function, E3 ligases, sumoylation sites, and/or size of the chains.

The same applies to other forms of post-translational modifications described for MDA5. MDA5 has been reported to be phosphorylated at different sites which prevents its activation (Wies *et al.*, 2013; Takashima *et al.*, 2015). It is still under investigation which kinases – in addition to RIOK3 (Takashima *et al.*, 2015) - are essential for this process. In sum, MDA5 endogenous co-IP could

further validate these findings and potentially reveal the kinases required for this process.

Furthermore, our preliminary experiments suggested MDA5 was attached to ubiquitin chains. Free (unanchored) K63-polyubiquitin chains were proposed to bind and activate MDA5 (Jiang *et al.*, 2012a). This is an *in vitro* model that suggests MDA5 works as a receptor for free ubiquitin chains and thereby does not require a ubiquitin ligase. Another model suggests its oligomerization through filament formation would be necessary to support signalling (Wu *et al.*, 2013).

These studies were performed in cell-free systems and thus still require further validation in more physiological contexts. Although these data suggest these events would lead to MDA5 signalling, this still need to be confirmed in cells. One could address, for example, the availability of free ubiquitin chains in cells infected with picornaviruses and whether MDA5 precipitates some of these chains. It would be interesting to identify the type of ubiquitination and what its relevance is to the stabilisation of MDA5 oligomers.

In attention to some of these observations, more recently, FLAG-MDA5 was shown to interact with TRIM65 leading to MDA5 K63-polyubiquitination at lysine 743 (Lang *et al.*, 2016). Another study suggested that MDA5 is polyubiquitinated by TRIM65 upon enterovirus infection, and this was required for signalling (Meng *et al.*, 2017).

Importantly, in cell cultures, TRIM65 was shown to regulate MDA5, but not RIG-I or TLRs. *In vivo*, TRIM65 KO mice were more susceptible to and did not induce IFN I upon EMCV challenge (Lang *et al.*, 2016).

Additionally, MDA5 ubiquitination was proposed to stabilise its oligomerization. The authors described the formation of aggregates in HeLa cells

by IF and semi-denaturing agarose gels that were dependent on MDA5 K743 and the presence of TRIM65 (Lang *et al.*, 2016).

The study above has thus identified a role for K63 polyubiquitination-mediated activation of MDA5 dependent on a ubiquitin ligase using both human and mouse systems.

As for HMW bands, α-FLAG mAb and the antibodies generated in our study revealed the presence of LMW bands for MDA5. The appearance of these bands was also more associated to cell responses to type I IFNs rather than the transfection of RNAs or virus infection.

The bands were detectable in both HEK293 and human skin fibroblasts. However, in general, HEK293 cells required often stronger stimuli (e.g. Sendai virus infection or higher levels of IFN-A/D treatment) to facilitate their detection.

I performed co-IP experiments with purified mAb17 of endogenous protein or α-FLAG mAb upon 3XFLAG-hMDA5 expression. After overnight incubation of cleared cell lysates with these antibodies, I was able to recover some of these LMW bands (not shown). Additionally, the detection of the LMW products was specific as they were not detected in MDA5 KO cells.

As mentioned above, I was not able to co-IP all LMW bands observed by WB (not shown). This is likely due to: i) possible altered conformation of MDA5 proteins in native conditions; ii) some of these bands might have lower affinity – or not being recognised - for mAb17 in IP assays, but can be detected by WB in denaturing conditions; iii) MDA5 ligands and/or protein binding partners could potentially block the accessibility of mAb17 to its epitope.

Based on our WB assays (Figure 13C), all the purified mAbs here might bind MDA5 within a region spanning aminoacids 295-827 - part of the helicase

domain. This region is predicted to be in direct contact with dsRNA by adopting a C-shaped structure (Wu *et al.*, 2013).

Hence, it is indeed feasible to conceive that protein conformation could affect accessibility and recognition by the purified mAbs. To explore this further, it is important to identify the actual epitope recognised by these antibodies.

Another unexplored issue that could be of interest for further studies is the nature of these LMW bands. These bands are suggestive of cleavage products, alternative translational start sites and/or alternative mRNAs.

Initially, MDA5 was described as a mouse protein named “HELICARD” (Kovacsovics *et al.*, 2002). The authors described a 45kDa cleavage product found in several mouse tissues and upon overexpression in 293T cells. Cells treated with FasL or TRAIL to induce apoptosis generated three more products of 41, 30, 28kDa. In addition, a 120kDa product was observed in a mouse lymphoma cell line (Kovacsovics *et al.*, 2002).

These proteins were found to be products of caspase 3 and 8 cleavage. Caspase 8 was responsible for the generation of the products of 30 and 28kDa, while caspase 3 generated the 41kDa band. All these bands were predicted to contain the CARD domain as they were detected by an antibody against this domain (Kovacsovics *et al.*, 2002).

The authors then generated three constructs and overexpressed them individually in 293T cells to check for their cellular localisation. The full-length and CARD (1-278aa) constructs located in the cytoplasm, while the ΔCARD (252-1025aa) construct located to the nucleus. The latter was shown to accelerate DNA fragmentation in cells treated with FasL (Kovacsovics *et al.*, 2002).

Human MDA5 was also found to be cleaved in cells infected with viruses (Barral *et al.*, 2007). In this study, the authors used a rabbit polyclonal antibody raised against the first 335aa of the MDA5 protein. HeLa cells were treated with HMW poly I:C to trigger MDA5 and hours later were infected with poliovirus (*Enterovirus*, *Picornarviridae*). The authors observed poliovirus infection induces PARP cleavage (a hallmark of apoptosis) and enhances MDA5 cleavage in a caspase and proteasome-dependent manner (Barral *et al.*, 2007).

Employing the same antibody used above, another study showed that MDA5 could be cleaved upon infection with enteroviruses independent of caspases and the proteasome. In this study, the cells were not primed with IFN I or MDA5 agonist prior to infection. Instead, untreated cells were infected with enteroviruses (e.g. CVB3) at a very high moi and MDA5 was found to be cleaved by the viral protease $2A^{pro}$ (Feng *et al.*, 2014).

Our results demonstrate that putative MDA5 cleavage products can be detected after exposure of cells to several stimuli, including IFN-A/D treatment. Although we have not investigated this further, our data suggest mechanisms by which MDA5 can be cleaved in the absence of virus infection as described above. In support to this, MDA5 has also been described to be K48-ubiquitinated by RNF125 and targeted for proteasomal degradation (Arimoto *et al.*, 2007).

The mechanisms by which human MDA5 can be cleaved by cellular caspases and degraded by the proteasome remains to be elucidated. How many products are generated and what are their roles? Could these products modulate the induction of antiviral IFNs and contribute to apoptosis of infected cells? It is important to investigate the physiological context (including cell types) of these

putative cleavage products as well as their possible relationships with cell death pathways.

MAVS has been shown to form rod-shaped prion-like fibrils on mitochondria (Hou *et al.*, 2011; Xu *et al.*, 2014). These structures can activate other MAVS molecules and are essential to trigger antiviral cytokines (Hou *et al.*, 2011). MAVS is also targeted to degradation, for example, by RNF125 and MARCH5 (Arimoto *et al.*, 2007; Yoo *et al.*, 2015).

Jonathan Kagan's group reported a new mechanism by which MAVS activation can also be controlled (Brubaker *et al.*, 2014). His group performed ribosome profiling and reported that the MAVS mRNA is polycistronic. This means the mRNA contains alternative start codons. Indeed, they identified that the MAVS mRNA contain a methionine at position 142 and thus generates a truncated protein (50kDa), miniMAVS. They found miniMAVS to be a negative regulator of full-length MAVS-mediated activation of type I IFNs (Brubaker *et al.*, 2014).

More recently, these findings were extended by another group (Qi *et al.*, 2017). This group generated three antibodies to target MAVS at its N-terminus, middle region, and C-terminus. They identified MAVS produced six different products, including its canonical full-length protein. Indeed, it was found MAVS contains six distinct methionines (M1/142/303/358/367/449) (Qi *et al.*, 2017).

The authors demonstrated that all truncated forms of MAVS, namely M2 to M6, had inhibitory effects on the activation of the type I IFN signalling pathway. These truncated forms inhibited MAVS prion-like aggregation. This was described as a mechanism to prevent and control MAVS activation (Qi *et al.*, 2017).

Interestingly, the *IFIH1* (MDA5) gene was also predicted to be polycistronic, and at least two truncated products were predicted by ribosomal profiling experiments (Brubaker *et al.*, 2014).

Here, our antibodies detected several truncated forms of MDA5 that could correspond to alternative translated products. I cloned two of these predicted truncated forms of MDA5 and co-expressed with the full-length protein. I did not find evidence of blockage of MDA5-mediated IFN induction (not shown). More experiments are, however, needed to rule out this possibility as it seems practical to speculate truncated proteins can block the aggregation of filament-prone proteins, such as MAVS and MDA5.

Another mechanism by which RLR signalling can be negatively regulated is by alternative splice variants. A RIG-I splice variant was found to have an internal deletion (36-80aa) within its CARD1 domain. This affects binding of TRIM25 and thus K63-polyubiquitination-mediated activation. In turn, this internally truncated protein was found to inhibit full-length RIG-I IFN-mediated antiviral activity (Gack *et al.*, 2008).

To the best of my knowledge, a similar mechanism has never been proposed for MDA5. Here, we deleted the entire *IFIH1* promoter plus several of the first aa of MDA5 CARD1 domain using CRISPR/Cas9 technique (Figure 10). Surprisingly, we found a truncated mRNA can still be detected. This strongly suggests *IFIH1* has an alternative promoter that is not IFN-inducible.

The presence of this mRNA was verified with several primers for RT-PCR and RT-qPCR (Figure 10). WB analysis with purified mAb17 further demonstrated no protein signal was enhanced (or detected) upon IFN-A/D

stimulation in HEK293.pΔIFIH1 cells (Figure 10B). Yet, at high concentrations of protein lysates (Figure 10B), two weak bands were observed in WB with mAb17.

If confirmed, our initial results from 5'RACE and primer extension experiments would indicate MDA5 has an alternative mRNA that is potentially 5'capped and thus could be translated. I cloned an MDA5 containing a truncated CARD1 domain based on our CRISPR strategy and existence of a downstream methionine. This construct was unable to induce IFN upon overexpression (not shown).

Additionally, an IFN-inducible protein was detected in the HEK293.FS MDA5 KO system. In this case, a nucleotide insertion was expected to lead to mRNA degradation of the full-length protein. Therefore, I suggest this cell line can also be exploited to investigate the existence of putative alternative mRNAs and/or alternative translation products for human MDA5.

Once the existence of other forms of MDA5 is validated, it will be relevant to investigate: i) their ability to modulate canonical MDA5 activation; ii) contribute to cell-death related pathways; iii) restrict cell growth in cancer and viral infections; iv) generate filaments on dsRNAs with or without IFN-independent direct effector-like functions.

Given all the above, it is tempting to speculate a model for MDA5 activation and control: upon recognition of an RNA agonist, MDA5 is activated following conformational change. This requires dephosphorylation, sumoylation, and K63-polyubiquitination. K63-polyubiquitination stabilises MDA5 oligomer formation leading to MAVS activation and IFN I induction. IFN I induces ISGs, including MDA5. Upregulation of MDA5 mRNA(s) and protein lead to the generation of several truncated MDA5 products. These products may interfere in MDA5

oligomerisation as well as compete for RNA ligands and K63-polyubiquitination. Concomitantly, caspase–mediated cleavage and K48-mediated proteasomal degradation terminate MDA5 induction. Some cleavage products may modulate mechanisms of cell death and, alongside with the effects of type I IFN, may interfere with cell growth mechanisms.

This model lacks the subcellular localisation and signalling platform for MDA5. Some studies have investigated the roles of stress granules as the signalling platform for RLRs (Langereis, Feng and van Kuppeveld, 2013; Ng *et al.*, 2013). However, this is an interesting open question that was not tested in this study.

In addition, it is believed MDA5 can potentially signal from MAVS localised in mitochondria, MAMs, and peroxisomes (Odendall *et al.*, 2014; Bender *et al.*, 2015). The contribution and dynamics of each of these signalling platforms are yet to be further clarified.

The physiological ligand for MDA5 still remains to be identified. It would be a revealing finding to validate whether MDA5 indeed binds to long dsRNA in cells. This is important as the current concept is that MDA5 forms long filaments along dsRNAs and these probably have the ability to trigger type I IFNs and/or antiviral effector-like functions (Peisley *et al.*, 2011, 2012; Berke *et al.*, 2012; Wu *et al.*, 2013; Yao *et al.*, 2015; Meng *et al.*, 2017). Evidence for such filaments was, however, never found in another system than cell-free systems.

Here, non-purified mouse ascites raised against human MDA5 detected bright punctae and filamentous structures in HEK293 cells transfected with V-EMCV-RNA. Another MDA5 stimulus (HMW poly I:C), and RIG-I stimuli failed to show similar structures. As transfection of V-EMCV-RNA leads to viral

replication, the appearance and detection of filaments may be detectable at certain time points. This would not be the case for a non-replicative system such as HMW poly I:C. *In situ* hybridisation assays could contribute to identify whether EMCV-RNAs can be found as filamentous structures.

Within the same cells presenting these structures, dsRNAs were co-detected by J2 mAb. Co-localisation was not observed. This may be explained due to protection of these RNAs by MDA5 filaments.

Importantly, the same structures were detected in HEK293.pΔIFIH1 MDA5 KO cells. HEK293.FS cells were not tested. Additionally, purified mAb 15 (and 16) was never able to detect filaments. 3XFLAG-hMDA5 or a similar construct (e.g. HALO-hMDA5) also do not form filaments in fixed samples or live-cell imaging, respectively. Collectively, this suggests non-purified ascite 15 contains non-specific antibodies that detect a protein other than MDA5.

If later proven that HEK293.pΔIFIH1 cells contain a translatable truncated MDA5 mRNA, the conclusion above will need to be revisited. Furthermore, siRNAs against MDA5 could also provide additional evidence whether these filaments could correspond to a truncated MDA5 protein.

The bright punctae and filaments do not seem to represent upregulation of MDA5 (or another protein). They probably indicate relocalisation of a diffusively distributed protein that accumulates around specific sites.

This idea was based on analysis of IF staining with ascite 15 and purified mAb15. Ascite 15 showed a clear upregulation of MDA5 after transfection of the artificial RIG-I agonist IVT-RNA in WT HEK293 cells, but not in MDA5 KO cells (Figure 11A). In the latter case, the staining remains weak and diffuse in mock-treated and IVT-RNA transfected cells. However, transfection of V-EMCV-RNA

into both cell systems leads to bright foci, but the diffuse background remains low.

Purified mAb 15 (and 16) were specific in detecting MDA5. They did not detect MDA5 in untreated cells (Figure 11B). This is in line with WBs probed with mAb17 that shows MDA5 expression is very low or undetectable in untreated lysates (Figure 13). IF staining with mAb15 showed upregulation of MDA5 upon stimulation of RLR signalling or IFN-A/D treatment as expected (Figure 11B).

IF staining with mAb15, however, revealed a diffuse cytoplasmic staining even in the presence of MDA5 ligands. Upon modifications on the IF staining protocol (yet to be validated in MDA5 KO system), some aggregates could be visualised in HEK293 cells upon V-EMCV-RNA transfection and EMCV infection.

Interestingly, a polyclonal antibody against MAVS showed a considerable modification in MAVS's morphology from mitochondria-like (Sendai virus-infected cells) to punctate structures (EMCV-infected cells). It is important to take into account that EMCV is cytotoxic and may lead to cellular modifications due to cell death or other related pathways. Also, MAVS staining remains to be validated by a MAVS KO cell line system.

Staining of primary human skin fibroblasts with mAb15 also showed reduced detection of MDA5 in untreated/uninfected cells. Upon Sendai virus infection, MDA5 was highly upregulated and was found diffusely throughout the cytoplasm. Upon transfection of V-EMCV-RNA, the staining revealed an increase in the appearance of aggregates and a diffuse staining. The aggregate-type staining overtook the diffuse staining after direct EMCV infection (Figure 12).

Given the above, a possible interpretation is that a diffuse staining for MDA5 represents upregulation of the protein after IFN I expression. The

aggregates may represent relocalisation of MDA5 to sites potentially containing RNA ligands. In support of this view, HEK293 cells infected with EMCV revealed several cells co-staining for MDA5 aggregates, morphologically-altered MAVS, and dsRNAs.

MDA5 subcellular localisation can potentially be explored with purified mAb15. For such, a careful optimisation must be envisaged alongside with live-cell imaging. For the latter, it is important to observe that N-terminally or C-terminally tagged constructs (tagged CARD or CTD domains, respectively) may not corroborate with mAb15 staining in fixed samples.

The issue is further complicated by the possibility this antibody detects alternative forms of human MDA5 which could lead to misinterpretation of which MDA5 species form certain structures.

In sum, we generated several mouse ascites and purified mAbs that can detect human MDA5. WB suggested that MDA5 undergoes post-translational modifications and generation of LMW products. The specificity of these findings is corroborated by an MDA5 KO cell line and siRNAs. This cell line also suggested the existence of an alternative IFN-independent promoter for *IFIH1*. Finally, the purified mAbs can be used in IF assays to detect MDA5 structures and their localisation formed during EMCV infection.

CHAPTER 4

4 DEVELOPMENT AND OPTIMISATION OF TECHNIQUES TO IDENTIFY AND CHARACTERISE MDA5 RNA LIGANDS

MDA5 was discovered in 2002 in human and mouse as an ISG with ATPase activity upon binding dsRNAs *in vitro* (Kang *et al.*, 2002; Kovacsovics *et al.*, 2002). Later, MDA5 was found to protect mice from infection with long dsRNA-generating viruses, such as picornaviruses (Gitlin *et al.*, 2006; Kato *et al.*, 2006).

Cell-free systems have shown MDA5 binds to the dsRNA phosphate backbone by forming a C-shaped ring (Wu *et al.*, 2013). This binding triggers monomers to oligomerize in a head-to-tail fashion. This results in MDA5 filaments along these dsRNAs. Longer dsRNAs tend to stabilise these filaments by decreasing MDA5 ATPase-dependent dissociation (Peisley *et al.*, 2011, 2012; Berke *et al.*, 2012; Wu *et al.*, 2013).

Transfection of synthetic HMW poly I:C, a mimic of long dsRNA, into cultured cells triggers IFN I in an MDA5-mediated manner (Gitlin *et al.*, 2006; Kato *et al.*, 2008). This is also the case for transfection of total RNAs from cells infected with picornaviruses, such as V-EMCV-RNA (Pichlmair *et al.*, 2009; Feng *et al.*, 2012; Jiang *et al.*, 2012a).

As mentioned above, replication of picornaviruses generates long dsRNAs, called replicative forms. These HMW RNAs can be isolated and purified from infected cells. Transfection of these purified products also leads to MDA5-

mediated IFN responses. Finally, MDA5 has ATPase activity upon binding to these purified replicative forms (Feng *et al.*, 2012).

These studies have led to the assumption that the MDA5 PAMP could be any long dsRNA species independently of its sequence. However, direct evidence from living cells demonstrating direct interactions between MDA5 and RNA ligands is missing.

Furthermore, it was shown that transfection of purified RNA species from EMCV-infected cells triggers MDA5 (Pichlmair *et al.*, 2009). This activation was dependent on higher-order HMW RNA species (a mix of ssRNAs and dsRNAs), but not ssRNAs or dsRNAs alone. Importantly, the authors pre-treated the cells with ribavirin to prevent EMCV replication and, thus possibly, the generation of replication by-products (Pichlmair *et al.*, 2009).

Native IP of human LGP2 from cells infected with EMCV co-purified a short ssRNA species that triggers MDA5 (Deddouche *et al.*, 2014). In a different study, PAR-CLIP experiments showed that MDA5 binds to ssRNAs in Mev-infected cells (Runge *et al.*, 2014). It is noteworthy that both co-IP studies did not define a specific PAMP for MDA5.

In addition to virus-derived RNA species, MDA5 is also believed to recognise cellular RNAs. Indeed, MDA5 is thought to sense: i) RNA from endogenous retroviruses during cancer treatment with DNA-demethylating agents (Chiappinelli *et al.*, 2015; Roulois *et al.*, 2015); ii) inverted Alu repeats in the context of the autoinflammatory disease AGS and in *ADAR1* KO mice (Rice *et al.*, 2012, 2014; Liddicoat *et al.*, 2015; Pestal *et al.*, 2015); iii) cellular and/or viral RNAs in the autoimmune disease T1D (Smyth *et al.*, 2006; Nejentsev *et al.*, 2009; Looney *et al.*, 2015; Gorman *et al.*, 2017).

These studies lack experimental evidence of which RNA species are directly bound by MDA5. MDA5-RNA co-IP has been considered challenging and, as such, there is currently no technique available to confidently precipitate RNAs bound by MDA5.

In an attempt to stabilise protein-RNA interactions, PAR-CLIP was used to co-IP RNAs associated with MDA5 (Runge *et al.*, 2014). PAR-CLIP involves the addition of 4-thiouridine to allow protein-RNA crosslinking with UV-C light. However, this method introduces a crosslinking bias towards uridine bases. Furthermore, this process induces cell toxicity and has a lower bioinformatics resolution than other available methods (Huppertz *et al.*, 2014).

iCLIP was demonstrated to overcome these issues and was shown to provide protein binding sites at single nucleotide resolution (e.g., Huppertz *et al.*, 2014). Here, we aimed at applying the iCLIP method to MDA5 to firstly demonstrate that MDA5 indeed binds RNAs, and secondly to sequence MDA5-associated RNAs. Thereafter, we developed a bioassay to verify whether cellular RNAs have the potential to trigger IFN I in an MDA5-dependent manner.

4.1 OPTIMISATION OF INDIVIDUAL-NUCLEOTIDE RESOLUTION UV CROSSLINKING AND IMMUNOPRECIPITATION (iCLIP) FOR HUMAN MDA5

Native protein-RNA co-IPs have been successful for some RLRs, such as RIG-I and LGP2 (Rehwinkel *et al.*, 2010b; Deddouche *et al.*, 2014; Goubau *et al.*, 2014) . Here, I attempted to use a similar protocol to precipitate MDA5 ligands. I used purified mAb17 for the endogenous MDA5 protein or α-FLAG antibody for cells overexpressing 3X-FLAG-hMDA5. In both cases, IPs failed to

precipitate MDA5 immunostimulatory RNAs in both mock- and EMCV-infected cells (not shown).

Considering MDA5-RNA interactions are likely to be dynamic, we reasoned UV-crosslinking could facilitate the precipitation of MDA5-associated RNAs. We therefore next tested the iCLIP technique (Huppertz *et al.*, 2014).

We used the commercial α-FLAG mAb for all experiments described here. We intended to optimise and validate an iCLIP protocol to be later used for endogenous MDA5 using one of the mAbs generated in this study.

I used 293T-TLA cells to overexpress 3XFLAG-hMDA5 as they expressed the lowest levels of endogenous MDA5 among the cell lines I have tested (Figure 10C, D). These cells also provided a better transfection efficiency with the lower amounts of plasmid in comparison to HEK293 (not shown).

Next, I transfected cells and left them uninfected or infected with EMCV (moi 0.1) for 16-24 hours. After this incubation time, cells were UV-crosslinked or not (mock) (Figure 14A).

We then optimised the IP protocol to test whether an RNA species is bound to MDA5. Figure 14A illustrates the steps from UV-crosslinking until RNA radiolabelling with radioactive γ-32^{P}-ATP.

Importantly, after UV-crosslinking, the cells were lysed in RIPA buffer and treated with RNAse A (Figure 14A). RNase A cleaves ssRNAs and dsRNA stretches that are not protected by bound protein. Its cleavage also generates RNAs with 5'OH and 3'P ends (Huppertz *et al.*, 2014).

RNAse A was inactivated and lysates were cleared. After this stage, MDA5 was IPed with α-FLAG mAb in two separate co-IP rounds (Huppertz *et al.*, 2014). After the first co-IP was performed, bound fractions were treated with a

6M Urea Cracking Buffer (Table 5) to disrupt possible interactions of MDA5 with other protein binding partners. A second IP was then executed to rescue and enrich for MDA5-RNA complexes (Figure 14B).

This protocol was able to IP MDA5 protein as shown by WB (Figure 14B, C). RNA 3'P ends were then dephosphorylated to ligate a pre-adenylated adaptor (Figure 14A). (These adaptors were only ligated in experiments aiming to prepare RNA libraries for Illumina Sequencing.)

To visualise RNAs possibly associated to MDA5, I radiolabelled the RNAs 5'OH ends with γ-32^{P}-ATP (Figure 14A, C). This involves a reaction in the presence of PNK. This enzyme was omitted in one reaction designated as negative control. Another negative control was the use of non-UV crosslinked samples in the presence of PNK (Figure 14C).

Using the samples and negative controls described above, I observed MDA5 protein was IPed in all conditions (Figure 14C). RNAs were only detected in samples that were UV-crosslinked and incubated with the PNK enzyme. Interestingly, I detected RNAs associated with MDA5 in either the presence or absence of EMCV infection (Figure 14C, D). This data shows that ectopically expressed MDA5 binds to cellular and, probably, viral RNAs.

To further validate the specificity of this protocol, I introduced an additional negative control. I transfected separate cells with HA-hMDA5 and used α-FLAG mAb for IP. WB confirmed the expression of 3XFLAG-hMDA5 and HA-hMDA5 (see Input, Figure 14D). After the IP, only 3XFLAG-hMDA5 was detected in the bound fractions.

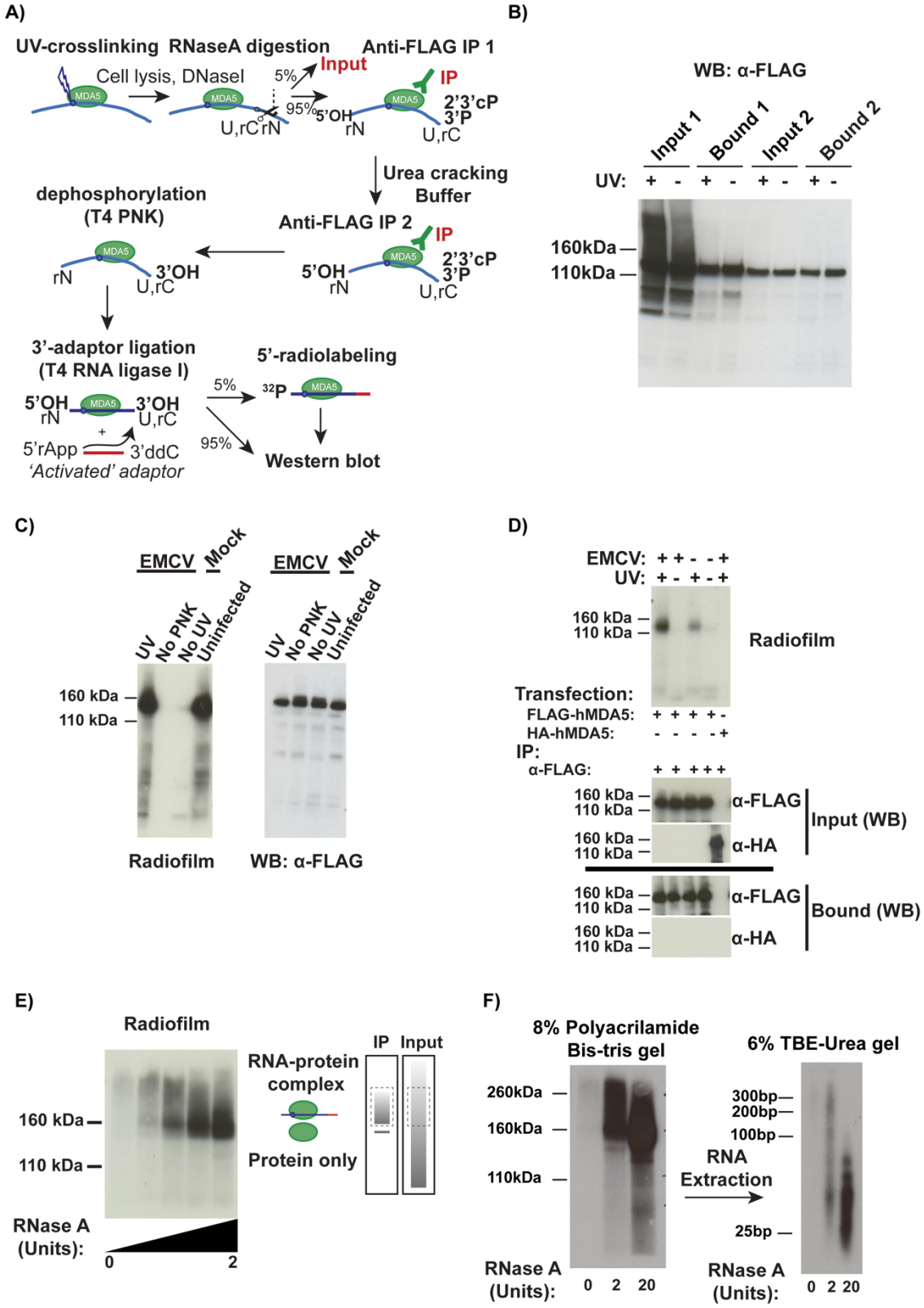


Figure 14 - Co-immunoprecipitation (co-IP) of RNAs associated with human MDA5. A) A diagram summarises the steps to perform MDA5-RNA co-IP. In sum, 293T-TLA cells were transfected with 3XFLAG-hMDA5 and (un)infected (EMCV) cells were mock or UV-crosslinked. After cell lysis, samples were treated with RNAse A following by lysate clearing and α-FLAG IP. Urea cracking buffer containing 6M urea was used to disrupt potential protein binding partners. 3XFLAG-hMDA5 was rescued with a second round of α-FLAG IP. RNAs associated to MDA5 were dephosphorylated and a pre-adenylated adaptor was ligated to their 3' ends for future

sequencing. For visualisation of RNAs bound by MDA5, radioactive (32P)ATP was ligated to the RNAs 5'-OH ends with aid of T4 polynucleotide kinase (PNK). B) MDA5 protein was detected by Western Blot (WB). The input and bound fractions of both rounds of α-FLAG IP are indicated as described in "A". C) RNAs (radiofilm) and proteins (WB) were detected in samples infected or not with EMCV. Two negative controls were used: i) samples radiolabelled with (32P)ATP in the absence of the enzyme PNK; ii) samples that were mock UV-crosslinked. D) Similar as in "C", but an HA-tagged MDA5 was used as additional negative control. E) RNase A was titrated as indicated. A scheme was drawn in the right to indicate at high RNase A concentrations, a band corresponding to MDA5 runs on a polyacrylamide gel at the expected size. However, MDA5-RNA interactions form higher molecular weight complexes at low concentrations of RNase A. F) As described in "E", different concentrations of RNase A were used. A band shift is seen at low RNase A concentrations. Proteins were digested with Proteinase K and RNAs were purified with Phenol-Chloroform extraction. Purified RNAs were run on a TBE-Urea gel and different sizes could be seen according to the concentration (20: high/ 2: low) of RNAse A was used. All experiments were performed at least in biological duplicates. The schemes in "A" and in "E (right scheme)" were provided by Dr. Jonathan Maelfait and were originally based on Huppertz *et al.*, 2014

Furthermore, radioactively labelled RNAs were only detected in samples after UV-crosslinking and with 3XFLAG-hMDA5, but not with HA-hMDA5 (Figure 14D). Hence, MDA5 α-FLAG co-IP was demonstrated to be specific and generated low or undetectable background.

The treatment of cell lysates with high amounts of RNAse A was previously shown to shorten crosslinked RNAs to short protein-protected fragments (Huppertz *et al.*, 2014). Indeed, the band on the radiofilm runs close to the expected molecular weight of MDA5 (Figures 12C, D).

Decreasing concentrations of RNase A are expected to produce RNAs of different sizes. Longer RNAs increase the molecular weight of protein-RNA complexes that will migrate in polyacrylamide gels as HMW products (band super shifts) (Huppertz *et al.*, 2014).

Based on this, I performed an RNase A titration experiment to reveal whether MDA5-RNA complexes can form HMW bands (Figure 14E, F). Indeed, I observed a band super shift for MDA5 with decreasing amounts of RNase A (Figure 14E, F). Samples lacking RNAse A treatment did not show a signal for radioactive RNA (Figure 14E, F). This is probably due to the lack of generation

of RNA substrates for PNK-mediated radiolabelling and/or HMW products that did not migrate in the gels. Hence, these experiments showed that MDA5 has the ability to bind RNA.

I further validated that MDA5 was associated with RNAs in samples treated with low concentrations of RNase A. I extracted the RNAs bound by MDA5 and, as expected, I observed short-sized RNAs in samples with high concentrations of RNAse A and longer RNAs when RNase A was used at lower concentrations (Figure 14F). Altogether, these data reveal that MDA5 can form complexes in association with RNA.

Importantly, to achieve success with this protocol and its controls, the double co-IP containing the Urea Cracking Buffer step was essential. Initial experiments lacking the Urea Cracking Buffer and the second co-IP steps led to the detection of putative non-specific products (Figure 15A, B). For example, the first co-IP alone revealed the presence of other bands in the radioactive (RNA) exposure film (Figure 15A, B). This finding suggested the presence of a possible contaminating RNA-binding protein.

32p-labelled RNAs were detected after the first co-IP even in non-UV crosslinked samples (Figure 15A). These were considered non-specific signals as they were also present in samples lacking the PNK enzyme during the radiolabelling step (Figure 15B).

All these issues were, however, addressed after the introduction of more stringent co-IP conditions (Urea Cracking Buffer step) followed by a second co-IP (Figure 14).

After confirming the presence of RNAs associated to 3XFLAG-hMDA5 (Figure 14E, F), I repeated this experiment and added an adaptor to the 3'end of

these RNAs (Figure 14A). After RNA purification, I performed an RT step, based on these adaptor sequences, to generate cDNAs (Figure 15C).

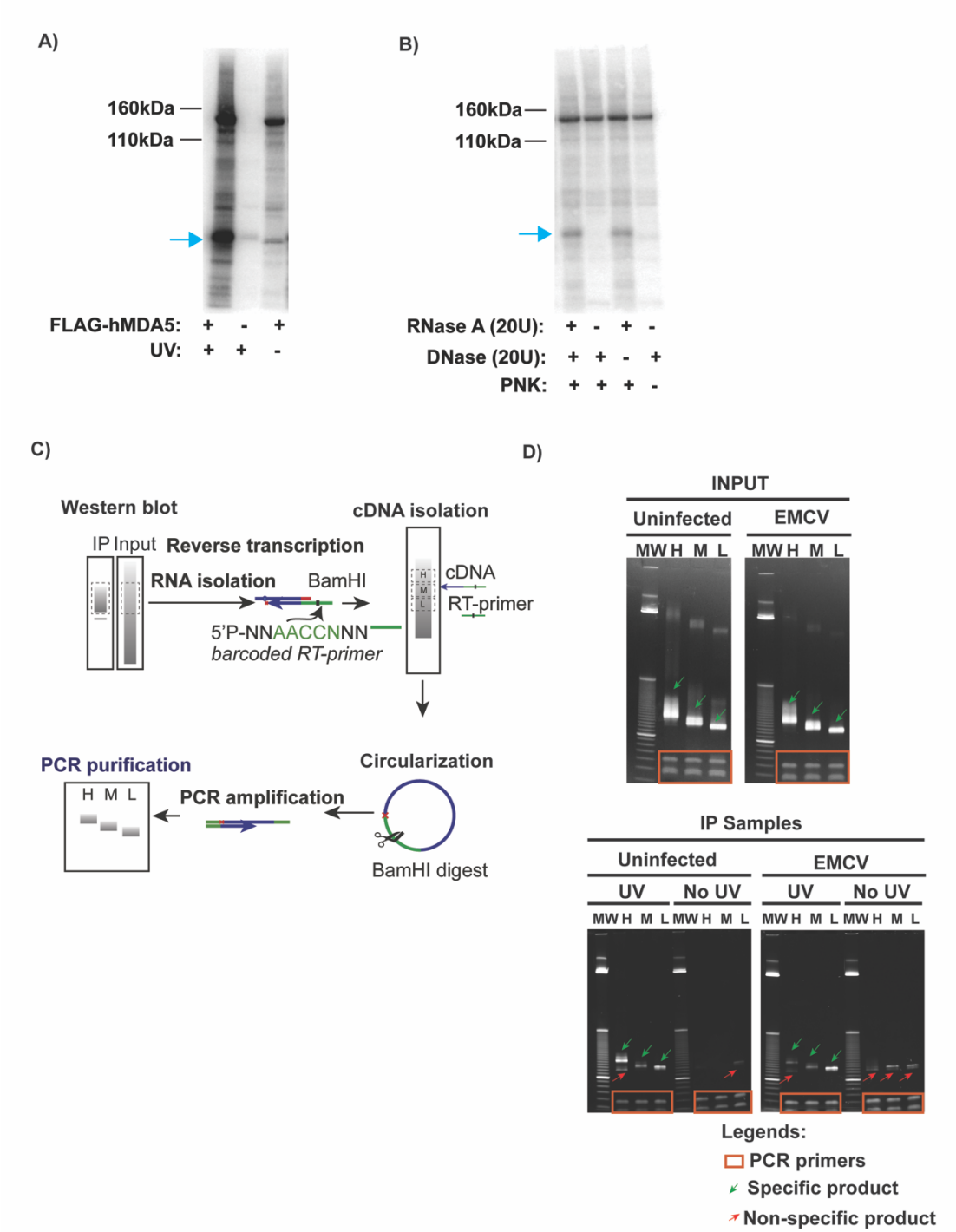


Figure 15 - Essential and further optimisation steps for MDA5 UV-crosslinking and immunoprecipitation (iCLIP) technique. "A" and "B" represent 3XFLAG-hMDA5 immunoprecipitation (IP) with α-FLAG in a single step and in the absence of stringent conditions such as the Urea Cracking Buffer. A) 293T-TLA cells were transfected or not with a 3XFLAG-hMDA5 construct and were left untreated- or treated with UV. Radiofilm (radioactively labelled RNA) is shown. B) Same as in "A", but samples were treated or not with RNase A, DNase or T4 polynucleotide kinase (PNK) for radiolabelling. C) Optimisation steps to generate complementary DNAs (cDNAs) for deep sequencing. In brief, RNAs were isolated from nitrocellulose membranes after western blot and used for reverse transcription (RT) to generate cDNAs. These cDNAs were gel purified and size-fractionated in H (high), Medium (M), and Low (L) bands. They were

circularised and again linearised with BamHI enzyme digestion. Products were used for polymerase chain reaction (PCR) amplification. D) PCR amplicons from size-matched input controls (13-16 cycles) or IPed RNAs from samples infected or not with EMCV (18-21 cycles). Specific and non-specific products as well as primers are indicated. Blue arrows in "A" and "B" indicate putative co-immunoprecipitating RNA-binding protein. A, B: representative of 2 biological replicates. D: representative of at least 3 biological replicates. "C" scheme was prepared by Dr. Jonathan Maelfait based on (Huppertz *et al.*, 2014).

The cDNAs were purified and size-fractionated into H, M and L molecular weight fragments (Figure 15C). These cDNAs were circularised and cleaved at a BamHI restriction enzyme site present on the adaptor. This step was important to generate linear cDNA fragments containing Forward and Reverse primer sites for PCR amplification (Figure 15C).

Size-matched input controls were treated separately as described in Van Nostrand *et al.* (2016). Here, I also size fractionated the input-derived cDNAs as described above. By PCR, I was able to amplify all H, M, and L cDNA fragments in samples from the size-matched input and co-IPed bound fractions (Figure 15D).

Non-UV crosslinked samples demonstrated the presence of short-sized non-specific bands in the PCR (Figure 15D). In some experiments, I purified and sequenced the specific bands from PCR experiments with no more than 18 cycles. However, sequencing analysis revealed most of the sequences were PCR duplicates. Therefore, further optimisation and protocol troubleshooting are required to reduce the number of PCR cycles and presence of PCR contaminating bands prior to new sequencing attempts.

The results presented above (Figure 14) show that ectopically expressed MDA5 binds to RNAs in cells infected or not with EMCV. All iCLIP experiments were performed with 293T-TLA cells transfected with a 3XFLAG-hMDA5 construct. I therefore aimed to address whether MDA5 overexpression, in this

experimental set up, induced type I IFNs and if this could be related to its ability to bind cellular RNAs.

As expected, 3XFLAG-hMDA5 overexpression led to the induction of IFN I (Figure 16A). Hence, we hypothesized that, upon overexpression, MDA5 binds cellular RNAs and induces type I IFNs.

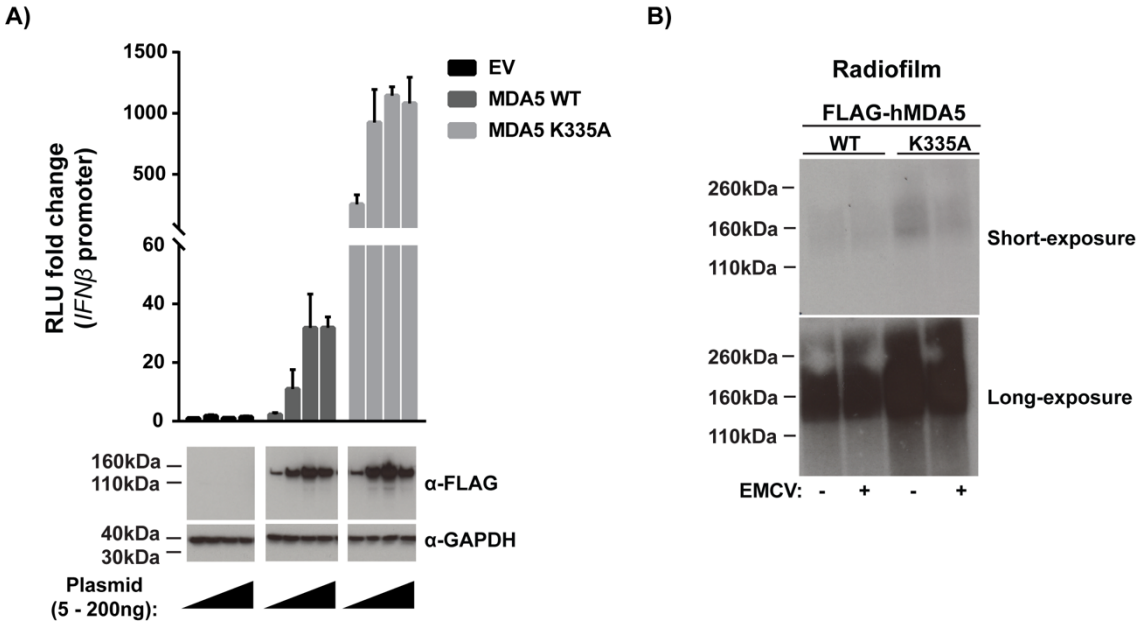


Figure 16 - Effects on interferon (IFN) induction of wild-type (WT) and ATPase mutant MDA5 upon overexpression in 293T-TLA cells. A) 3XFLAG-containing WT and ATPase mutant (K335A) MDA5 constructs were transfected in 293T-TLA cells. Protein expression was detected by Western-blot using an α-FLAG antibody. IFN-β promoter reporter was used to detect the induction of type I interferons measured by Relative Luciferase Units (RLU). B) Cell lysates from cells treated as in "A" were separately used for UV-crosslinking and Immunoprecipitation (iCLIP). RNAs were radiolabelled with γ-32p-ATP and radiofilms are shown. Cells were mock- or infected with EMCV (moi 0.1). In "A", experiments were performed in technical and biological triplicates. Graph corresponds to a representative experiment and bars are Standard Deviations (SD). "B" represents one biological replicate.

To test this hypothesis, I generated an MDA5 ATPase mutant, K335A. It has been demonstrated in cell-free systems that this mutation decreases the dissociation kinetics of MDA5 from dsRNAs (Peisley *et al.*, 2011).

In line with this, the K335A mutant induced much higher levels of type I IFN in comparison to the WT construct upon overexpression. At the same time, WT and K335A mutants produced similar amounts of protein (Figure 16A).

Furthermore, I compared WT and K335A MDA5 constructs in their ability to bind cellular RNAs upon overexpression. A stronger signal for radiolabelled RNA species was found to be associated to K335A in comparison to WT MDA5 (Figure 16B). These data suggested the ATPase mutant construct binds to cellular RNAs with higher affinity/stability and this is probably correlated with a stronger induction of type I IFNs. Moreover, MDA5 is likely to be able to trigger type I IFN signalling upon binding to cellular RNAs.

EMCV-infected samples presented a weaker signal for radiolabelled RNAs than mock-infected samples (Figure 16B). This is probably due to virus-induced cell death.

4.2 DEVELOPMENT OF CELL-BASED BIOASSAYS TO ASSESS THE IMMUNOSTIMULATORY POTENTIAL OF CELLULAR RNAS

Next, I aimed at investigating whether RNAs from uninfected cells can trigger MDA5-dependent type I IFNs. To test this, first I established a bioassay in HEK293 cells stably expressing a luciferase *IFN-β* promoter. This cell line was rendered deficient for RIG-I, MDA5 or MAVS using CRISPR technique. All these four cell lines were generated in our laboratory by Dr. Alice Mayer.

The assay involved seeding these reporter cell lines at high density in 96-well plates (Figure 17A). These cells were pre-treated or not with IFN-A/D up to 24hs prior to transfection with high amount of total RNAs. These RNAs were previously extracted from cell cultures infected or not with viruses (Figure 17A).

For RIG-I agonists, a robust IFN response was found without pre-treatment with IFN-A/D (not shown; see Rehwinkel *et al.*, 2010b). However, IFN-A/D pre-treatment was essential to enhance MDA5-dependent responses in these systems (for an example, see Figure 17C). For that reason, in all of the following experiments, these reporter cells were pre-treated with IFN-A/D before transfection.

To validate the WT and KO reporter cell lines, we transfected IVT-RNA or V-EMCV-RNA, as RIG-I or MDA5 agonists, to verify the induction of type I IFNs (Figure 17B). Indeed, IVT-RNA only induced the IFN-β reporter in WT and MDA5 KO cells. V-EMCV-RNA-mediated IFN responses were stronger in WT and RIG-KO cells, and much reduced in MDA5 KO cells. Both stimuli did not induce IFNs in MAVS KO cells (Figure 17B). MAVS KO cells had the ability to induce IFNs to these stimuli upon overexpression of a MAVS construct (not shown). In sum, these data validated the KO reporter systems in a functional assay.

I then tested whether total RNAs extracted from uninfected A549 cells could induce IFNs. Transfection of total RNAs from these cells induced the IFN-β reporter only if reporter cells were pre-treated with at least 10U/ml of IFN-A/D. This induction was largely dependent on the expression of MDA5 (Figure 17C).

Using a fixed concentration of IFN-A/D of 30U/ml, the finding above was also extended to total RNAs from other cell lines, such as 293T-TLA cells (Figure 17D), Huh7.5, and HeLa cells (not shown). These data suggested that MDA5 can respond to transfection of total RNAs from uninfected cells and induce type I IFNs in a MAVS-dependent manner.

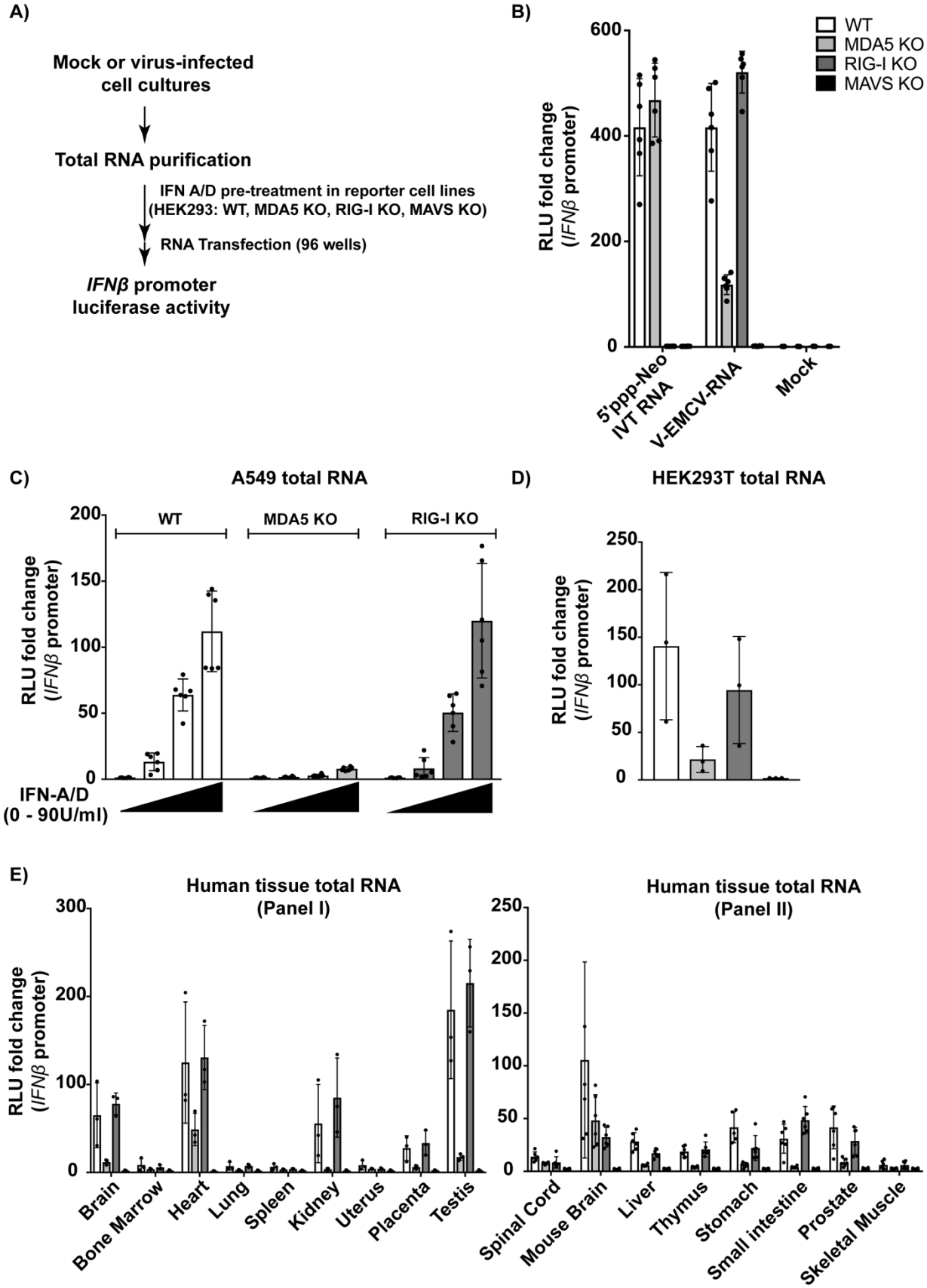

A)
Mock or virus-infected cell cultures
Total RNA purification
IFN A/D pre-treatment in reporter cell lines (HEK293: WT, MDA5 KO, RIG-I KO, MAVS KO)
RNA Transfection (96 wells)
IFNβ promoter luciferase activity
B)
WT
MDA5 KO
RIG-I KO
MAVS KO
RLU fold change (IFNβ promoter)
600
400
200
0
5'ppp-Neo IVT RNA
V-EMCV-RNA
Mock
C)
A549 total RNA
WT
MDA5 KO
RIG-I KO
RLU fold change (IFNβ promoter)
200
150
100
50
0
IFN-A/D (0 - 90U/ml)
D)
HEK293T total RNA
RLU fold change (IFNβ promoter)
250
200
150
100
50
0
E)
Human tissue total RNA (Panel I)
RLU fold change (IFNβ promoter)
300
200
100
0
Brain
Bone Marrow
Heart
Lung
Spleen
Kidney
Uterus
Placenta
Testis
Human tissue total RNA (Panel II)
250
200
150
100
50
0
Spinal Cord
Mouse Brain
Liver
Thymus
Stomach
Small intestine
Prostate
Skeletal Muscle

Figure 17 - Transfection of cell and tissue total RNAs into HEK293-IFN-β promoter reporter cells. A) The presented scheme describes a bioassay using HEK293 cells stably expressing a luciferase IFN-β promoter reporter. Wild-type (WT) and RIG-I/MDA5/MAVS KO reporter systems were used. These cells were pre-treated with IFN-A/D as indicated. Relative Luciferase Units (RLU) was measured the following day post-transfection. B) Lipofectamine-only (Mock), RIG-I (5'ppp-Neo-IVT-RNA) or MDA5 (V-EMCV-RNA) agonists were transfected (4ng) into the reporter cells. C) Titration of recombinant of IFN-A/D in the reporter cell lines prior to transfection of total RNA from uninfected A549 cells. IFN-A/D concentrations (U/ml): 0, 10, 30, 90. D) Reporter cells were treated with 30U/ml of IFN-A/D and transfected with total RNAs from 293T-TLA cells. E) Commercially available DNase-treated human tissue total RNAs were used in the bioassay, as indicated. C-E) 100ng of total RNAs were transfected. Bars represent standard deviations (SD). B, C and E (panel II) were performed in biological duplicates and technical triplicates; dots represent technical replicates. D and E (panel I) were performed in biological triplicates and technical triplicates; dots here represent average of each biological replicate.

Given the results above, I also tested whether total RNAs from human tissues could induce IFNs (Figure 17E). I transfected these RNAs and found most of them induced MDA5-dependent IFN responses. Interestingly, human testis total RNA was the strongest inducer among all tissues (Figure 17E).

In addition to RNA from human testis, RNA samples from human brain, heart, and kidney induced relevant levels of IFNs. Mouse brain total RNA also induced the IFN-β reporter. However, this induction was partially dependent on both RIG-I and MDA5, and fully dependent on MAVS. Total RNAs from other tissues, such as spinal cord and bone marrow, induced none or low levels of IFNs.

To further confirm transfection of total RNAs from human tissues could induce MDA5-mediated IFN responses, I set up a different bioassay. I transfected RNAs into primary human skin fibroblasts – without IFN pre-treatment – and transferred the cell supernatants to an Interferon-Sensitive Response Element (ISRE) reporter cell line (Figure 18A). This reporter cell line was generated by Dr. Jonathan Maelfait in our laboratory (Bridgeman *et al.*, 2015).

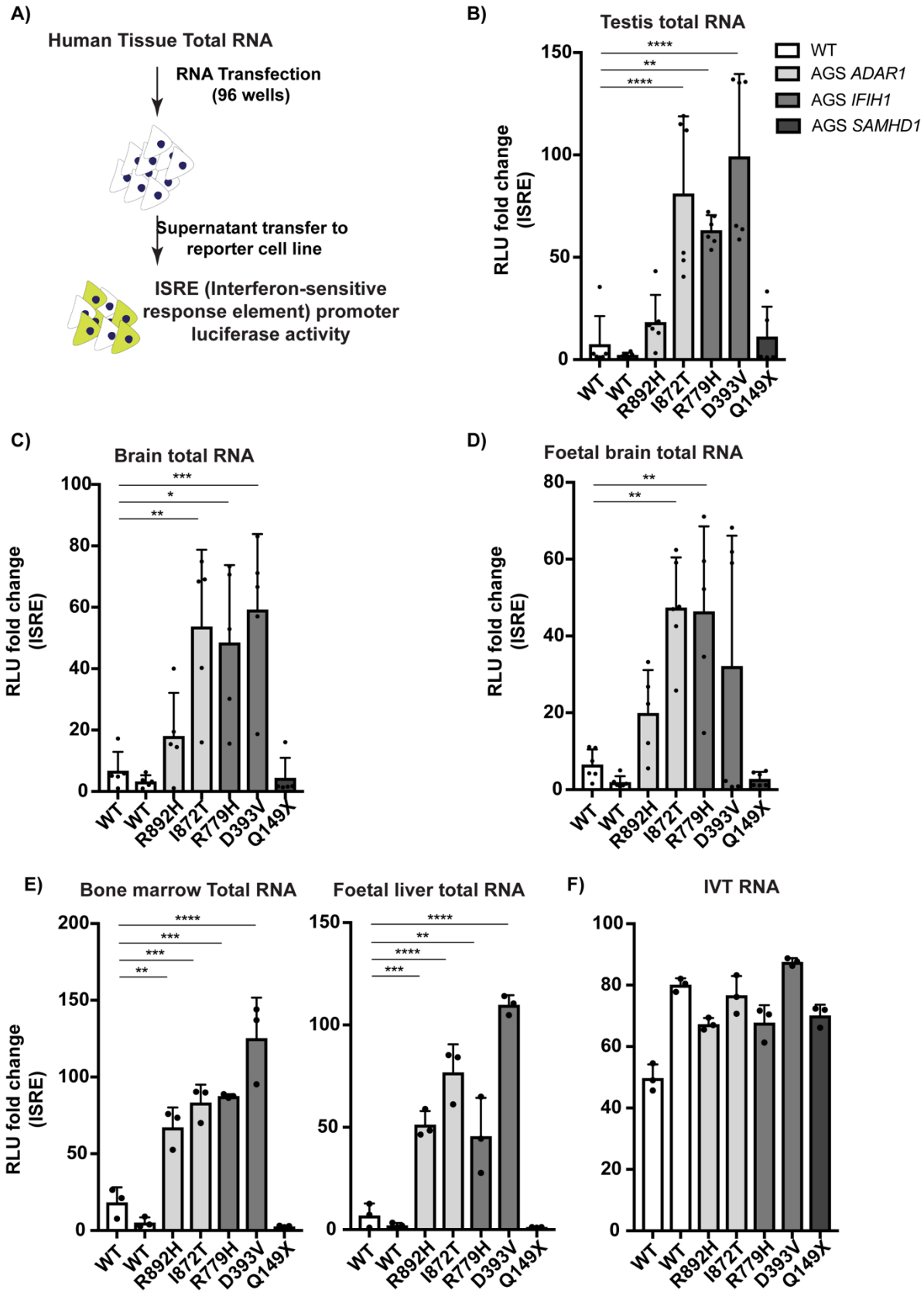

A)
Human Tissue Total RNA
RNA Transfection
(96 wells)
Supernatant transfer to
reporter cell line
ISRE (Interferon-sensitive
response element) promoter
luciferase activity
B)
Testis total RNA
RLU fold change
(ISRE)
WT
AGS ADAR1
AGS IFIH1
AGS SAMHD1
WT
WT
R892H
I872T
R779H
D393V
Q149X
C)
Brain total RNA
D)
Foetal brain total RNA
E)
Bone marrow Total RNA
Foetal liver total RNA
F)
IVT RNA

Figure 18 - Transfection of human tissue total RNA into primary human skin fibroblasts. A) The bioassay is the depicted in the presented scheme. In brief, primary human skin fibroblasts were transfected with total RNAs from human tissues. Fibroblasts from healthy donors (WT) or AGS patients were used. AGS patients had mutations in different genes as indicated. Supernatants of cells transfected with total RNAs from human testis (B; 25ng), adult brain (C; 50ng), fetal brain (D; 50ng), bone marrow and fetal liver (E; 100ng), or RIG-I agonist IVT-RNA (F; 0.4ng) were transferred to a reporter cell line. This cell line stably expresses an interferon-sensitive response element (ISRE) reporter (luciferase). Relative Luciferase Units (RLU) was measured. Bars represent Standard Deviations (SD). All experiments were performed in technical triplicates; dots represent technical replicates in B, D, E and F and the average of each biological replicate in C. B and D were performed in biological duplicates; C in biological quintuplicates; E and F in biological simplicates. Stars (*) represent statistical significance: * ($p<0.05$), ** ($p<0.01$), *** ($p<0.001$), **** ($p<0.0001$), one-way ANOVA.

For this assay, I used the human skin fibroblast cultures that were previously presented (Figure 13D). These are fibroblasts from healthy donors or AGS patients and were provided by Dr. Yanick Crow (University of Manchester, UK). Importantly, I performed RT-qPCR in untreated fibroblasts and did not detect induction of IFNs or ISGs at the baseline level (not shown).

Transfection of total RNAs from human testis, adult and foetal brain induced IFNs in all fibroblasts (Figure 18B-D). This induction was stronger in fibroblasts from AGS patients containing mutations in the *ADAR1* and *IFIH1* genes, but not in the *SAMHD1* gene (Figure 18B-E).

In contrast to the previous bioassay (Figure 17E), transfection of bone marrow and foetal liver total RNAs into human skin fibroblasts induced expression of IFNs (Figure 18E). As a control, transfection of IVT-RNA (RIG-I agonist) induced similar amounts of IFN across all fibroblasts (Figure 18F). In sum, fibroblasts from *IFIH1* and *ADAR1* AGS patients are more sensitive to RNA transfection and generate an IFN response that is likely MDA5-mediated.

4.3 DISCUSSION

As previously mentioned, co-IP in native conditions has become a common approach to study RIG-I agonists (e.g., Rehwinkel *et al.*, 2010b; Goubau *et al.*, 2015). A similar protocol has also been established for LGP2 (Deddouche *et al.*, 2014). However, MDA5 IP in native conditions does not enrich for a fraction containing immunostimulatory RNAs (not shown).

RIG-I has been shown to have high affinity for 5'-triphosphate RNAs (Pichlmair *et al.*, 2006; Veit Hornung *et al.*, 2006; Kowalinski *et al.*, 2011b; Kolakofsky, Kowalinski and Cusack, 2012). In turn, phosphatase treatment disrupts RIG-I-dependent RNA immunostimulatory activity (Pichlmair *et al.*, 2006; Veit Hornung *et al.*, 2006; Rehwinkel *et al.*, 2010b). This high affinity for 5'-triphosphates possibly facilitates the success of co-IP in native conditions for RIG-I agonists.

In contrast, MDA5 is predicted to bind to the phosphate backbone of dsRNA (Wu *et al.*, 2013). In addition, MDA5 generates filaments on dsRNA. The dynamics of these filaments relate to MDA5's ATPase activity (Peisley *et al.*, 2011; Berke *et al.*, 2012).

A model proposed by Sun Hur's lab suggests that several MDA5 monomers bind to dsRNA in different regions leading to multiple nucleation sites. Hence, longer dsRNAs generate more nucleation sites and thus longer filaments. MDA5 ATPase activity disassembles these filaments as part of a dynamic process (Peisley *et al.*, 2011, 2012). All these experiments were performed in cell-free systems.

With this current model, we suspect that during a native co-IP, MDA5 may disassemble from its agonists. Thus, we aimed to stabilise MDA5-RNA

interactions. We adapted an iCLIP protocol (Huppertz *et al.*, 2014) to UV crosslink bound RNAs to MDA5.

We generated a stringent and specific protocol to co-IP 3XFLAG-MDA5-associated RNAs (Figure 14). The stringency of this protocol was required to achieve specificity (Figure 15).

Without the Urea Cracking Buffer step, I observed that MDA5 co-IPed other putative RNA-binding proteins (Figure 15). In addition, a kinase was possibly pulled down along with MDA5. This was evident from apparent protein phosphorylation in negative control reactions lacking the PNK enzyme (Figure 15).

These observations are interesting and could be combined with Mass Spectrometry analysis to reveal putative MDA5 binding partners. Here, instead, we extended our protocol by including the highly stringent Urea Cracking Buffer step to reveal RNAs associated to MDA5 only.

We demonstrated that MDA5 binds to RNAs in 293T-TLA cells upon overexpression (Figure 14). This interaction was visible in uninfected cells or in cells infected with EMCV. Furthermore, we generated specific cDNA products from MDA5 bound fractions that will be used for sequencing in the future (Figure 15). With this, we described here for the first time direct MDA5 interaction with RNAs in living cells.

Prior to our study, another report showed by IF assays possible interactions between MDA5 and dsRNAs (Triantafilou *et al.*, 2012). The authors used dsRNAs pre-conjugated with fluorophores to detect their interaction with endogenous MDA5 in fixed cells. MDA5 was then shown to re-localise to sites

containing dsRNAs. This phenomenon led to the conclusion that MDA5 binds to dsRNAs in living cells; however, this interaction could be indirect.

In the study mentioned above, validation and specificity data for the antibodies used are lacking. Moreover, it is essential to assess whether RNA labelling affects its binding to MDA5 (e.g. in cell-free systems) and IFN I/III induction. Also, the interactions between MDA5 and dsRNAs could be alternatively explored with super-resolution microscopy.

Finally, MDA5 re-localisation and proximity to dsRNAs are indications that MDA5 may bind dsRNAs. However, this method is not a direct confirmation that these RNA species are bound by MDA5 leading to its activation.

Evidences from studies using recombinant MDA5 and synthetic RNAs suggest MDA5 has preference for binding long dsRNAs. Most studies were performed in cell-free systems (Peisley *et al.*, 2011, 2012; Berke *et al.*, 2012; Yao *et al.*, 2015). In line with this observation, transfection of HMW poly I:C into cells triggers MDA5-dependent IFN I responses (Kato *et al.*, 2006, 2008).

MDA5-dependent IFN induction has also been observed after transfection of total RNAs from cells infected with long dsRNA-generating viruses or of purified replicative intermediates (Pichlmair *et al.*, 2009; Feng *et al.*, 2012; Jiang *et al.*, 2012a; Triantafilou *et al.*, 2012). An interesting exception is JEV that generates long dsRNAs but appears not to trigger MDA5 upon infection or RNA transfection (Kato *et al.*, 2006; Y.-M. Loo *et al.*, 2008). It would therefore be interesting to evaluate the differences between the dsRNAs from several types of viruses and their likelihood to trigger MDA5.

Altogether, these data suggest MDA5 becomes activated in the presence of long-dsRNAs. However, experiments demonstrating direct association

between MDA5 and dsRNAs in living cells leading to IFN I induction have not been reported. This issue is further complicated by multiple other studies suggesting different agonists for MDA5 (Pichlmair *et al.*, 2009; Deddouche *et al.*, 2014; Runge *et al.*, 2014).

MDA5-dependent IFN I responses were shown to be activated by higher-order HMW RNAs, and not by purified ssRNAs and dsRNAs (Pichlmair *et al.*, 2009). In addition, a short (170bp) virus-derived hairpin RNA bound by LGP2 can trigger MDA5 (Deddouche *et al.*, 2014). As for the other studies described above, these studies also lack evidence that MDA5 directly binds to these RNA species.

To date, the most direct evidence for RNAs association to MDA5 comes from one PAR-CLIP study (Runge *et al.*, 2014). The authors found in the MDA5 bound fractions ssRNA species containing AU rich sequences. Nonetheless, no specific motif or structure was identified and characterised to trigger MDA5.

As discussed before, PAR-CLIP has the risk of artefactually introducing uridine-rich sequences and cell toxicity. The nucleotide resolution is also lower than for the iCLIP (Huppertz *et al.*, 2014). Given these reasons, we established an adapted iCLIP protocol to determine RNAs bound by MDA5.

With our stringent double IP/Urea Cracking Buffer protocol, we can clearly show that MDA5 binds to RNA (Figures 12, 13). Runge *et al*. (2014) did not establish whether their protocol enriches RNA species derived from other RNA-binding proteins co-precipitating with MDA5. Our data suggested this is an actual possibility (Figure 15). It is thus important to avoid possible cross-contaminating material that could affect the identification of MDA5 ligands/agonists.

Taken together, physiological agonists for MDA5 are to be identified. We plan to use our iCLIP protocol to unravel MDA5 agonists in overexpression

systems. In addition, for the future, we aim to adapt this protocol to endogenous MDA5 co-IP using the antibodies generated in this study (see Chapter 3).

To achieve this successfully, we may need to overcome limitations of the iCLIP technique. UV-crosslinking is expected to covalently link nucleobases to proteins in close proximity (Huppertz *et al.*, 2014). This may complicate MDA5-RNA crosslinking as it has been suggested that MDA5 binds to the phosphate backbones in dsRNAs, possibly, without a primary sequence preference (Wu *et al.*, 2013). Therefore, bioinformatics analysis will need to differentiate crosslinking sites from actual binding sites. Some identified sequences might also have been crosslinked due to an irrelevant transitory interaction.

Recently, a method called RNA hybrid iCLIP (hiCLIP) was developed to facilitate the identification of dsRNA species associated to RNA-binding proteins (Sugimoto *et al.*, 2015, 2017). In hiCLIP, a key step was the insertion of a linker between the two strands of a dsRNA molecule. This method improved the accuracy of the identification of RNA duplexes bound to STAUFEN 1 protein (Sugimoto *et al.*, 2015). MDA5-RNA co-IP could also potentially benefit from using the hiCLIP technique.

Interestingly, MDA5 has also been suggested to bind to cellular RNAs, possibly dsRNA-generating inverted repeat Alu elements (Rice *et al.*, 2012, 2014; Liddicoat *et al.*, 2015). Given the nature of their highly repetitive sequences, mapping of Alu elements against the human genome could be complicated by the short reads (25-50bp) generated by the iCLIP protocol. In an attempt to overcome this issue, we are currently titrating the concentrations of RNase A to generate libraries of at least 100bp (Figure 14F).

As previously described, our iCLIP data showed MDA5 binds to RNAs even in uninfected cells. In parallel, we observed ectopically expressed MDA5 induces type I IFNs in mock-infected cells (Figure 16). This suggests that overexpressed MDA5 binds self RNAs and these can possibly trigger the induction of type I IFNs.

This is further supported by the use of the MDA5 ATPase mutant K335A that triggered a potent IFN I response (Figure 16). MDA5 ATPase mutant K335A was shown to increase MDA5 affinity for dsRNAs on a test tube (Peisley *et al.*, 2012). In line with this, our data suggested enrichment of RNA species bound by the mutant MDA5 construct using the iCLIP protocol (Figure 16B).

This finding was expected and is in agreement with experiments in cell-free systems (Peisley *et al.*, 2012). In future experiments, it would be interesting to identify the RNAs bound by MDA5 K335A in comparison to the WT protein.

Mutations in the *IFIH1* (MDA5) gene were found to be associated with AGS by two independent groups (Oda *et al.*, 2014; Rice *et al.*, 2014). Both groups agreed these are gain-of-function mutations. One study suggested that mutant MDA5 still requires an endogenous RNA ligand for IFN I induction (Rice *et al.*, 2014). In contradiction, the other study suggested protein conformational changes could lead to spontaneous activation of MDA5 (Oda *et al.*, 2014). Our iCLIP protocol could be used to detect whether more RNA species are associated to MDA5 harbouring AGS mutations.

ADAR1 is a gene thought to act as a negative regulator of MDA5 signalling by A-to-I editing of otherwise immunostimulatory dsRNAs. Loss of *ADAR1* in mice leads to embryonic lethality correlated with an MDA5-dependent type I IFN signature (Liddicoat *et al.*, 2015; Pestal *et al.*, 2015). In agreement with this

observation, *ADAR1* loss-of-function mutations in humans result in AGS and in a type I IFN signature (Rice *et al.*, 2012).

In all of these cases, a yet-to-be tested hypothesis is that MDA5 senses dsRNA from inverted Alu repeat elements, which may be present in the cell cytosol (Rice *et al.*, 2012; Liddicoat *et al.*, 2015). We thus expect the iCLIP protocol described here will help us elucidate which types of cellular RNAs are bound by MDA5.

Interestingly, MDA5 is also activated by unidentified cellular RNAs in other contexts. One example is the putative sensing of RNAs derived from endogenous retroviruses after cancer treatment with DNA demethylating agents (Chiappinelli *et al.*, 2015; Roulois *et al.*, 2015). Furthermore, T1D has been associated with *IFIH1* gene SNPs (Smyth *et al.*, 2006; Rice *et al.*, 2012, 2014; Oda *et al.*, 2014; Gorman *et al.*, 2017).

To further determine whether cellular RNAs have the potential to trigger MDA5 signalling, I developed two bioassays that involve transfection of total RNAs into cell culture systems. Prior to this, it had been established that only transfection of total RNAs from cells infected with viruses could trigger type I IFNs (Pichlmair *et al.*, 2009; Rehwinkel *et al.*, 2010b; Jiang *et al.*, 2012a).

I hypothesized that the systems used before did not achieve enough sensitivity to detect MDA5-immunostimulatory RNAs derived from uninfected cells. To increase the sensitivity, I first developed a bioassay in HEK293 cells stably expressing a luciferase reporter under the control of the IFN-β promoter. The following aspects were found to be important: i) seeding a high number of cells (e.g. $3x10^4$ cells/well) in 96-well plates for the bioassay; ii) treatment of cells

with recombinant IFN-A/D 16-24 hours prior to RNA transfection; iii) transfection of 100ng per well of total RNA from uninfected cells.

The IFN-A/D pre-treatment was crucial for the triggering of the luciferase reporter upon transfection of MDA5 but not RIG-I agonists (Figure 17C). This treatment might increase the sensitivity of the system by upregulating the expression of MDA5 and LGP2, a positive regulator of MDA5 signalling (Bruns *et al.*, 2014; Deddouche *et al.*, 2014; Uchikawa *et al.*, 2016). Interestingly, transfection of total RNAs from uninfected cells generated IFN I responses that were mainly MDA5-dependent.

A second bioassay involved human skin fibroblasts from healthy donors or from patients with AGS. In this bioassay, IFN-A/D pre-treatment was not required and these cells also responded to smaller amounts of total RNA (e.g. 25 – 100ng of RNAs per well). Proteome differences between HEK293 and human skin fibroblasts may explain the differences in sensitivity between both systems.

Therefore, the set up of the second bioassay allowed for the cell supernatants to be harvested after RNAs were transfected and washed away. These supernatants were transferred to a HEK293 cell line stably expressing a luciferase reporter under the control of the ISRE promoter. Using this system, we observed that IFN induction was higher in cells from AGS patients containing mutations in the *ADAR1* and *IFIH1* genes, as compared to cells with mutations on the *SAMHD1* gene or healthy controls fibroblasts (Figure 18).

The findings from both bioassays support the hypothesis MDA5 has the ability to become activated by total RNAs extracted from uninfected cells. They further support the notion that an endogenous RNA ligand can potentially trigger MDA5 in autoinflammatory and/or autoimmune diseases.

Importantly, AGS is a neurological disorder (Crow and Manel, 2015) and thus we asked whether human brain could contain immunostimulatory RNAs. Both bioassays confirmed RNAs derived from adult and fetal whole brains, and adult cerebellum, but not spinal cord, contain MDA5-dependent immunostimulatory potential (Figures 15E, 16C).

In the bioassay with HEK293 cells, we observed MDA5-dependent responses following transfection of a panel of total RNAs from different human tissues and cell cultures. Our controls were IVT-RNA, that only triggered RIG-I, and V-EMCV-RNA, which mainly triggered MDA5 (Figure 17B). In addition, several human tissues did not induce (or induced low levels) of the luciferase reporter.

Although total RNAs derived from bone marrow or fetal liver, for example, induced low levels of IFN in HEK293 cells, they triggered IFN I in human skin fibroblasts. This induction was higher in fibroblasts containing *IFIH1* and *ADAR1* mutations. These data suggest AGS-related fibroblasts are more sensitive to RNA transfection than cells from healthy control volunteers and HEK293 cells.

Interestingly, RNA from mouse brain triggered a fully MAVS-dependent response that required both MDA5 and RIG-I (Figure 17E). This finding could be relevant for studies using mice with AGS-related mutations in *Ifih1* or *Adar1* genes. In particular, it is tempting to speculate that these mice may not present a neurological phenotype as mouse brain RNA may contain a mixture of MDA5 and RIG-I agonists. This could help to explain why there is currently no mouse model for AGS.

I incubated human brain total RNAs with RNase type III (to cleave dsRNAs only) or RNAse type I (to cleave ssRNAs only). I found the immunostimulatory

response was dependent on the presence of dsRNAs (not shown). This is line with the concept that MDA5 senses dsRNAs, as discussed above.

In addition, I tested total RNAs from 293T WT or *ADAR1* KO cells in our bioassays. I expected the *ADAR1* KO cells to contain RNAs with a higher immunostimulatory activity. However, I found the responses to be similar between RNAs derived from WT and *ADAR1* KO cells (not shown). As *ADAR1* is an important gene for survival in mice (Liddicoat *et al.*, 2015; Pestal *et al.*, 2015), it is possible that KO cell cultures develop mechanisms for survival that avoids chronical MDA5 signalling.

Another interesting finding was that total RNAs from human testis elicited the strongest MDA5-mediated type I IFN responses (Figure 17E). After we determine the RNA species bound by MDA5 in uninfected cells, it will be interesting to compare the expression of these RNA species in different human tissues.

Importantly, it will be relevant to understand how the human testis could avoid spontaneous induction of MDA5 if a high proportion of the RNAs expressed in this organ are MDA5 agonists. The testis expresses an ADAR-related protein, namely testis nuclear RNA-binding protein (TENR) (Nishikura, 2015), which may play an important role in this context.

Although TENR has no deaminase activity (Nishikura, 2015), it would be interesting to investigate whether it has the ability to bind to MDA5 stimulatory RNAs. TENR binding to RNAs could sterically block the access of MDA5 to immunostimulatory RNAs. Generation of TENR KO and TENR/IFIH1 KO mice may reveal MDA5-mediated inflammatory responses in testis.

An additional possibility is that expression of MDA5 is low in human testis allowing expression of its stimulatory RNAs.

In Chapter 3, I discussed that MDA5 may be cleaved and may have alternative translation products upon IFN-A/D treatment (e.g. Figure 13). The generation of alternative truncated translation products has been demonstrated recently for MAVS to avoid chronical activation of type I IFN (Qi *et al.*, 2017). Considering this, MDA5 putative shorter products could likely be a regulatory mechanism to avoid self-RNA sensing. In addition, this mechanism could be particularly relevant in some tissue and/or cell types.

In sum, our work established a stringent iCLIP protocol to purify RNAs bound by MDA5. In these conditions, we demonstrate MDA5 indeed binds to RNAs. This protocol can now be adapted to endogenous MDA5-RNA co-IP and identification of the ligands/agonists. Furthermore, we suggest ectopic expression of MDA5 or transfection of total RNAs from uninfected cell cultures and human tissues can trigger MDA5-mediated IFN responses.

CHAPTER 5

5 ACTIVATION AND INHIBITION OF THE TYPE I INTERFERON RESPONSE BY ZIKA VIRUS

Several viruses within the *Flaviviridae* family trigger antiviral type I IFNs and have developed effective means to block this host response. For example, HCV triggers RIG-I and MDA5 by generating distinct PAMPs (Saito *et al.*, 2008b; Schnell *et al.*, 2012; Cao *et al.*, 2015). In turn, the HCV protease has been shown to overcome the induction of type I IFNs by cleaving the adaptor protein MAVS (Li *et al.*, 2005; Horner *et al.*, 2011; Bender *et al.*, 2015).

Both RIG-I and MDA5 are also involved in sensing flaviviruses, such as WNV and DENV (Fredericksen *et al.*, 2008; Nasirudeen *et al.*, 2011; Errett *et al.*, 2013). Interestingly, JEV was found to trigger only RIG-I, but not MDA5 (Kato *et al.*, 2006).

In the case of WNV and DENV, it is believed RIG-I mediates an early response while MDA5 helps to maintain ISG expression (Fredericksen *et al.*, 2008). The IFN I response is mostly abrogated in mice lacking both sensors or MAVS (Errett *et al.*, 2013). Flaviviruses can block type I IFNs with aid of their NS proteins and, perhaps, by replicating within cytoplasmic vesicle-like compartments (Cumberworth *et al.*, 2017).

ZIKV is an emerging flavivirus and likely causes microcephaly in newborn babies (Faria *et al.*, 2016; Mlakar *et al.*, 2016). This link has been supported by animal models, especially immunodeficient mice (Cugola *et al.*, 2016; Lazear *et*

al., 2016; Miner *et al.*, 2016). These mouse models alongside with studies in human cell cultures revealed that ZIKV replication is sensitive to the effects of type I IFNs (Hamel *et al.*, 2015; Kumar *et al.*, 2016).

In this context, we asked two main questions: i) Does ZIKV replication generate RLR agonists? ii) Do ZIKV proteins block the type I IFN response?

In the next sections, I will describe several experiments that address these questions. I performed several experiments presented below together with Mr. Jonny Hertzog. He was a student reading in the MSc Integrated Immunology programme at the University of Oxford in 2016 (candidate 1002070).

He was supervised by Prof. Dr. Jan Rehwinkel (my current DPhil supervisor) and co-supervised by myself (day-to-day supervisor). Therefore, I indicate in the figure legends below which experiments were performed by or with me, by Jonny or by another experimentalist.

5.1 IDENTIFICATION OF RIG-I-LIKE RECEPTOR AGONISTS GENERATED DURING ZIKA VIRUS REPLICATION

Flavivirus infection and replication typically block the induction and/or effects of type I IFNs. We predicted that these mechanisms could make difficult the interpretation of the contribution of RLRs to sensing ZIKV. Hence, we attempted to identify whether ZIKV replication generates RNA PAMPs able to trigger RLRs by investigating total RNA extracts following ZIKV replication.

Our collaborators, Prof. Dr. Alain Kohl and Dr. Claire Donald (University of Glasgow, UK), infected A549 cells with a Brazilian ZIKV strain (PE243) at an MOI 5. After 20-24 hours, the cells were harvested and total RNA was purified

(A549_ZIKV). (This arrangement was important as we did not have the set up to use ZIKV in our facilities by the time of these experiments.)

We received the RNAs and tested them in our bioassay based on HEK293 cells stably expressing a luciferase reporter under the control of the IFN-β promoter. As we were not interested in the IFN induction mediated by the transfection of total RNAs from uninfected cells (A549), we did not pre-treat HEK293 cells with IFN-A/D prior to transfection (described in Chapter 4).

As expected, transfection of total RNAs from uninfected A549 cells did not trigger IFNs (Figure 19A). In contrast, I found that A549_ZIKV RNA induced IFN I, and this was largely dependent on RIG-I and fully dependent on MAVS (Figure 19A). I used IVT-RNA as a control that specifically activates RIG-I. Residual IFN induction was observed in RIG-I KO HEK293 cells transfected with A549_ZIKV RNA but not with IVT-RNA (Figure 19A). These data suggest that ZIKV replication generates RLR, mostly RIG-I, RNA PAMPs.

Other studies reported similar assays using IVT-RNA and total RNAs from cells infected with Influenza virus (Pichlmair *et al.*, 2006; Rehwinkel *et al.*, 2010b). These studies demonstrated RIG-I activation was dependent on the presence of 5'-triphosphates present in base-paired RNAs (Pichlmair *et al.*, 2006; Rehwinkel *et al.*, 2010b). To test the requirement for 5'-phosphates, I treated IVT-RNA (control) and A549_ZIKV RNA with AP to remove 5'-phosphates from the RNAs and then tested them in our bioassay (Figure 19B).

I observed that the A549_ZIKV RNA immunostimulatory activity was mostly abrogated upon treatment with AP (Figure 19B). At a high RNA concentration (50ng), limited IFN induction was still detectable after transfection. In contrast, IVT-RNA treated with AP did not induce IFN at any concentration

(Figure 19B). These observations suggest A549_ZIKV RNA contains 5'-phosphate bearing RNAs able to trigger RIG-I as well as a small RIG-I-independent immunostimulatory activity.

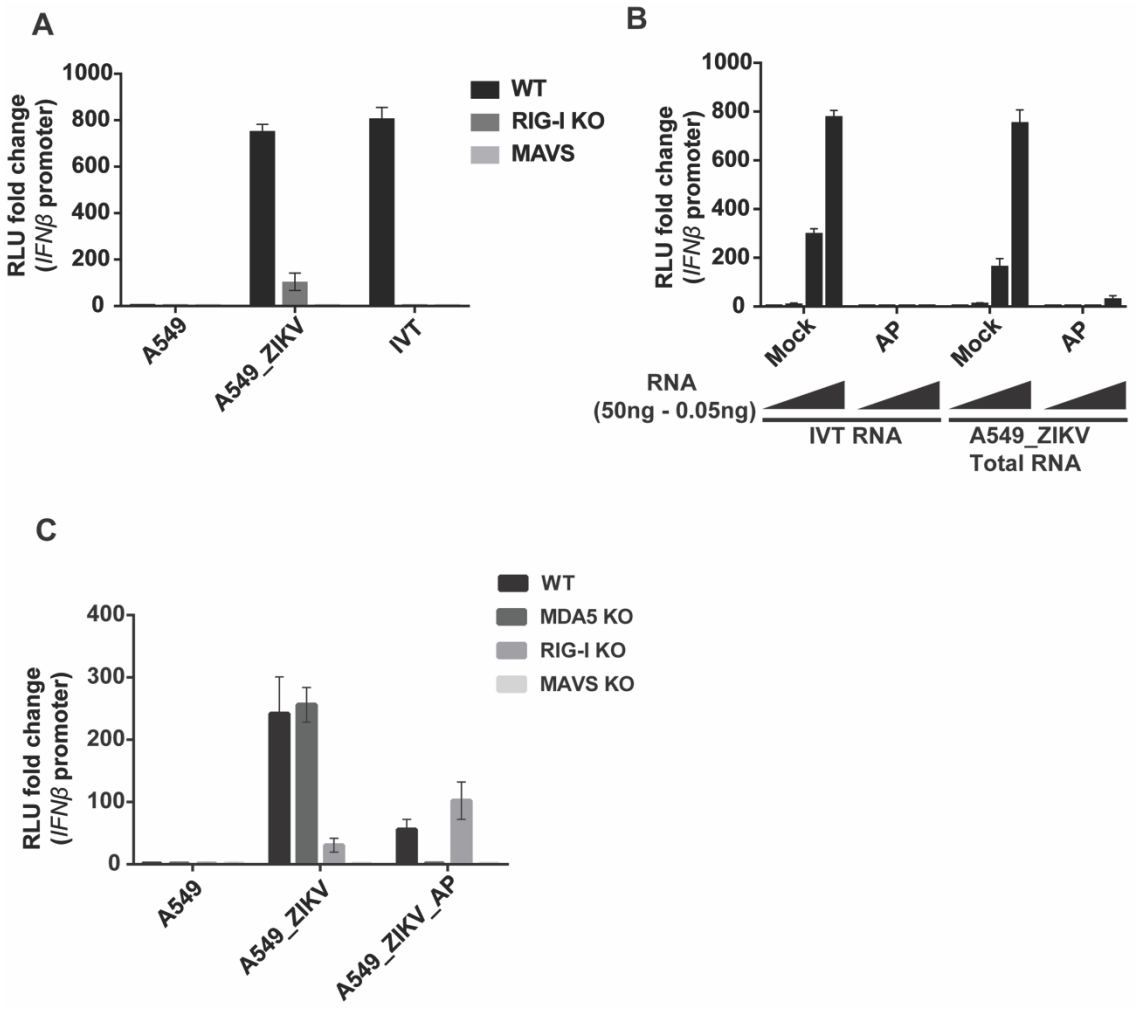


Figure 19 – Detection of immunostimulatory activity in total RNAs extracted from A549 cells infected with Zika virus (ZIKV). A) 100ng of total RNA from uninfected A549 cells or from cells infected with ZIKV (ZIKV_A549) were transfected into HEK293 cells (wild-type, WT; RIG-I or MAVS knockout, KO) stably expressing a luciferase reporter under the control of the IFN-β promoter. B) A549_ZIKV and IVT-RNA were mock treated or treated with AP (Alkaline phosphatase) and transfected into WT HEK293 reporter cells. 50, 5, 0.05ng or no RNA was transfected per well. C) HEK293 reporter cells were pre-treated with 3U/ml of IFN-A/D for one day prior to transfection with the indicated total RNAs (50ng). WT, MDA5/RIG-I/MAVS KO HEK293 reporter cells were used. Relative Luciferase Units (RLU) was measured. Bars represent Standard Deviations (SD) of technical triplicates. Experiments were performed in biological duplicates. Contributions: All RNA material was provided by Prof. Alain Kohl and Dr. Claire Donald (University of Glasgow, UK). I used the provided RNA extracts and performed all the experiments presented in this figure.

To test the latter hypothesis, I investigated whether MDA5 made a contribution to IFN induction upon A549_ZIKV RNA transfection (Figure 19C). As discussed in Chapter 4, to better identify the presence of MDA5 agonists in total RNA extracts, HEK293 reporter cells should be pre-treated with IFN-A/D.

Previously, I pre-treated HEK293 reporter cells with at least 10 or, often, 30U/ml of IFN-A/D (Figure 19C). Here, to avoid detection of IFN induction by total RNAs from uninfected cells, I rather pre-treated the reporter cells with 3U/ml of IFN-A/D (Figure 19C).

Indeed, I observed that transfection of total RNA from uninfected A549 cells did not trigger type I IFNs (Figure 19C). Transfection of A549_ZIKV RNAs triggered a potent induction of IFN I in WT and MDA5 KO cells.

A small induction was observed in RIG-I KO cells while MAVS KO cells did not trigger any response (Figure 19C). This experiment reproduced our previous findings that A549_ZIKV RNA contains strong RIG-I stimuli.

I then removed the 5'phosphates from A549_ZIKV RNA with AP treatment and observed that the remaining IFN induction was mediated by MDA5 (Figure 19C). This suggests that ZIKV infection in A549 cells generates RIG-I and MDA5 agonists, with RIG-I probably being the more sensitive sensor to detect RNA products of ZIKV replication.

5.2 GENERATION OF CONSTRUCTS TO EXPRESS ZIKA VIRUS PROTEINS

Next, we wished to test whether ZIKV proteins block the IFN I response. To achieve this, we first cloned DNA sequences encoding ZIKV proteins into

expression vectors for mammalian cells (Figure 20A). A V5-tag was added to the C-termini of all constructs.

Flaviviruses possess a single ORF coding for a polyprotein that is co-translationally cleaved by viral and host proteases (Figure 5A and 20A; King *et al*., 2012). In line with this, we further cloned some other possible constructs to generate proteins that are products of an incomplete cleavage process (Figure 20A).

After confirming the sequences of these plasmids, we used HEK293 cells for transfection and to test for protein expression. Most of the constructs expressed proteins at high levels as detected by WB using an α-V5 monoclonal antibody (Figure 20B-D).

Longer exposures were able to detect the proteins that were not readily detectable (Figure 20C). We further cloned a construct expressing eYFP tagged to NS5 protein, NSA5_eYFP (Figure 20D).

Most of the ectopically expressed proteins were found to migrate close to their expected sizes (Figure 20B-D). Some were also found to generate further products of different sizes.

Of note, Figures 18B-D depict the constructs initially used in our assays. Some constructs were cloned at later stages (e.g. NS2B-NS3) and were not included in this panel, but had their expression similarly confirmed (not shown).

EMCV-L, empty vector (pCDNA3.2), and pCDNA3.2-CAT (encoding for chloramphenicol acetyl transferase) were included as negative controls. We did not detect expression of EMCV L protein by WB, but observed its expected phenotype to block type I IFN response (Figure 20B).

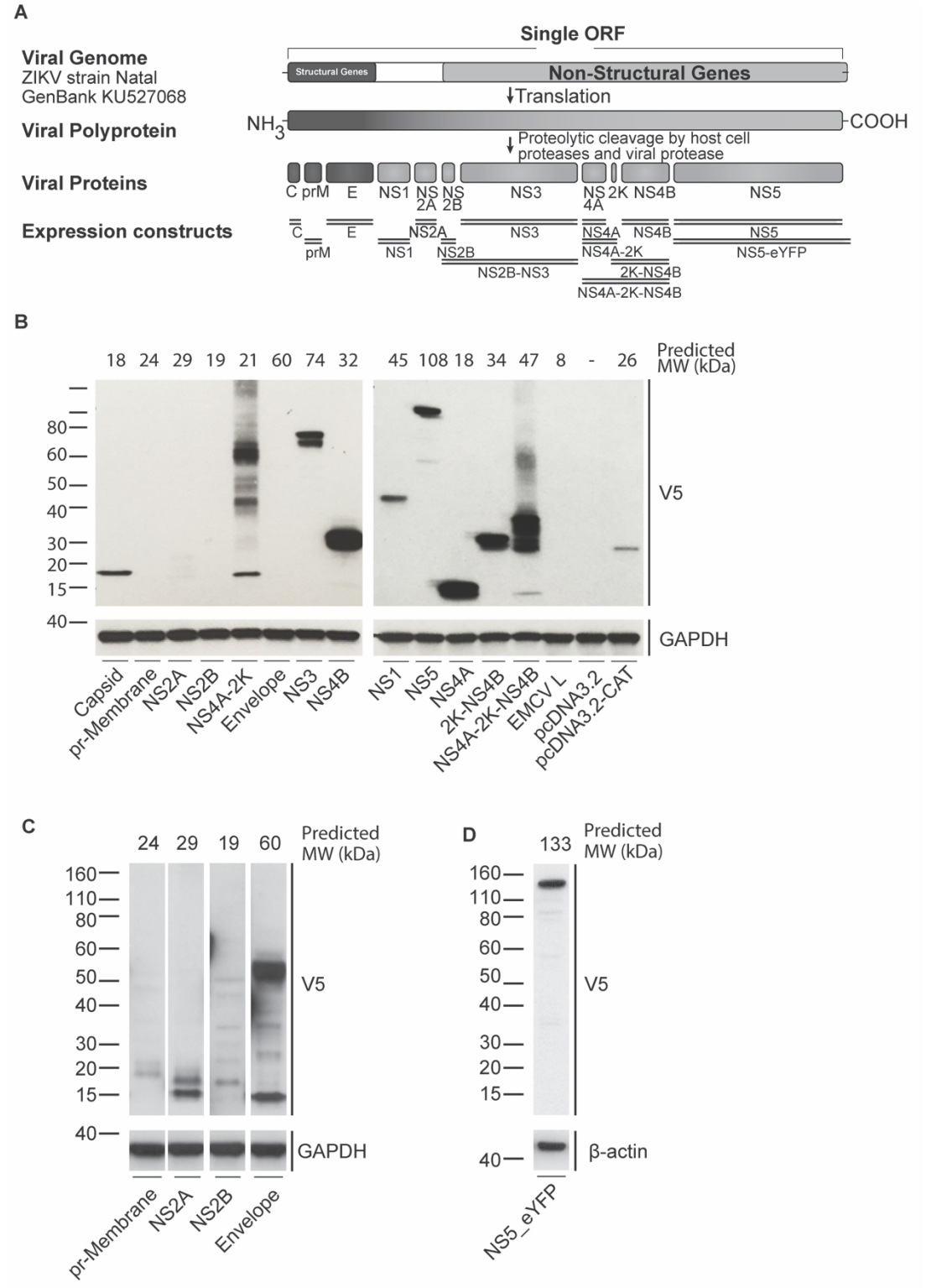


Figure 20 – Cloning and expression of Zika virus (ZIKV) proteins in HEK293 cells. A) As described in Figure 5, ZIKV proteins are represented. In addition, the expression constructs generated in this study are also depicted. B) Expression constructs containing a V5-Tag were transfected into HEK293 cells and lysates were tested by Western Blot (WB). Predicted Molecular Weights (MW) are indicated on the top (B, C, and D). C) Longer exposure of WB of some proteins represented in "B". D) Expression of the ZIKVA NS5_eYFP construct. GAPDH and β-actin were used as loading controls. Experiments were performed in biological duplicates. Contributions: this

Figure has been used in Mr. Jonny Hertzog Master's thesis (see main text). I designed and cloned most of the constructs. I performed all experiments together with Jonny with equal contribution.

5.3 ZIKA VIRUS (ZIKV) NS5 BLOCKS TYPE I INTERFERON SIGNALLING

Type I IFNs are well known to exert their antiviral effects via JAK/STAT signalling after engagement of IFNAR receptors. In turn, some flaviviruses can effectively block STAT proteins to avoid the induction of ISGs (Cumberworth *et al.*, 2017).

To test whether ZIKV could similarly block JAK/STAT signalling, we overexpressed individually or in combination constructs expressing ZIKV proteins. We used HEK293 reporter cells stably expressing a luciferase reporter under control of ISRE. After protein overexpression, we treated the cells with IFN-A/D to induce luciferase activity (Figure 21).

We observed that ZIKV NS5 and its fluorescent construct, NS5_eYFP, were the most potent inhibitors of ISRE induction (Figure 21A and E). To further assess whether other ZIKV proteins could exert inhibitory activities in combination with other proteins, we co-transfected three different plasmids (Figures 19B and C).

By using a matrix of plasmid combinations, we observed inhibition of ISRE induction in the presence of either ZIKV NS5 or EMCV L (Figure 21B). We then removed ZIKV NS5 from the combination with other proteins, and observed the other proteins did not block ISRE induction (Figure 21C). In sum, these data suggest that NS5 is the main viral protein that blocks JAK/STAT signalling.

We next tested whether the predicted viral protease NS2B-NS3 could inhibit ISRE induction (Figure 21D). We did not find evidence for NS2B-NS3-

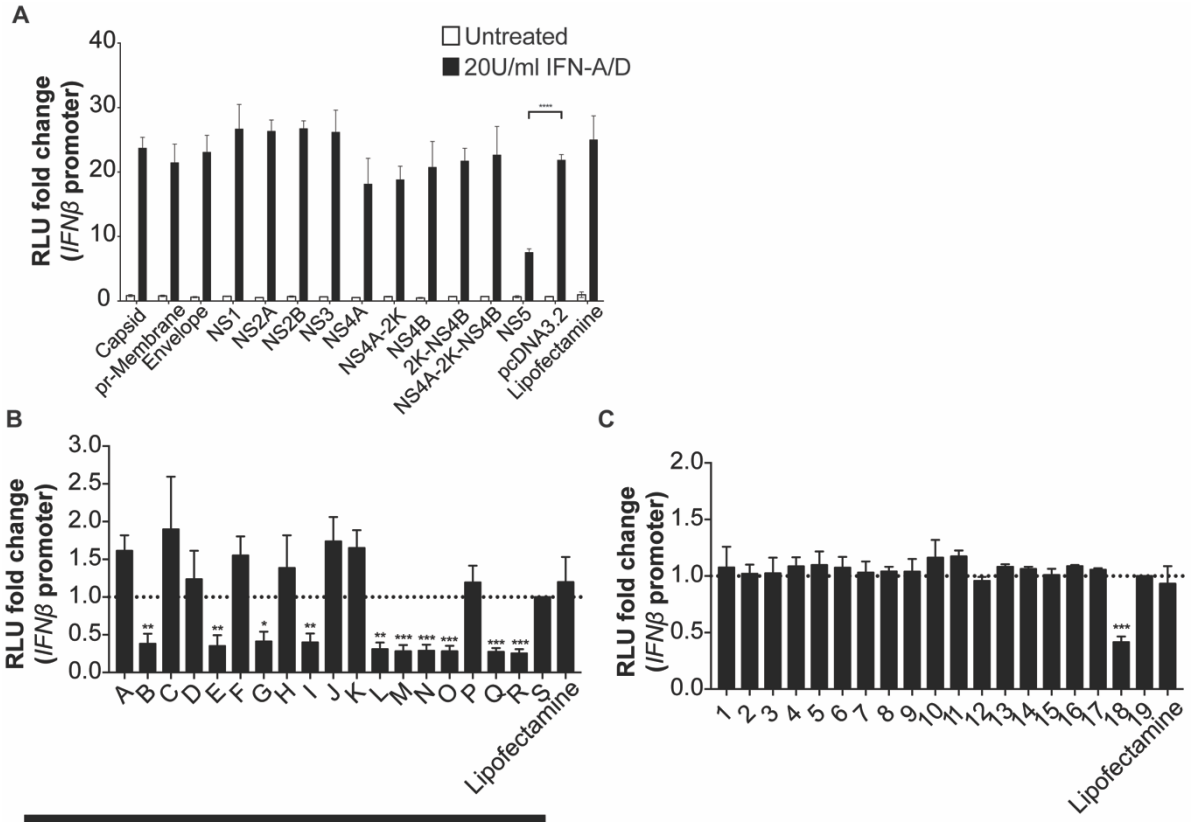
mediated blockade in this assay. However, NS4A showed weak inhibitory effects in some, but not all, of our experiments (Figure 21D).

Previous work in our lab had addressed the mechanisms by which ZIKV NS5 blocks JAK/STAT signalling. These experiments revealed that ZIKV NS5 degraded STAT2 and blocked the phosphorylation of STAT1 (Master's thesis: "Mini screen identifies Zika virus non-structural protein 5 as an antagonist of type I interferon induced antiviral gene expression", University of Oxford, 2016). Blockade of STAT1 phosphorylation was especially observed after 24 hour incubation with IFN-A/D, but not in shorter incubation windows, e.g. 30-60min.

Importantly, the data presented in Figure 21 were confirmed by RT-qPCR for ISGs and WB for RIG-I, which is encoded by an ISG (Master's thesis: "Mini screen identifies Zika virus non-structural protein 5 as an antagonist of type I interferon induced antiviral gene expression", University of Oxford, 2016).

NS5 is the biggest viral protein containing methyltransferase and an RdRp domains (King *et al.*, 2012). DENV NS5 was also shown to contain an NLS (nuclear localisation signal) (Pryor *et al.*, 2007). We aligned ZIKV NS5 sequences with other flaviviruses, including DENV, and mapped the putative NLS on ZIKV (Figure 22A).

We mutated candidate residues in the ZIKV NS5_eYFP construct and assessed NS5 localisation by live-cell imaging (Figure 22B). These experiments showed NS5 is mainly located in the cell nucleus due to the presence of an NLS. I further confirmed this finding in a cell fractionation experiment followed by WB (not shown).



Group	ZIKV proteins
A	C, pr-M, NS2A, NS2B, E
B	NS3, NS4B, NS1, **NS5**, NS4A
C	NS4A2KNS4B, NS2BNS3, C, pr-M, NS2A
D	NS2B, E, NS3, NS4B, NS1
E	**NS5**, NS4A, NS4A2KNS4B, NS3BNS3, C
F	pr-M, NS2A, NS2B, E, NS3
G	NS4B, NS1, **NS5**, NS4A, NS4A2KNS4B
H	NS2BNS3, C, pr-M, NS2A, NS2B
I	E, NS3, NS4B, NS1, **NS5**
J	NS4A, NS4A2KNS4B, NS2BNS3, C, pr-M
K	NS2A, NS2B, E, NS3, NS4B
L	NS1, **NS5**, NS4A, NS4A2KNS4B, NS2BNS3
M	C, NS3, NS4B, NS1, **NS5**
N	pr-M, NS4B, NS1, **NS5**, NS4A2KNS4B
O	NS2B, **NS5**, NS4A, NS4A2KNS4B, E
P	NS3, NS4A2KNS4B, NS2BNS3, E, NS4B
Q	NS2A, **NS5**, NS4A, NS4B, NS1
R	EMCV L protein, empty vector (20 ng)
S	empty vector (25 ng)

Group	ZIKV proteins
1	C, pr-M, E
2	NS1, NS2A, NS2BNS3
3	NS4A2KNS4B, C, pr-M
4	E, NS1, NS2A
5	NS2BNS3, NS4A2KNS4B, C
6	pr-M, E, NS1
7	NS2A, NS2BNS3, NS4A2KNS4B
8	C, NS1, NS2A
9	Pr-M, NS2A, NS2BNS3
10	E, NS2BNS3, NS4A2KNS4B
11	NS1, C, NS4A2KNS4B
12	NS2A, C, pr-M
13	NS2BNS3, C, E
14	NS4A2KNS4B, E, NS1
15	NS2BNS3, NS4A2KNS4B, pr-M
16	NS2BNS3, NS4A2KNS4B, NS2A
17	NS2BNS3, NS4A2KBNS4B, NS1
18	**NS5**, empty vector (10 ng)
19	empty vector (15 ng)

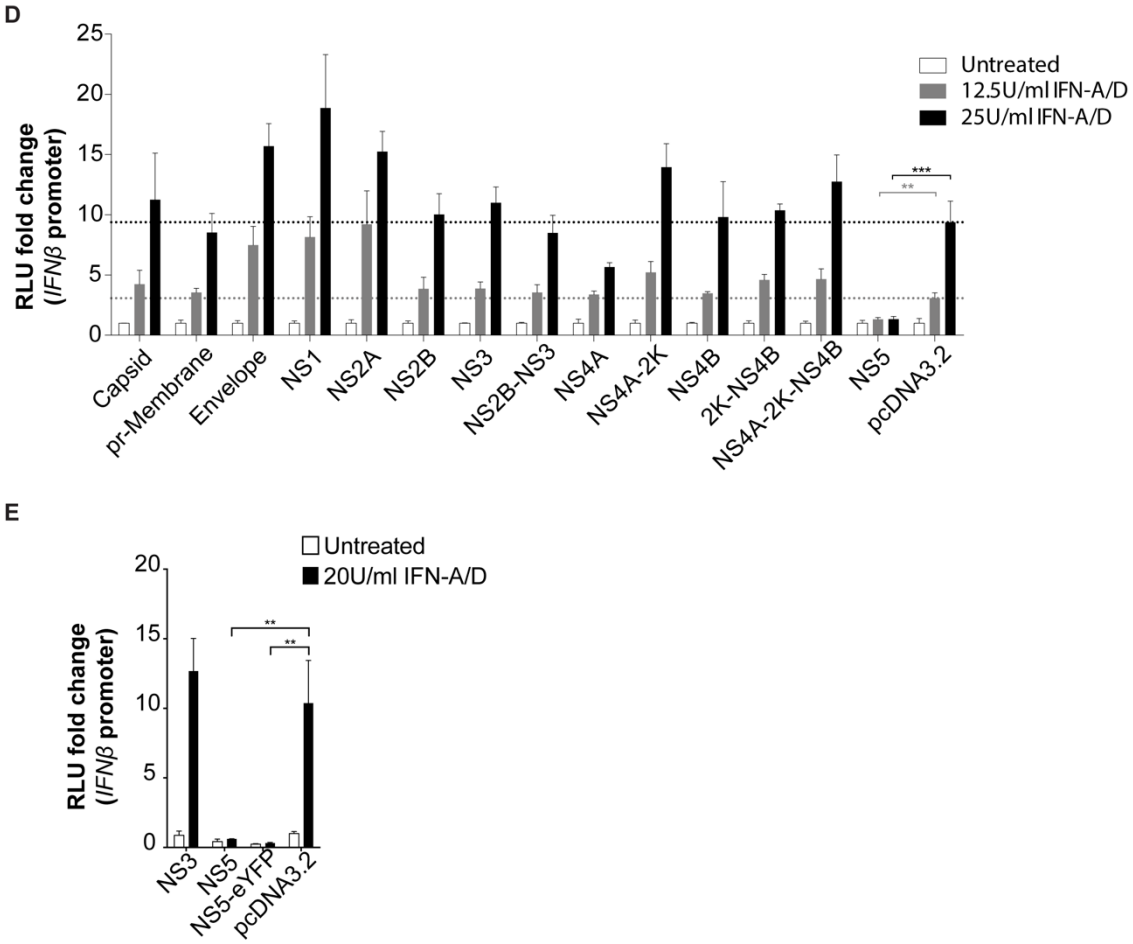


Figure 21 – The effects of Zika virus (ZIKV) protein overexpression in HEK293 cells. ZIKV protein-coding plasmids were transfected individually (A, D, and E) or in combinations (B and C) into HEK293 reporter cells. Tables in B and C describe the plasmid combinations used. These reporter cells stably expressed luciferase under the control of ISREs (Interferon-Stimulated Response Element). After overexpression, the cells were treated with recombinant IFN-A/D. Relative Luciferase Units (RLUs) were measured. Bars represent Standard Deviations (SD) of experiments in technical and biological triplicates. Contributions: Experiments in A, D, and E were performed by me and Mr. Jonny Hertzog. Experiments in B and C were performed by Dr. Rachel Rigby. Stars (*) represent statistical significance: * ($p<0.05$), ** ($p<0.01$), *** ($p<0.001$), **** ($p<0.0001$), one-way ANOVA.

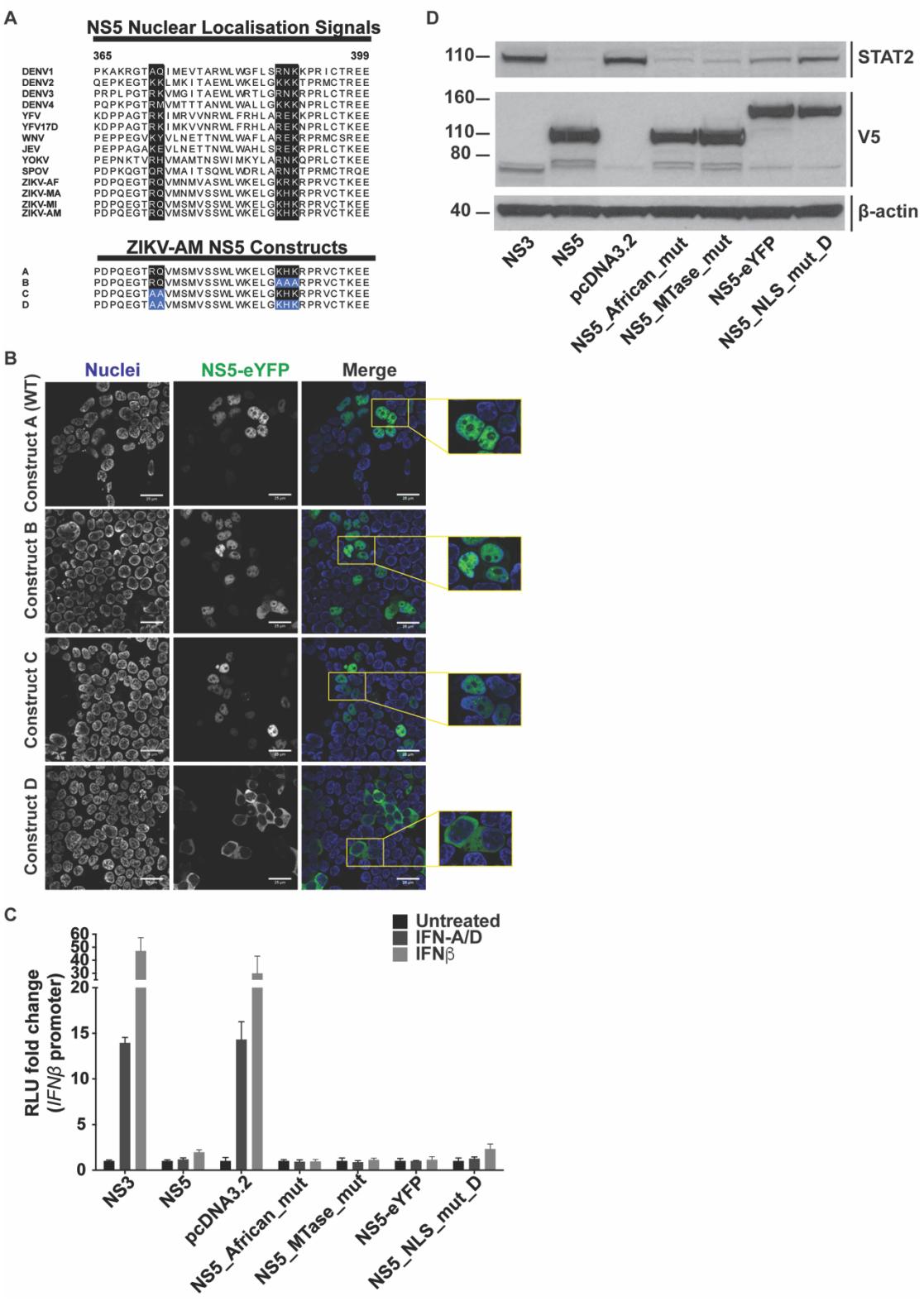


Figure 22 – Overexpression of Zika virus (ZIKV) NS5 mutants. A) Alignment of flaviviral NS5 sequences containing putative α-importin Nuclear Localisation Signals (NLS; in black). ZIKV-AM (America) genotype was used to generate mutants A-D (mutations shown in blue). DENV: Dengue virus; YFV: Yellow fever virus; WNV: West Nile virus; JEV: Japanese encephalitis virus; YOKV: Yokose virus; SPOV: Spondweni virus; ZIKV: Zika virus – AF: Africa, MA: Malaysia, MI: Micronesia, AM: America. B) Wild-type or NLS mutant ZIKV NS5_eYFP ectopic expression in HEK293 cells. Cells were visualised by live-cell imaging. C) HEK293 reporter cells expressing luciferase under the control of an ISRE (Interferon-Stimulated Response Element) were

transfected with ZIKV WT and mutant (mut) constructs. After overexpression, the cells were treated with IFN I, as indicated. NS5_African_mut (M2634V and M3392V, respective to the full-length genome nucleotides). NS5_MTase_mut (Methyltransferase domain mutant: E218A, respective to NS5 aminoacids). Relative Luciferase Units were measured. D) Western blot for the cell lysates presented in "C". Constructs were probed with an α-V5 antibody and endogenous STAT2 with a specific antibody. β-actin was probed as loading control. Microscopy bars in "B": 25μm. Bars in "C" represent standard deviations. Experiments were performed in technical triplicates (C) and biological triplicates (B, C, and D). Contributions: I performed the analysis and experiment in A and B. Mr. Jonny Hertzog performed experiments C and D.

Furthermore, we generated other NS5 mutant constructs. The NS5 E218A is expected to abrogate its CAP1 (2'-O-methylation) methyltransferase activity (NS5_MTase_Mut) (Ray *et al.*, 2006; Yangsheng Zhou *et al.*, 2007). In addition, Brazilian ZIKV strains from the current outbreak contain two mutations (M2634V and M3392V) on NS5. We reverted these residues to the ZIKV African genotype (ZIKV_African_mut).

We tested the ability of all these constructs to block ISRE induction (Figure 22C). Interestingly, all these mutant constructs blocked ISRE induction similarly to the WT construct. In support of this, they were also capable of inducing STAT2 degradation (Figure 22D). Taken together, natural NS5 mutations found in Brazilian strains as well as MTase and NLS-related residues are unlikely to be related to NS5's ability to block JAK/STAT signalling.

5.4 DISCUSSION

We first aimed at exploring whether ZIKV replication has the potential to generate RLRs agonists. To demonstrate this, we transfected total RNAs extracted from A549 cells infected with ZIKV into HEK293 reporter cells. This approach has been widely used to define RLR agonists from virus-infected cells. Conventionally, total RNAs from virus-infected cells have been transfected into WT or MDA5/RIG-I/MAVS KO MEFs (mouse embryonic fibroblasts) (Pichlmair *et*

al., 2009; Rehwinkel *et al.*, 2010b; Jiang *et al.*, 2012b). Our study has used a similar experimental set up employing a human cell line for the bioassay. We demonstrated that ZIKV replication produced RLR agonists.

This is consistent with a previous study showing that ZIKV replication produces detectable amounts of dsRNAs in infected cells (Grant *et al.*, 2016). As discussed in previous chapters, dsRNAs – including those detected by J2 mAb – may be related to MDA5 activation. Interestingly, our assays rather indicated MDA5 contribution was minor in comparison to RIG-I.

To a large extent, IFN I induction after ZIKV_A549 RNA transfection was RIG-I-dependent and sensitive to AP treatment. Flaviviruses are known to contain a 5'-triphosphorylated (5'ppp) genomes (King *et al.*, 2012). Given that RIG-I detects 5'-pp or 5'-ppp groups on viral RNA genomes (Pichlmair *et al.*, 2006; Rehwinkel *et al.*, 2010b; Goubau *et al.*, 2015), we hypothesized that RIG-I directly senses ZIKV RNAs. RIG-I IPs under native conditions could be used to address this question.

We are currently infecting human cells with live ZIKV to verify whether its replication induces type I IFNs in an RLR-dependent manner. We will compare these findings with our total RNA transfection data.

During the course of WNV and DENV replication, RIG-I and MDA5 were both found to contribute to the induction of IFN I (Yueh-Ming Loo *et al.*, 2008; Nasirudeen *et al.*, 2011; Errett *et al.*, 2013; Sprokholt *et al.*, 2017). RIG-I is thought to be an early mediator of IFN I activation while MDA5 sustains the response for longer periods. Simultaneous ablation of both sensors or their adaptor MAVS abrogated IFN I induction and was lethal in infected mice (Fredericksen *et al.*, 2008; Errett *et al.*, 2013). Hence, experiments in WNV and

DENV reveal an important role for RLR-mediated host protection against flaviviruses, with RIG-I and MDA5 playing complimentary roles.

Interestingly, although JEV has been shown to accumulate detectable levels of cytoplasmic dsRNAs (e.g., Uchida *et al.*, 2014), the survival of infected mice and IFN I induction seem to be exclusively RIG-I-dependent (Kato *et al.*, 2006). In contrast to WNV and DENV, ZIKV and JEV are thus likely examples of flaviviruses being primarily recognised by RIG-I. It would be interesting to test whether JEV has the ability to trigger MDA5 in a human and more sensitive system as the one described here in our study.

The conclusion that JEV is primarily sensed by RIG-I came initially from studies in mice (Kato *et al.*, 2006). More recently, mouse models for ZIKV infection have also been established (Cugola *et al.*, 2016; Lazear *et al.*, 2016; Miner *et al.*, 2016).

Surprisingly, MAVS KO mice showed similar susceptibility to ZIKV infection than WT mice (Lazear *et al.*, 2016). The authors observed that only IFNAR1 KO or triple IRF3/IRF5/IRF7 KO mice suffered from enhanced viral replication and neurological damage. It is important to note that low doses of viral inoculum were used in these studies in C57BL/6 mice - aged 5-6 weeks old (Lazear *et al.*, 2016).

Although IFNAR1 and triple IRF3/IRF5/IRF7 KO mice were susceptible to virus replication, the sensor(s) and adaptor(s) that trigger type I IFNs and promote survival were not tested (Lazear *et al.*, 2016). Perhaps, mice can detect ZIKV replication by multiple different sensors such as RLRs, TLRs, and/or cGAS/STING.

Indeed, a role for nucleic acid sensing in ZIKV mouse models was described in another study using intra-vaginal inoculation (Yockey *et al.*, 2016). The vaginal mucosa was shown to support ZIKV replication, ultimately leading to the infection of the foetal brain in pregnant mice. In this model, the ablation of MAVS led to an increase in viral replication. Viral replication was further enhanced after the infection of double MAVS/TLR7 KO or double IRF3/IRF7 KO mice. These observations suggest that both RLRs and TLRs provide protection against ZIKV infection. In addition, the authors observed that the cGAS/STING pathway was dispensable (Yockey *et al.*, 2016).

Naturally, mice are resistant to infection with DENV and thus animal models have been challenging (Zompi and Harris, 2012). Most of the studies describing susceptible models have used suckling mice, immunodeficient mice, and/or DENV mouse-adapted strains at high MOIs (Zompi and Harris, 2012; Zellweger and Shresta, 2014). One of the reasons for the resistance of mice to DENV may come from its inability to degrade mouse STAT2 (Ashour *et al.*, 2010). In contrast, AG126 mice (lacking IFNAR1) are highly susceptible and have been explored to study the DENV infection-mediated ADE (Balsitis *et al.*, 2010).

Similar to DENV, ZIKV was found to degrade human but not mouse STAT2 (Grant *et al.*, 2016). As for DENV, ZIKV strains might possess different abilities to infect and replicate in animals. It is possible that different mouse models result in different phenotypes depending on mouse strain, age, sex, viral strain, viral inoculum titre, route of inoculation, etc. Given these factors, studies in mouse models to identify the roles of individual RLRs and/or TLRs upon ZIKV infection are interesting to be further explored.

In vitro, the advantage of using RNA transfections to investigate immunostimulatory RNAs is the absence of viral inhibitors and evasion mechanisms that come to play in the course of virus replication. Flaviviruses, for example, are expected to replicate within cytoplasmic vesicle-like membranes which may might prevent dsRNA detection by cytosolic sensors (Welsch *et al.*, 2009; Överby *et al.*, 2010; Espada-Murao and Morita, 2011; Uchida *et al.*, 2014; Takamatsu, Uchida and Morita, 2015). These pore-containing vesicles are expected to be replication complexes containing dsRNAs and viral proteins (Welsch *et al.*, 2009).

To gain further insight into this issue, exploratory studies have been associating the kinetics of vesicle formation and dsRNA detection in the cytosol with the induction of type I IFNs (Överby *et al.*, 2010; Espada-Murao and Morita, 2011; Uchida *et al.*, 2014; Takamatsu, Uchida and Morita, 2015). These authors observed different dsRNA cytosolic exposure kinetics comparing JEV, WNV, and DENV. Importantly, the formation and stability of vesicles containing viral replication complexes depend on the type of cells infected.

Furthermore, it is possible to conceive that early detection of dsRNAs by RLRs is more detrimental to viral replication than late detection. I therefore suggest a speculative model: RIG-I detects viral 5'ppp-RNAs in the cytosol upon probable leakage from vesicle-like replication complexes. Although flaviviruses modify the 5'ends of their genomes with a CAP1 group (King *et al.*, 2012), different cell types and their replication machineries might lead to the generation of unprotected or incompletely modified RNAs. RIG-I-mediated IFN induction upregulates other ISGs, including *IFIH1* that encodes MDA5. MDA5, in turn, requires access to longer dsRNAs to become activated and this may be

prevented by the interaction of viral RNAs with viral and host proteins. Hence, ZIKV and JEV potentially generate MDA5 agonists that are less accessible to MDA5 than is the case for WNV and DENV, e.g. due to protein binding, RNA modifications, and/or kinetics of replication within membranous complexes.

Flaviviral RNAs contain a CAP1 (me^7-GpppN-me^2) structure that is produced by the replication complex formed between NS3 and NS5. NS3 has helicase and triphosphatase activities while NS5 has MTase (important for capping) and RdRp activities (Dong *et al.*, 2014).

Capping of flaviviral RNAs is also thought to be a viral strategy to avoid recognition by 5'phophate-binding proteins, such as RIG-I and IFIT1 (Daffis *et al.*, 2010; Szretter *et al.*, 2012; Schuberth-Wagner *et al.*, 2015).

Our studies demonstrated that ZIKV replication generated 5-phosphate bearing RNAs that trigger RIG-I upon transfection. It is thus unclear whether 5' RNA capping by ZIKV factory a mechanism that prevents recognition by RIG-I and/or IFIT1.

Flaviviruses thus employ several mechanisms to defeat the immune system. This idea led us to investigate whether ZIKV proteins could block the type I IFN system. To initially test this, we cloned and overexpressed ZIKV proteins in HEK293 cells. This approach, however, has the disadvantage of not mimicking the physiological context of virus replication. For example, vesicle-like structures containing replication factories are not formed in this system.

On the other hand, overexpression of constructs encoding ZIKV proteins is useful as a rapid means to screen for viral proteins with strong activity to block the type I IFN system. By overexpressing ZIKV constructs in isolation or in combinations, we observed that NS5 was the main viral protein blocking ISRE

and ISG induction upon IFN I treatment. Our data demonstrate that ZIKV NS5 blocks JAK/STAT signalling.

Further experiments demonstrated that NS5 degraded STAT2 (Figure 22D) at any time point tested and inhibited STAT1 phosphorylation at late time points (e.g. 16-24hs) post IFN-A/D treatment (not shown). While our work was in progress, Adolfo Garcia Sastre's lab reported similar findings regarding STAT2 degradation (Grant *et al.*, 2016). The basic mechanism by which ZIKV NS5 targets STAT2 for degradation, however, has not been revealed to date.

Other studies have been published since then and all agree with NS5's role in targeting human STAT2 (Kumar *et al.*, 2016; Bowen *et al.*, 2017; Chaudhary *et al.*, 2017). Similar to our study, Bowen *et al*. (2017) have found that ZIKV infection of human dendritic cells also led to inhibition of STAT1 phosphorylation.

In contrast, Chaudhary *et al*. (2017) suggested that ZIKV infection promotes STAT1-STAT1 homodimer formation and thus facilitates induction of IFN-γ, a type II IFN, to enhance virus replication. The authors have used overexpression of STAT1 to demonstrate homodimerization in HEK293 cells. Further experiments were performed in JEG3 (human placenta choriocarcinoma) cells (Chaudhary *et al.*, 2017). Whether the role of NS5 in promoting STAT1 homodimer formation is due to its overexpression, the time point and/or cell-type remains to be seen.

Importantly, we studied human STATs at endogenous levels in 293T-TLA and HEK293 cells. Furthermore, we used constructs based on the sequence of a Brazilian ZIKV strain isolated from a microcephaly case (Mlakar *et al.*, 2016). Differences in viral strains could account for different results.

Up to this date, all investigated flavivirus NS5 proteins have been found to block JAK/STAT signalling. In addition to DENV (Ashour *et al.*, 2009, 2010) and ZIKV, other examples are: i) tick-borne encephalitis virus (TBEV: *Flaviviridae*, *Flavivirus*) NS5 blocks the phosphorylation of JAK1 and TYK2 (Best *et al.*, 2005); ii) YFV NS5 interacts with and blocks STAT2, but only in the presence of IFN I (Laurent-Rolle *et al.*, 2014); iii) WNV NS5 blocks STAT1 phosphorylation (Laurent-Rolle *et al.*, 2010). In sum, all flaviviruses appear to have evolved to avoid the induction of ISGs, thereby preventing the establishment of a cellular antiviral state.

There is a multitude of other mechanisms by which flaviviruses can avoid the mosquito and human immune systems, including by the use of several NS proteins (Lindenbach and Rice, 1999; Diamond, 2003; Fernandez-Garcia *et al.*, 2009; Zeidler *et al.*, 2017).

Here, we found little evidence that ZIKV NS proteins other than NS5 can block JAK/STAT signalling. NS4A alone, but not in conjunction with the peptide 2K, showed a small inhibitory effect in some experiments (Figure 21D). Another study found that NS1 and NS4A block this pathway in addition to NS5, which was the most potent inhibitor (Kumar *et al.*, 2016). Altogether, more studies are needed to define whether other ZIKV NS proteins block the immune system. Given the limitations of overexpression systems, conclusions are difficult to be drawn apart from the clear evidence presented for NS5.

Reverse genetic experiments could be used to generate mutant or chimeric viruses to reveal the role of ZIKV proteins in counteracting the immune system. In this context, different cell lines could be explored alongside animal models. In addition, viral counterdefence mechanisms could be further explored

at the level of RLR/TLR sensing as well as humoral- and T cell-mediated responses. Finally, it would be interesting to investigate whether some of these mechanisms contribute to ZIKV pathogenesis by providing infection across the placental barrier and foetal infection.

We showed that some NS5 mutations found only in the current ZIKV epidemic strains did not affect its ability to block ISRE induction (Figure 22C). These mutations were previously predicted to be unlikely to affect NS5's functions (Faria *et al.*, 2016). Importantly, we confirmed this prediction experimentally with regards to its role in blocking type I IFN signalling. There are, however, several other major differences between NS5 proteins from American/Asian and African strains of ZIKV. Hence, comparative studies could provide further insights into putatively different functions employed by NS5 proteins from different ZIKV genotypes and strains.

These NS5 mutations are found in close proximity to conserved residues important for MTase and RdRp interdomain interactions – based on a JEV NS5 full-length structure (Lu and Gong, 2013). Indeed, the ZIKV NS5 full-length structure was recently shown to be more closely related to the NS5 structure from JEV than that of DENV NS5 (Zhao *et al.*, 2017).

In fact, in terms of aminoacid sequence, ZIKV NS5 can be grouped along with encephalopathogenic flaviviruses (e.g. WNV and JEV), whereas ZIKV groups with DENV in respect to its surface E protein (Barba-Spaeth *et al.*, 2016). Given these observations, it is tempting to speculate that ZIKV infection and humoral responses may resemble those of DENV while its replication and fitness capabilities are similar to other encephalitic viruses.

Inhibition of JAK/STAT mediated by ZIKV NS5 was unaffected by a CAP1 MTase mutant. This result suggests its conserved MTase residue (E218A) may not be involved in protein-protein interactions. We predict protein-protein interactions are likely to be relevant for NS5-mediated JAK/STAT inhibition.

Given this idea, we asked whether protein localisation could disrupt NS5's inhibitory activity. Flaviviruses replicate in the cytoplasm; yet, their NS5 proteins are nuclear. The reasons for this are unclear (Lopez-Denman and Mackenzie, 2017). In terms of the inhibition of the immune system, one study suggested that nuclear localisation is not required to block IFN I signalling (Kumar *et al.*, 2013). Another recent study demonstrated that DENV NS5 nuclear localisation affects RIG-I splicing leading to the accumulation of RIG-I immature pre-mRNA (De Maio *et al.*, 2016).

Here, we identified and validated the NLS of ZIKV NS5 (Figure 22A and B) based on a previous study using DENV (Pryor *et al.*, 2007). We demonstrated that NS5 nuclear localisation does not affect NS5's ability to block JAK/STAT signalling (Figure 22C). It will be relevant to study whether this subcellular localisation could also affect the splicing of other immune-related genes and/or affect RLR/TLR sensing.

We found that ZIKV NS5 WT and NLS mutants can both block ISRE induction (Figure 22C). WT NS5 proteins from flaviviruses have the ability to shuttle between the nucleus and cytoplasm through NLS and Nuclear Export Signals (NES) (Lopez-Denman and Mackenzie, 2017). Therefore, we suggest NS5 blocks the activity of human STATs in its cytoplasmic localisation. This could be further verified by generating an NS5 construct mutant for its NES.

A closer inspection of NS5's nuclear localisation revealed the presence of nuclear speckles (not shown). Grant *et al*. (2016) also observed these speckles, which appear to be exclusive for ZIKV and are not visible for NS5 from other tested flaviviruses. By using FRAP (Fluorescence Recovery After Photobleaching), our group observed that these speckles are highly dynamic and are thus unlikely to be surrounded by membranes (not shown). It would be interesting to characterise the sub-nuclear localisations of ZIKV NS5 in comparison with NS5 proteins from other flaviviruses and explore their roles in viral replication and/or immune system counteraction.

In summary, we provided data that ZIKV replication generates RLR agonists. Our *in vitro* assays suggest that RIG-I is the main RLR sensor that detects ZIKV RNAs. For future studies, it would be interesting to sequence and characterise the ZIKV-derived 5'ppp-bearing RNAs that trigger RIG-I. Our iCLIP protocol could also be used to investigate whether MDA5 also binds to ZIKV RNAs.

We observed that ZIKV NS5 strongly blocks JAK/STAT signalling. The mechanisms that NS5 employs to target STAT2 and phospho-STAT1 remain to be identified. We demonstrated that ZIKV NS5 contains a functional NLS. The role of its nuclear localisation requires further studies. In addition, other putative mechanisms of inhibition of the immune system by ZIKV proteins await exploitation.

The flaviviral NS5 protein is the longest viral protein containing two important domains: CAP1 MTase and RdRp (King *et al.*, 2012). It is also a potent inhibitor of the human immune system as previously discussed. These roles

seem to be very well conserved amongst flaviviruses. NS5 therefore is an interesting target for drug design and vaccine development against flaviviruses.

CHAPTER 6

6 CONCLUSIONS

We generated and validated mouse monoclonal antibodies against hMDA5. More than 20 mouse ascites were tested and many were found to be specific in WB. Ascites 15 and 16 successfully IPed endogenous MDA5 protein. The purity of the ascites, however, limited their use in IF. For example, ascites 15 and 16 detected filamentous structures in cells in the presence of V-EMCV-RNA; however, by using a HEK293 MDA5 KO cell line, we found that these structures do not correspond to MDA5. In sum, several of the antibodies we generated are reliable to detect MDA5 by WB and work in IP assays, but require further validation for IF assays.

Next, we purified some MDA5 mAbs from hybridoma cell culture supernatants. We found that mAbs 15, 16, and 17 detect specific signals for MDA5 at endogenous expression level by WB. mAb 17 was the most sensitive in this technique. Furthermore, it detected several other bands suggestive of post-translational modifications as well as cleavage and/or alternative translation products. The canonical protein and all other putative forms were readily detectable under IFN-inducing conditions and after treatment with recombinant IFN. mAbs 15 and 16 also detected alternative MDA5 forms upon overexpression. The specificity of the antibodies was validated by siRNAs and by using the HEK293.ΔIFIH1 MDA5 KO cell line. All mAbs recognise an epitope within the helicase domain. Taken together, we generated purified MDA5 mAbs

that detected hMDA5 with high specificity. In addition, MDA5 may be controlled or regulated through the generation of modified or cleaved forms of the protein.

The existence of truncated MDA5 products was also supported by the presence of truncated RNAs species on the MDA5 KO cell line. This cell line lacks the annotated promoter, transcription start site (TSS), and the canonical protein start codon. The presence of these RNA species also suggested the existence of an alternative, IFN-independent MDA5 promoter. Further studies are required to confirm these predictions and to show whether a truncated MDA5 protein is expressed and functional.

Purified mAbs 15 and 16 were specific in IF and detected MDA5 in WT but not in KO human cells. MDA5 staining was found across the cytoplasm after cells received recombinant IFN-I or IFN-inducing treatments. Together with the WB data, these results confirm that MDA5 is an ISG and that its expression is very low or undetectable in unstimulated cells.

In primary human skin fibroblasts, a punctate staining was observed in IF assays using mAbs15 and 16. These structures were present in cells containing EMCV RNA either after V-EMCV-RNA transfection or EMCV infection. Further studies are required to characterise these structures and to determine whether they are related with MDA5 signalling.

To test whether MDA5 binds to RNAs, we employed the iCLIP protocol using 3XFLAG-hMDA5 in 293T cells. We opted for a highly stringent IP protocol to specifically enrich a fraction containing MDA5-RNA complexes. Indeed, we found that high stringency was required, and led a specific and reliable IP protocol was developed.

In these conditions, we detected that MDA5 bound to RNAs upon overexpression. This is the first report demonstrating that MDA5 indeed associates with RNAs in living cells. RNAs binding to MDA5 was seen in cells infected or not with EMCV. This strongly suggests that MDA5 binds cellular RNAs in addition to viral RNAs in these conditions.

Currently, we are preparing samples for deep sequencing of these RNAs. Sequencing will definitely reveal whether MDA5 binds to cellular and/or viral RNAs. In addition, we are now applying this method to endogenous MDA5 by using the antibodies generated in this study.

By using RNase A titrations, we demonstrated that MDA5 binds to RNAs of different - including long - sizes. This suggests that MDA5 is likely to form HMW complexes with associated RNAs in living cells. We are now aiming to sequence long (>100bp) RNAs bound by MDA5, which will also facilitate genome mapping by bioinformatics.

In addition to the RNA binding data, we found that 3XFLAG-hMDA5 overexpression led to the induction of the *IFN-β* promoter. We tentatively correlated the IFN-I induction with cellular RNA binding (virus-infected cells were not used in these experiments). This suggestion is reinforced by using an ATP-hydrolysis mutant (K335A) construct previously shown by others to confer higher affinity for dsRNAs in cell-free systems. We observed that the mutant construct bound to more RNAs than the WT construct and induced more IFN-I. At the same time, both WT and mutant constructs expressed proteins at comparable levels. Thus, hMDA5 is likely activated by cellular RNAs to induce type I IFNs.

We also developed two RNA transfection-based bioassays. The first assay involved RNA transfection into HEK293 cells stably expressing the *IFN-β*

promoter. In order to observe MDA5-mediated responses, HEK293 cells had to be pre-treated with IFN prior to transfection. In this setting, we demonstrated that cellular RNAs from uninfected cells trigger IFN-I in an MDA5- and MAVS-dependent manners.

Similar findings were made after transfection of total RNAs from human tissues. Importantly, we found that human brain RNAs had MDA5-immunostimulatory potential. Furthermore, human testis RNA had the most potent MDA5-dependent activity. Interestingly, mouse brain RNAs induced IFN-I with a mixed MDA5/RIG-I-dependency. Different levels or absence of immunostimulatory potential amid several human tissue RNAs demonstrated the specificity of the protocol.

The second bioassay made use of primary human skin fibroblasts and involved collection of supernatants after transfection. Fibroblasts from AGS patients revealed that cells containing *IFIH1* and *ADAR1* mutations were more responsive to RNA transfections. In comparison, WT and AGS cells containing a *SAMHD1* mutation induced weaker IFN-I responses. However, this bioassay was less specific to RNA transfection than the bioassay involving HEK293 cells. Nonetheless, transfection of human fibroblasts further supported the notion that cellular RNAs contain MDA5-stimulatory potential.

We also used the bioassay in HEK293 cells in a different project. We found that ZIKV replication in A549 cells led to the accumulation of both MDA5 and RIG-I RNA agonists. Of note, the immunostimulatory activity was largely dependent on RIG-I and on the presence 5’-phosphates, suggesting a minor contribution of MDA5. Further studies involving virus infection and, perhaps,

animal models are needed to elucidate the roles of RLRs in the recognition of ZIKV.

We performed a mini-screen by testing constructs expressing ZIKV proteins for their ability to block type I IFN signalling. We found that NS5 is a potent inhibitor of this pathway. We collected data showing that NS5 targeted total STAT2 and phospho-STAT1. The mini-screen did not identify other ZIKV proteins that had clear inhibitory activities. Studies involving mutant and chimeric viruses could expand these results and contribute to a more detailed understanding of how ZIKV proteins block JAK/STAT and, possibly, other antiviral signalling pathways.

We identified the ZIKV NS5 NLS and found that NS5 is mostly located in the nucleus, where it formed speckles of unknown functions. A NLS mutant NS5 protein found in the cytoplasm retained activity to block JAK/STAT signalling. This suggests that NS5 targets STAT1 and 2 in the cytoplasm.

Our findings also revealed that two mutations found in NS5 from ZIKV strains from the current outbreak did not influence the proteins ability to block type I IFN signalling. Similarly, a construct containing a mutation in its MTase domain remains active. Therefore, NS5 blocks JAK/STAT signalling independently of its nuclear localisation, virus strain, and MTase activity.

In conclusion, this study provides validated reagents to explore the MDA5 signalling pathway. Indeed, our MDA5-specific antibodies are of great interest to the field and have already been distributed to multiple laboratories in the UK, Europe and USA. Our characterisation of MDA5 revealed several interesting aspects of its activation by RNA and led to new open questions. With some additional experiments, we expect that some of these novel findings will provide

a more detailed understanding of MDA5's role in the context of virus infection, as well as autoinflammatory and autoimmune diseases. It is already clear how divergent MDA5 is from RIG-I in terms of RNA sensing, dynamics, and control. Yet, much less is known about MDA5 than RIG-I. Hence, the protocols and reagents described here will be useful tools for interesting future studies of MDA5, including its physiological agonists.

REFERENCES

Ablasser, A. *et al.* (2009) 'RIG-I-dependent sensing of poly(dA:dT) through the induction of an RNA polymerase III–transcribed RNA intermediate', *Nature Immunology*. Nature Publishing Group, 10(10), pp. 1065–1072. doi: 10.1038/ni.1779.

Ablasser, A. *et al.* (2013) 'Cell intrinsic immunity spreads to bystander cells via the intercellular transfer of cGAMP', *Nature*, 503(7477), pp. 530–534. doi: 10.1038/nature12640.

Aguirre, S. *et al.* (2012) 'DENV Inhibits Type I IFN Production in Infected Cells by Cleaving Human STING', *PLoS Pathogens*, 8(10). doi: 10.1371/journal.ppat.1002934.

Aguirre, S. *et al.* (2017) 'Dengue virus NS2B protein targets cGAS for degradation and prevents mitochondrial DNA sensing during infection', *Nature Microbiology*. Nature Publishing Group, 2(March), p. 17037. doi: 10.1038/nmicrobiol.2017.37.

Almine, J. F. *et al.* (2017) 'IFI16 and cGAS cooperate in the activation of STING during DNA sensing in human keratinocytes', *Nature Communications*, 8, p. 14392. doi: 10.1038/ncomms14392.

Arimoto, K. -i. *et al.* (2007) 'Negative regulation of the RIG-I signaling by the ubiquitin ligase RNF125', *Proceedings of the National Academy of Sciences*, 104(18), pp. 7500–7505. doi: 10.1073/pnas.0611551104.

Ashour, J. *et al.* (2009) 'NS5 of Dengue Virus Mediates STAT2 Binding and Degradation', *Journal of Virology*, 83(11), pp. 5408–5418. doi: 10.1128/JVI.02188-08.

Ashour, J. *et al.* (2010) 'Mouse STAT2 restricts early dengue virus replication', *Cell Host and Microbe*, 8(5), pp. 410–421. doi: 10.1016/j.chom.2010.10.007.

Balsitis, S. J. *et al.* (2010) 'Lethal antibody enhancement of dengue disease in mice is prevented by Fc modification', *PLoS Pathogens*, 6(2). doi: 10.1371/journal.ppat.1000790.

Barba-Spaeth, G. *et al.* (2016) 'Structural basis of potent Zika-dengue virus antibody cross-neutralization.', *Nature*. Nature Publishing Group, 536(7614), pp. 48–53. doi: 10.1038/nature18938.

Bardina, S. V. *et al.* (2017) 'Enhancement of Zika virus pathogenesis by preexisting antiflavivirus immunity', *Science*, 356(6334), pp. 175–180. doi: 10.1126/science.aal4365.

Barral, P. M. *et al.* (2007) 'MDA-5 Is Cleaved in Poliovirus-Infected Cells', *Journal of Virology*, 81(8), pp. 3677–3684. doi: 10.1128/JVI.01360-06.

Bender, S. *et al.* (2015) 'Activation of Type I and III Interferon Response by

Mitochondrial and Peroxisomal MAVS and Inhibition by Hepatitis C Virus', *PLoS Pathogens*, 11(11), pp. 1–30. doi: 10.1371/journal.ppat.1005264.

Berke, I. C. *et al.* (2012) 'MDA5 assembles into a polar helical filament on dsRNA.', *Proceedings of the National Academy of Sciences of the United States of America*, 109(45), pp. 18437–41. doi: 10.1073/pnas.1212186109.

Best, S. M. *et al.* (2005) 'Inhibition of interferon-stimulated JAK-STAT signaling by a tick-borne flavivirus and identification of NS5 as an interferon antagonist.', *Journal of virology*, 79(20), pp. 12828–12839. doi: 10.1128/JVI.79.20.12828-12839.2005.

Bowen, J. R. *et al.* (2017) 'Zika Virus Antagonizes Type I Interferon Responses during Infection of Human Dendritic Cells', *PLoS Pathogens*, 13(2), pp. 1–30. doi: 10.1371/journal.ppat.1006164.

Bridgeman, A. *et al.* (2015) 'Viruses transfer the antiviral second messenger cGAMP between cells', *Science*, 349(6253), pp. 1228–1232. doi: 10.1126/science.aab3632.

Brubaker, S. W. *et al.* (2014) 'A bicistronic MAVS transcript highlights a class of truncated variants in antiviral immunity', *Cell*. Elsevier Inc., 156(4), pp. 800–811. doi: 10.1016/j.cell.2014.01.021.

Brubaker, S. W. *et al.* (2015) *Innate Immune Pattern Recognition: A Cell Biological Perspective*, *Annual Review of Immunology*. doi: 10.1146/annurev-immunol-032414-112240.

Bruns, A. M. *et al.* (2014) 'The Innate Immune Sensor LGP2 Activates Antiviral Signaling by Regulating MDA5-RNA Interaction and Filament Assembly', *Molecular Cell*. Elsevier Inc., 55(5), pp. 771–781. doi: 10.1016/j.molcel.2014.07.003.

Cao, X. *et al.* (2015) 'MDA5 plays a critical role in interferon response during hepatitis C virus infection', *Journal of Hepatology*, 62(4), pp. 771–778. doi: 10.1016/j.jhep.2014.11.007.

Chan, Y. K. and Gack, M. U. (2016) 'A phosphomimetic-based mechanism of dengue virus to antagonize innate immunity', *Nature Immunology*, 17(5), pp. 523–530. doi: 10.1038/ni.3393.

Chaudhary, V. *et al.* (2017) 'Selective activation of interferon-γ signaling by Zika virus NS5 protein', *Journal of Virology*, (May), p. JVI.00163-17. doi: 10.1128/JVI.00163-17.

Chen, L.-L. and Yang, L. (2017) 'ALUternative Regulation for Gene Expression', *Trends in Cell Biology*, 27(7), pp. 480–490. doi: 10.1016/j.tcb.2017.01.002.

Chen, Q. *et al.* (2016) 'Carcinoma–astrocyte gap junctions promote brain metastasis by cGAMP transfer', *Nature*, 533(7604), pp. 493–498. doi: 10.1038/nature18268.

Chiang, C. and Gack, M. U. (2017) ‘Post-translational Control of Intracellular Pathogen Sensing Pathways’, *Trends in Immunology*. Elsevier Ltd, 38(1), pp. 39–52. doi: 10.1016/j.it.2016.10.008.

Chiappinelli, K. B. *et al.* (2015) ‘Inhibiting DNA Methylation Causes an Interferon Response in Cancer via dsRNA Including Endogenous Retroviruses’, *Cell*, 162(5), pp. 974–986. doi: 10.1016/j.cell.2015.07.011.

Chiu, Y. H., MacMillan, J. B. and Chen, Z. J. (2009) ‘RNA Polymerase III Detects Cytosolic DNA and Induces Type I Interferons through the RIG-I Pathway’, *Cell*. Elsevier Ltd, 138(3), pp. 576–591. doi: 10.1016/j.cell.2009.06.015.

Choi, S. J. *et al.* (2016) ‘HDAC 6 regulates cellular viral RNA sensing by deacetylation of RIG-I’, *Embo*, 35(4), pp. 1–14. doi: 10.15252/embj.201592586.

Clausen, M. P. *et al.* (2013) ‘Pathways to optical STED microscopy’, *NanoBioImaging*, 1(1), pp. 1–12. doi: 10.2478/nbi-2013-0001.

Cong, L. *et al.* (2013) ‘Multiplex genome engineering using CRISPR/Cas systems.’, *Science (New York, N.Y.)*, 339(6121), pp. 819–23. doi: 10.1126/science.1231143.

Crow, Y. J. and Manel, N. (2015) ‘Aicardi–Goutières syndrome and the type I interferonopathies’, *Nature Reviews Immunology*. Nature Publishing Group, 15(7), pp. 429–440. doi: 10.1038/nri3850.

Cugola, F. R. *et al.* (2016) ‘The Brazilian Zika virus strain causes birth defects in experimental models’, *Nature*. Nature Publishing Group, 534(7606), pp. 267–271. doi: 10.1038/nature18296.

Cumberworth, S. L. *et al.* (2017) ‘Inhibition of type I interferon induction and signalling by mosquito-borne flaviviruses’, *Cellular Microbiology*, 19(5), pp. 1–8. doi: 10.1111/cmi.12737.

Daffis, S. *et al.* (2010) ‘2’-O methylation of the viral mRNA cap evades host restriction by IFIT family members.’, *Nature*. Nature Publishing Group, 468(7322), pp. 452–6. doi: 10.1038/nature09489.

Deddouche, S. *et al.* (2014) ‘Identification of an LGP2-associated MDA5 agonist in picornavirus-infected cells’, *eLife*, 3, p. e01535. doi: 10.7554/eLife.01535.

Dejnirattisai, W. *et al.* (2016) ‘Dengue virus sero-cross-reactivity drives antibody-dependent enhancement of infection with zika virus’, *Nature Immunology*. Nature Publishing Group, 17(9), pp. 1102–1108. doi: 10.1038/ni.3515.

Devarkar, S. C. *et al.* (2016) ‘Structural basis for m7G recognition and 2′-O-methyl discrimination in capped RNAs by the innate immune receptor RIG-I’, *Proceedings of the National Academy of Sciences*, 113(3), pp. 596–601. doi: 10.1073/pnas.1515152113.

Diamond, M. S. (2003) ‘Evasion of innate and adaptive immunity by flaviviruses’, *Immunology and Cell Biology*, 81(3), pp. 196–206. doi: 10.1046/j.1440-1711.2003.01157.x.

Dixit, E. *et al.* (2010) ‘Peroxisomes Are Signaling Platforms for Antiviral Innate Immunity’, *Cell*. Elsevier Ltd, 141(4), pp. 668–681. doi: 10.1016/j.cell.2010.04.018.

Dong, H. *et al.* (2014) ‘Flavivirus RNA methylation’, *Journal of General Virology*, 95(PART 4), pp. 763–778. doi: 10.1099/vir.0.062208-0.

Eggeling, C., Willig, K. I. and Barrantes, F. J. (2013) ‘STED microscopy of living cells - New frontiers in membrane and neurobiology’, *Journal of Neurochemistry*, 126(2), pp. 203–212. doi: 10.1111/jnc.12243.

Errett, J. S. *et al.* (2013) ‘The essential, nonredundant roles of RIG-I and MDA5 in detecting and controlling West Nile virus infection’, *J Virol*, 87(21), pp. 11416–11425. doi: 10.1128/JVI.01488-13.

Espada-Murao, L. A. and Morita, K. (2011) ‘Delayed Cytosolic Exposure of Japanese Encephalitis Virus Double-Stranded RNA Impedes Interferon Activation and Enhances Viral Dissemination in Porcine Cells’, *Journal of Virology*, 85(13), pp. 6736–6749. doi: 10.1128/JVI.00233-11.

Faria, N. R. *et al.* (2016) ‘Zika virus in the Americas: Early epidemiological and genetic findings’, *Science*, 352(6283), pp. 345–349. doi: 10.1126/science.aaf5036.

Feng, Q. *et al.* (2012) ‘MDA5 Detects the Double-Stranded RNA Replicative Form in Picornavirus-Infected Cells’, *Cell Reports*. The Authors, 2(5), pp. 1187–1196. doi: 10.1016/j.celrep.2012.10.005.

Feng, Q. *et al.* (2014) ‘Enterovirus 2Apro targets MDA5 and MAVS in infected cells.’, *Journal of virology*, 88(6), pp. 3369–78. doi: 10.1128/JVI.02712-13.

Fernandez-Garcia, M. D. *et al.* (2009) ‘Pathogenesis of Flavivirus Infections: Using and Abusing the Host Cell’, *Cell Host and Microbe*. Elsevier Inc., 5(4), pp. 318–328. doi: 10.1016/j.chom.2009.04.001.

Franchi, L., Muñoz-Planillo, R. and Núñez, G. (2012) ‘Sensing and reacting to microbes through the inflammasomes’, *Nature Immunology*, 13(4), pp. 325–332. doi: 10.1038/ni.2231.

Fredericksen, B. L. *et al.* (2008) ‘Establishment and Maintenance of the Innate Antiviral Response to West Nile Virus Involves both RIG-I and MDA5 Signaling through IPS-1’, *Journal of Virology*, 82(2), pp. 609–616. doi: 10.1128/JVI.01305-07.

Fu, J. *et al.* (2011) ‘MDA5 is SUMOylated by PIAS2β in the upregulation of Type I interferon signaling’, *Molecular Immunology*. Elsevier Ltd, 48(4), pp. 415–422. doi: 10.1016/j.molimm.2010.09.003.

Gack, M. U. *et al.* (2007) 'TRIM25 RING-finger E3 ubiquitin ligase is essential for RIG-I-mediated antiviral activity', *Nature*, 446(7138), pp. 916–920. doi: 10.1038/nature05732.

Gack, M. U. *et al.* (2008) 'Roles of RIG-I N-terminal tandem CARD and splice variant in TRIM25-mediated antiviral signal transduction.', *Proceedings of the National Academy of Sciences of the United States of America*, 105(43), pp. 16743–16748. doi: 10.1073/pnas.0804947105.

Gack, M. U. *et al.* (2010) 'Phosphorylation-Mediated Negative Regulation of RIG-I Antiviral Activity', *Journal of Virology*, 84(7), pp. 3220–3229. doi: 10.1128/JVI.02241-09.

Gao, D. *et al.* (2015) 'Activation of cyclic GMP-AMP synthase by self-DNA causes autoimmune diseases', *Proceedings of the National Academy of Sciences*, 112(42), pp. E5699–E5705. doi: 10.1073/pnas.1516465112.

Gentili, M. *et al.* (2015) 'Transmission of innate immune signaling by packaging of cGAMP in viral particles', *Science*, 349(6253), pp. 1232–1236. doi: 10.1126/science.aab3628.

Gitlin, L. *et al.* (2006) 'Essential role of mda-5 in type I IFN responses to polyriboinosinic:polyribocytidylic acid and encephalomyocarditis picornavirus.', *Proceedings of the National Academy of Sciences of the United States of America*, 103(22), pp. 8459–64. doi: 10.1073/pnas.0603082103.

Gorman, J. A. *et al.* (2017) 'The A946T variant of the RNA sensor IFIH1 mediates an interferon program that limits viral infection but increases the risk for autoimmunity', *Nature Immunology*, 18(7). doi: 10.1038/ni.3766.

Goubau, D. *et al.* (2014) 'Antiviral immunity via RIG-I-mediated recognition of RNA bearing 5′-diphosphates', *Nature*, 514(7522), pp. 372–375. doi: 10.1038/nature13590.

Goubau, D. *et al.* (2015) 'Europe PMC Funders Group Antiviral immunity via RIG-I-mediated recognition of RNA bearing 5 ′ -diphosphates', 514(7522), pp. 372–375. doi: 10.1038/nature13590.Antiviral.

Govero, J. *et al.* (2016) 'Zika virus infection damages the testes in mice', *Nature*. Nature Publishing Group, 540(7633), pp. 438–442. doi: 10.1038/nature20556.

Grant, A. *et al.* (2016) 'Zika Virus Targets Human STAT2 to Inhibit Type i Interferon Signaling', *Cell Host and Microbe*, 19(6), pp. 882–890. doi: 10.1016/j.chom.2016.05.009.

Halstead, S. B. (2014) 'Dengue Antibody-Dependent Enhancement : Knowns and Unknowns', *Microbiology Spectrum*, 2(6), pp. 1–18. doi: 10.1128/microbiolspec.AID-0022-2014.Correspondence.

Hamel, R. *et al.* (2015) 'Biology of Zika Virus Infection in Human Skin Cells', *Journal of Virology*, 89(17), pp. 8880–8896. doi: 10.1128/JVI.00354-15.

Hao, Q. *et al.* (2015) 'A non-canonical role of the p97 complex in RIG-I antiviral signaling', *The EMBO Journal*, 34(23), pp. 2903–2920. doi: 10.15252/embj.201591888.

Hartner, J. C. *et al.* (2009) 'ADAR1 is essential for the maintenance of hematopoiesis and suppression of interferon signaling', *Nature Immunology*, 10(1), pp. 109–115. doi: 10.1038/ni.1680.

He, S. *et al.* (2015) 'Viral pseudo-enzymes activate RIG-I via deamidation to evade cytokine production', *Molecular Cell*. Elsevier Inc., 58(1), pp. 134–146. doi: 10.1016/j.molcel.2015.01.036.

Horner, S. M. *et al.* (2011) 'Mitochondrial-associated endoplasmic reticulum membranes {(MAM)} form innate immune synapses and are targeted by hepatitis C virus.', *Proc. Natl. Acad. Sci. {U.S.A.}*, 108(35), pp. 14590–14595. doi: 10.1073/pnas.1110133108.

Hornung, V. *et al.* (2006) '5'-Triphosphate RNA Is the Ligand for RIG-I', *Science*, 314(5801), pp. 994–997. doi: 10.1126/science.1132505.

Hornung, V. *et al.* (2006) '5'-Triphosphate RNA Is the Ligand for RIG-I', *Science*, 314(5801), pp. 994–997. doi: 10.1126/science.1132505.

Hornung, V. *et al.* (2014) 'OAS proteins and cGAS: unifying concepts in sensing and responding to cytosolic nucleic acids', *Nature Reviews Immunology*. Nature Publishing Group, 14(8), pp. 521–528. doi: 10.1038/nri3719.

Hou, F. *et al.* (2011) 'MAVS forms functional prion-like aggregates to activate and propagate antiviral innate immune response', *Cell*. Elsevier, 146(3), pp. 448–461. doi: 10.1016/j.cell.2011.06.041.

Hu, M.-M. *et al.* (2017) 'Innate immunity to RNA virus is regulated by temporal and reversible sumoylation of RIG-I and MDA5', *The Journal of Experimental Medicine*, 214(4), pp. 973–989. doi: 10.1084/jem.20161015.

Huang, S. L. *et al.* (2000) 'Cloning and characterization of a novel retinoid-inducible gene 1(RIG1) deriving from human gastric cancer cells', *Mol Cell Endocrinol*, 159(1–2), pp. 15–24. doi: S0303-7207(99)00207-5 [pii].

Huppertz, I. *et al.* (2014) 'iCLIP: Protein-RNA interactions at nucleotide resolution', *Methods*, 65(3), pp. 274–287. doi: 10.1016/j.ymeth.2013.10.011.

Jiang, F. *et al.* (2011) 'Structural basis of RNA recognition and activation by innate immune receptor RIG-I', *Nature*, 479(7373), pp. 423–427. doi: 10.1038/nature10537.

Jiang, X. *et al.* (2012a) 'Ubiquitin-Induced Oligomerization of the RNA Sensors RIG-I and MDA5 Activates Antiviral Innate Immune Response', *Immunity*, 36(6), pp. 973–959. doi: 10.1016/j.immuni.2012.03.022.

Jiang, X. *et al.* (2012b) 'Ubiquitin-Induced Oligomerization of the RNA Sensors RIG-I and MDA5 Activates Antiviral Innate Immune Response', *Immunity*, 36(6),

pp. 959–973. doi: 10.1016/j.immuni.2012.03.022.

Jønsson, K. L. *et al.* (2017) 'IFI16 is required for DNA sensing in human macrophages by promoting production and function of cGAMP', *Nature Communications*, 8, p. 14391. doi: 10.1038/ncomms14391.

Kang, D. *et al.* (2002) 'mda-5: An interferon-inducible putative RNA helicase with double-stranded RNA-dependent ATPase activity and melanoma growth-suppressive properties.', *Proceedings of the National Academy of Sciences of the United States of America*, 99(2), pp. 637–42. doi: 10.1073/pnas.022637199.

Kato, H. *et al.* (2006) 'Differential roles of MDA5 and RIG-I helicases in the recognition of RNA viruses', *Nature*, 441(7089), pp. 101–105. doi: 10.1038/nature04734.

Kato, H. *et al.* (2008) 'Length-dependent recognition of double-stranded ribonucleic acids by retinoic acid–inducible gene-I and melanoma differentiation–associated gene 5', *The Journal of Experimental Medicine*, 205(7), pp. 1601–1610. doi: 10.1084/jem.20080091.

Katzelnick, L. C., Coloma, J. and Harris, E. (2017) 'Dengue: knowledge gaps, unmet needs, and research priorities', *The Lancet Infectious Diseases*, 17(3), pp. e88–e100. doi: 10.1016/S1473-3099(16)30473-X.

King, A. M. Q. *et al.* (2012) 'Flaviviridae - Ninth Report of the International Committee on Taxonomy of Viruses', in *Virus Taxonomy*, pp. 1003–1020. doi: 10.1016/B978-0-12-384684-6.00086-0.

Kolakofsky, D., Kowalinski, E. V. A. and Cusack, S. (2012) 'A structure-based model of RIG-I activation', pp. 2118–2127. doi: 10.1261/rna.035949.112.2118.

Kovacsovics, M. *et al.* (2002) 'Overexpression of Helicard, a CARD-containing helicase cleaved during apoptosis, accelerates DNA degradation', *Current Biology*, 12(10), pp. 838–843. doi: 10.1016/S0960-9822(02)00842-4.

Kowalinski, E. *et al.* (2011a) 'Structural basis for the activation of innate immune pattern-recognition receptor RIG-I by viral RNA', *Cell*, 147(2), pp. 423–435. doi: 10.1016/j.cell.2011.09.039.

Kowalinski, E. *et al.* (2011b) 'Structural basis for the activation of innate immune pattern-recognition receptor RIG-I by viral RNA', *Cell*. Elsevier Inc., 147(2), pp. 423–435. doi: 10.1016/j.cell.2011.09.039.

Kumar, A. *et al.* (2013) 'Nuclear Localization of Dengue Virus Nonstructural Protein 5 Does Not Strictly Correlate with Efficient Viral RNA Replication and Inhibition of Type I Interferon Signaling', *Journal of Virology*, 87(8), pp. 4545–4557. doi: 10.1128/JVI.03083-12.

Kumar, A. *et al.* (2016) 'Zika virus inhibits type-I interferon production and downstream signaling', *EMBO reports*, 17(12), pp. 1766–1775. doi: 10.15252/embr.201642627.

Kuno, G. and Chang, G. J. J. (2007) 'Full-length sequencing and genomic characterization of Bagaza, Kedougou, and Zika viruses', *Archives of Virology*, 152(4), pp. 687–696. doi: 10.1007/s00705-006-0903-z.

Lang, X. *et al.* (2016) 'TRIM65-catalized ubiquitination is essential for MDA5-mediated antiviral innate immunity', *The Journal of Experimental Medicine*, p. jem.20160592. doi: 10.1084/jem.20160592.

Langereis, M. A., Feng, Q. and van Kuppeveld, F. J. (2013) 'MDA5 localizes to stress granules, but this localization is not required for the induction of type I interferon.', *Journal of virology*, 87(11), pp. 6314–25. doi: 10.1128/JVI.03213-12.

Laurent-Rolle, M. *et al.* (2010) 'The NS5 Protein of the Virulent West Nile Virus NY99 Strain Is a Potent Antagonist of Type I Interferon-Mediated JAK-STAT Signaling', *Journal of Virology*, 84(7), pp. 3503–3515. doi: 10.1128/JVI.01161-09.

Laurent-Rolle, M. *et al.* (2014) 'The interferon signaling antagonist function of yellow fever virus NS5 protein is activated by type i interferon', *Cell Host and Microbe*, 16(3), pp. 314–327. doi: 10.1016/j.chom.2014.07.015.

Lazear, H. M. *et al.* (2016) 'A Mouse Model of Zika Virus Pathogenesis', *Cell Host & Microbe*, 19(5), pp. 1–11. doi: 10.1016/j.chom.2016.03.010.

Li, C. *et al.* (2016) 'Correction: Zika Virus Disrupts Neural Progenitor Development and Leads to Microcephaly in Mice (Cell Stem Cell (2016) 19(5) (672) (S1934590916300844) (10.1016/j.stem.2016.04.017))', *Cell Stem Cell*. Elsevier, 19(5), p. 672. doi: 10.1016/j.stem.2016.10.017.

Li, T. *et al.* (2016) 'Antitumor Activity of cGAMP via Stimulation of cGAS-cGAMP-STING-IRF3 Mediated Innate Immune Response', *Scientific Reports*. Nature Publishing Group, 6(1), p. 19049. doi: 10.1038/srep19049.

Li, X.-D. *et al.* (2005) 'Hepatitis C virus protease NS3/4A cleaves mitochondrial antiviral signaling protein off the mitochondria to evade innate immunity', *Proceedings of the National Academy of Sciences*, 102(49), pp. 17717–17722. doi: 10.1073/pnas.0508531102.

Li, X.-D. *et al.* (2013) 'Pivotal Roles of cGAS-cGAMP Signaling in Antiviral Defense and Immune Adjuvant Effects', *Science*, 341(6152). Available at: http://science.sciencemag.org/content/341/6152/1390/tab-pdf (Accessed: 26 June 2017).

Liddicoat, B. J. *et al.* (2015) 'RNA editing by ADAR1 prevents MDA5 sensing of endogenous dsRNA as nonself', *Science*, 349(6252), pp. 1115–1120. doi: 10.1126/science.aac7049.

Lincez, P. J., Shanina, I. and Horwitz, M. S. (2015) 'Reduced expression of the MDA5 Gene IFIH1 prevents autoimmune diabetes', *Diabetes*, 64(6), pp. 2184–2193. doi: 10.2337/db14-1223.

Lindenbach, B. D. and Rice, C. M. (1999) 'Genetic Interaction of Flavivirus Nonstructural Proteins NS1 and NS4A as a Determinant of Replicase Function', 73(6), pp. 4611–4621.

Liu, S. *et al.* (2015) 'Phosphorylation of innate immune adaptor proteins MAVS, STING, and TRIF induces IRF3 activation', *Science*, 347(6227), p. aaa2630-aaa2630. doi: 10.1126/science.aaa2630.

Loo, Y.-M. *et al.* (2008) 'Distinct RIG-I and MDA5 Signaling by RNA Viruses in Innate Immunity', *Journal of Virology*, 82(1), pp. 335–345. doi: 10.1128/JVI.01080-07.

Loo, Y.-M. *et al.* (2008) 'Distinct RIG-I and MDA5 signaling by RNA viruses in innate immunity.', *Journal of virology*, 82(1), pp. 335–45. doi: 10.1128/JVI.01080-07.

Looney, B. M. *et al.* (2015) 'Effects of Type 1 Diabetes-Associated IFIH1 Polymorphisms on MDA5 Function and Expression', *Current Diabetes Reports*, 15(11), pp. 1–11. doi: 10.1007/s11892-015-0656-8.

Lopez-Denman, A. J. and Mackenzie, J. M. (2017) 'The IMPORTance of the nucleus during flavivirus replication', *Viruses*, 9(1), pp. 1–11. doi: 10.3390/v9010014.

Louber, J. *et al.* (2014) 'RIG-I self-oligomerization is either dispensable or very transient for signal transduction', *PLoS ONE*, 9(9). doi: 10.1371/journal.pone.0108770.

Lu, G. and Gong, P. (2013) 'Crystal Structure of the Full-Length Japanese Encephalitis Virus NS5 Reveals a Conserved Methyltransferase-Polymerase Interface', *PLoS Pathogens*, 9(8). doi: 10.1371/journal.ppat.1003549.

Maharaj, N. P. *et al.* (2012) 'Conventional Protein Kinase C- (PKC-) and PKC- Negatively Regulate RIG-I Antiviral Signal Transduction', *Journal of Virology*, 86(3), pp. 1358–1371. doi: 10.1128/JVI.06543-11.

De Maio, F. A. *et al.* (2016) 'The Dengue Virus NS5 Protein Intrudes in the Cellular Spliceosome and Modulates Splicing', *PLoS Pathogens*, 12(8), pp. 1–29. doi: 10.1371/journal.ppat.1005841.

Malathi, K. *et al.* (2007) 'Small self-RNA generated by RNase L amplifies antiviral innate immunity', *Nature*, 448(7155), pp. 816–819. doi: 10.1038/nature06042.

Mariathasan, S. *et al.* (2006) 'Cryopyrin activates the inflammasome in response to toxins and ATP', *Nature*, 440(7081), pp. 228–232. doi: 10.1038/nature04515.

Meng, J. *et al.* (2017) 'ARRDC4 regulates enterovirus 71-induced innate immune response by promoting K63 polyubiquitination of MDA5 through TRIM65', *Cell Death and Disease*. Nature Publishing Group, 8(6), p. e2866. doi: 10.1038/cddis.2017.257.

Miner, J. J. *et al.* (2016) 'Zika Virus Infection during Pregnancy in Mice Causes Placental Damage and Fetal Demise', *Cell*. Elsevier Inc., 165(5), pp. 1081–1091. doi: 10.1016/j.cell.2016.05.008.

Mlakar, J. *et al.* (2016) 'Zika Virus Associated with Microcephaly', *New England Journal of Medicine*, 374(10), pp. 951–958. doi: 10.1056/NEJMoa1600651.

Mogensen, T. H. (2009) 'Pathogen recognition and inflammatory signaling in innate immune defenses', *Clinical Microbiology Reviews*, 22(2), pp. 240–273. doi: 10.1128/CMR.00046-08.

Moreira, J. *et al.* (2016) 'Sexually acquired Zika virus: A systematic review', *Clinical Microbiology and Infection*. Elsevier Ltd, 23. doi: 10.1016/j.cmi.2016.12.027.

Morrison, J. *et al.* (2013) 'Dengue Virus Co-opts UBR4 to Degrade STAT2 and Antagonize Type I Interferon Signaling', *PLoS Pathogens*, 9(3). doi: 10.1371/journal.ppat.1003265.

Nasirudeen, A. M. A. *et al.* (2011) 'RIG-i, MDA5 and TLR3 synergistically play an important role in restriction of dengue virus infection', *PLoS Neglected Tropical Diseases*, 5(1). doi: 10.1371/journal.pntd.0000926.

Nejentsev, S. *et al.* (2009) 'Protect Against Type 1 Diabetes', 333(April), pp. 387–389.

Ng, C. S. *et al.* (2013) 'Encephalomyocarditis virus disrupts stress granules, the critical platform for triggering antiviral innate immune responses.', *Journal of virology*, 87(17), pp. 9511–22. doi: 10.1128/JVI.03248-12.

Nishikura, K. (2015) 'A-to-I editing of coding and non-coding RNAs by ADARs', *Nature Reviews Molecular Cell Biology*. Nature Publishing Group, 17(2), pp. 83–96. doi: 10.1038/nrm.2015.4.

Nistal-Villán, E. *et al.* (2010) 'Negative role of RIG-I serine 8 phosphorylation in the regulation of interferon-β production', *Journal of Biological Chemistry*, 285(26), pp. 20252–20261. doi: 10.1074/jbc.M109.089912.

Van Nostrand, E. L. *et al.* (2016) 'Robust transcriptome-wide discovery of RNA-binding protein binding sites with enhanced CLIP (eCLIP).', *Nature methods*, 13(November 2015), pp. 1–9. doi: 10.1038/nmeth.3810.

Oda, H. *et al.* (2014) 'Aicardi-goutières syndrome is caused by IFIH1 mutations', *American Journal of Human Genetics*. The American Society of Human Genetics, 95(1), pp. 121–125. doi: 10.1016/j.ajhg.2014.06.007.

Odendall, C. *et al.* (2014) 'Diverse intracellular pathogens activate type III interferon expression from peroxisomes', *Nature Immunology*, 15(8), pp. 717–726. doi: 10.1038/ni.2915.

Överby, A. K. *et al.* (2010) 'Tick-Borne encephalitis virus delays interferon induction and hides its double-stranded RNA in intracellular membrane

vesicles', *Journal of Virology*, 84(17), pp. 8470–8483. doi: 10.1128/JVI.00176-10.

Pålsson-McDermott, E. M. and O'Neill, L. A. J. (2004) 'Signal transduction by the lipopolysaccharide receptor, Toll-like receptor-4', *Immunology*, 113(2), pp. 153–162. doi: 10.1111/j.1365-2567.2004.01976.x.

Patel, J. R. *et al.* (2013) 'ATPase-driven oligomerization of RIG-I on RNA allows optimal activation of type-I interferon.', *EMBO reports*, 14(9), pp. 1–8. doi: 10.1038/embor.2013.102.

Paul, L. M. *et al.* (2016) 'Dengue virus antibodies enhance Zika virus infection', *Clinical & Translational Immunology*. Nature Publishing Group, 5(12), p. e117. doi: 10.1038/cti.2016.72.

Peisley, A. *et al.* (2011) 'Cooperative assembly and dynamic disassembly of MDA5 filaments for viral dsRNA recognition', *Proceedings of the National Academy of Sciences*, 108(52), pp. 21010–21015. doi: 10.1073/pnas.1113651108.

Peisley, A. *et al.* (2012) 'Kinetic mechanism for viral dsRNA length discrimination by MDA5 filaments.', *Proceedings of the National Academy of Sciences of the United States of America*, 109(49), pp. E3340-9. doi: 10.1073/pnas.1208618109.

Peisley, A. *et al.* (2014) 'Structural basis for ubiquitin-mediated antiviral signal activation by RIG-I', *Nature*. Nature Publishing Group, 509(7498), pp. 110–114. doi: 10.1038/nature13140.

Pestal, K. *et al.* (2015) 'Isoforms of RNA-Editing Enzyme ADAR1 Independently Control Nucleic Acid Sensor MDA5-Driven Autoimmunity and Multi-organ Development', *Immunity*. Elsevier Inc., 43(5), pp. 933–944. doi: 10.1016/j.immuni.2015.11.001.

Pichlmair, A. *et al.* (2006) 'RIG-I-Mediated Antiviral Responses to Single-Stranded RNA Bearing 5'-Phosphates', *Science*, 314(5801), pp. 997–1001. doi: 10.1126/science.1132998.

Pichlmair, A. *et al.* (2009) 'Activation of MDA5 Requires Higher-Order RNA Structures Generated during Virus Infection', *Journal of Virology*, 83(20), pp. 10761–10769. doi: 10.1128/JVI.00770-09.

Priyamvada, L. *et al.* (2016) 'Human antibody responses after dengue virus infection are highly cross-reactive to Zika virus', *Proceedings of the National Academy of Sciences*, 113(28), pp. 7852–7857. doi: 10.1073/pnas.1607931113.

Pryor, M. J. *et al.* (2007) 'Nuclear localization of dengue virus nonstructural protein 5 through its importin ??/??-recognized nuclear localization sequences is integral to viral infection', *Traffic*, 8(7), pp. 795–807. doi: 10.1111/j.1600-0854.2007.00579.x.

Pyzocha, N. K. *et al.* (2014) 'RNA-guided genome editing of mammalian cells', *Methods in Molecular Biology*, 1114, pp. 269–277. doi: 10.1007/978-1-62703-761-7_17.

Qi, N. *et al.* (2017) 'Multiple truncated isoforms of MAVS prevent its spontaneous aggregation in antiviral innate immune signalling.', *Nature communications*. Nature Publishing Group, 8, p. 15676. doi: 10.1038/ncomms15676.

Qiu, W. *et al.* (2013) 'ADAR1 is essential for intestinal homeostasis and stem cell maintenance', *Cell Death and Disease*, 4(4), p. e599. doi: 10.1038/cddis.2013.125.

Ray, D. *et al.* (2006) 'West Nile virus 5'-cap structure is formed by sequential guanine N-7 and ribose 2'-O methylations by nonstructural protein 5.', *Journal of virology*, 80(17), pp. 8362–70. doi: 10.1128/JVI.00814-06.

Rehwinkel, J. *et al.* (2010a) 'RIG-I Detects Viral Genomic RNA during Negative-Strand RNA Virus Infection', *Cell*, 140(3), pp. 397–408. doi: 10.1016/j.cell.2010.01.020.

Rehwinkel, J. *et al.* (2010b) 'RIG-I Detects Viral Genomic RNA during Negative-Strand RNA Virus Infection', *Cell*. Elsevier Ltd, 140(3), pp. 397–408. doi: 10.1016/j.cell.2010.01.020.

Rehwinkel, J. and Reis e Sousa, C. (2010) 'RIGorous Detection: Exposing Virus Through RNA Sensing', *Science*, 327(5963), pp. 284–286. doi: 10.1126/science.1185068.

Rehwinkel, J. and Reis e Sousa, C. (2013) 'Targeting the viral Achilles' heel: Recognition of 5'-triphosphate RNA in innate anti-viral defence', *Current Opinion in Microbiology*. Elsevier Ltd, 16(4), pp. 485–492. doi: 10.1016/j.mib.2013.04.009.

Rice, G. I. *et al.* (2012) 'Mutations in ADAR1 cause Aicardi-Goutières syndrome associated with a type I interferon signature', *Nature Genetics*. Nature Publishing Group, 44(11), pp. 1243–1248. doi: 10.1038/ng.2414.

Rice, G. I. *et al.* (2014) 'Gain-of-function mutations in IFIH1 cause a spectrum of human disease phenotypes associated with upregulated type I interferon signaling', *Nature Genetics*. Nature Publishing Group, 46(5), pp. 503–509. doi: 10.1038/ng.2933.

Roers, A., Hiller, B. and Hornung, V. (2016) 'Recognition of Endogenous Nucleic Acids by the Innate Immune System', *Immunity*, 44(4), pp. 739–754. doi: 10.1016/j.immuni.2016.04.002.

Roulois, D. *et al.* (2015) 'DNA-Demethylating Agents Target Colorectal Cancer Cells by Inducing Viral Mimicry by Endogenous Transcripts', *Cell*. Elsevier Inc., 162(5), pp. 961–973. doi: 10.1016/j.cell.2015.07.056.

Runge, S. *et al.* (2014) 'In Vivo Ligands of MDA5 and RIG-I in Measles Virus-

Infected Cells', *PLoS Pathogens*, 10(4). doi: 10.1371/journal.ppat.1004081.

Saito, T. *et al.* (2008a) 'Innate immunity induced by composition-dependent RIG-I recognition of hepatitis C virus RNA', *Nature*, 454(7203), pp. 523–527. doi: 10.1038/nature07106.

Saito, T. *et al.* (2008b) 'Innate immunity induced by composition-dependent RIG-I recognition of hepatitis C virus RNA', *Nature*, 454(7203), pp. 523–527. doi: 10.1038/nature07106.

Sato, S. *et al.* (2015) 'The RNA Sensor RIG-I Dually Functions as an Innate Sensor and Direct Antiviral Factor for Hepatitis B Virus', *Immunity*, 42(1), pp. 123–132. doi: 10.1016/j.immuni.2014.12.016.

Schermelleh, L., Heintzmann, R. and Leonhardt, H. (2010) 'A guide to super-resolution fluorescence microscopy', *Journal of Cell Biology*, 190(2), pp. 165–175. doi: 10.1083/jcb.201002018.

Schlee, M. and Hartmann, G. (2016) 'Discriminating self from non-self in nucleic acid sensing', *Nature Reviews Immunology*, 16(9), pp. 566–580. doi: 10.1038/nri.2016.78.

Schnell, G. *et al.* (2012) 'Uridine Composition of the Poly-U/UC Tract of HCV RNA Defines Non-Self Recognition by RIG-I', *PLoS Pathogens*, 8(8). doi: 10.1371/journal.ppat.1002839.

Schuberth-Wagner, C. *et al.* (2015) 'A Conserved Histidine in the RNA Sensor RIG-I Controls Immune Tolerance to N<inf>1</inf>-2'O-Methylated Self RNA', *Immunity*, 43(1), pp. 41–52. doi: 10.1016/j.immuni.2015.06.015.

Schulz, O. *et al.* (2010) 'NIH Public Access', 7(5), pp. 354–361. doi: 10.1016/j.chom.2010.04.007.Protein.

Seth, R. B. *et al.* (2005) 'Identification and characterization of MAVS, a mitochondrial antiviral signaling protein that activates NF-κB and IRF3', *Cell*, 122(5), pp. 669–682. doi: 10.1016/j.cell.2005.08.012.

Shi, J. *et al.* (2014) 'Inflammatory caspases are innate immune receptors for intracellular LPS', *Nature*. Nature Publishing Group. doi: 10.1038/nature13683.

Smyth, D. J. *et al.* (2006) 'A genome-wide association study of nonsynonymous SNPs identifies a type 1 diabetes locus in the interferon-induced helicase (IFIH1) region', *Nature genetics*, 38(6), pp. 617–619. doi: 10.1038/ng1800.

Sprokholt, J. K. *et al.* (2017) 'RIG-I–like Receptor Triggering by Dengue Virus Drives Dendritic Cell Immune Activation and T H 1 Differentiation', *The Journal of Immunology*, 198(12), pp. 4764–4771. doi: 10.4049/jimmunol.1602121.

Sugimoto, Y. *et al.* (2015) '{hiCLIP} reveals the in vivo atlas of {mRNA} secondary structures recognized by Staufen 1.', *Nature*. Nature Publishing Group, 519(7544), pp. 491–494. doi: 10.1038/nature14280.

Sugimoto, Y. *et al.* (2017) 'Using hiCLIP to identify RNA duplexes that interact with a specific RNA-binding protein', *Nature Protocols*. Nature Publishing Group, 12(3), pp. 611–637. doi: 10.1038/nprot.2016.188.

Sun, L. *et al.* (2013) 'Cyclic GMP-AMP Synthase Is', *Science*, 339, pp. 786–791. doi: 10.1126/science.1229963.

Sun, Z. *et al.* (2011) 'Phosphorylation of RIG-I by Casein Kinase II Inhibits Its Antiviral Response', *Journal of Virology*, 85(2), pp. 1036–1047. doi: 10.1128/JVI.01734-10.

Szretter, K. J. *et al.* (2012) '2′-O Methylation of the Viral mRNA Cap by West Nile Virus Evades Ifit1-Dependent and -Independent Mechanisms of Host Restriction In Vivo', *PLoS Pathogens*. Edited by M. U. Gack, 8(5), p. e1002698. doi: 10.1371/journal.ppat.1002698.

Takamatsu, Y., Uchida, L. and Morita, K. (2015) 'Delayed IFN response differentiates replication of west nile virus and japanese encephalitis virus in human neuroblastoma and glioblastoma cells', *Journal of General Virology*, 96(8), pp. 2194–2199. doi: 10.1099/vir.0.000168.

Takashima, K. *et al.* (2015) 'RIOK3-mediated phosphorylation of MDA5 interferes with its assembly and attenuates the innate immune response', *Cell Reports*. The Authors, 11(2), pp. 192–200. doi: 10.1016/j.celrep.2015.03.027.

Tang, W. W. *et al.* (2016) 'A Mouse Model of Zika Virus Sexual Transmission and Vaginal Viral Replication', *Cell Reports*. ElsevierCompany., 17(12), pp. 3091–3098. doi: 10.1016/j.celrep.2016.11.070.

Thrift, A. P., El-Serag, H. B. and Kanwal, F. (2016) 'Global epidemiology and burden of HCV infection and HCV-related disease', *Nature Reviews Gastroenterology & Hepatology*. Nature Publishing Group, 14(2), pp. 122–132. doi: 10.1038/nrgastro.2016.176.

Triantafilou, K. *et al.* (2012) 'Visualisation of direct interaction of MDA5 and the dsRNA replicative intermediate form of positive strand RNA viruses', *Journal of Cell Science*, 125(20), pp. 4761–4769. doi: 10.1242/jcs.103887.

Uchida, L. *et al.* (2014) 'The dengue virus conceals double-stranded RNA in the intracellular membrane to escape from an interferon response', *Scientific Reports*, 4, p. 7395. doi: 10.1038/srep07395.

Uchikawa, E. *et al.* (2016) 'Structural Analysis of dsRNA Binding to Anti-viral Pattern Recognition Receptors LGP2 and MDA5', *Molecular Cell*, 62(4), pp. 586–602. doi: 10.1016/j.molcel.2016.04.021.

Uraki, R. *et al.* (2017) 'Fetal Growth Restriction Caused by Sexual Transmission of Zika Virus in Mice', *The Journal of Infectious Diseases*, 215. doi: 10.1093/infdis/jix204.

Uzri, D. and Gehrke, L. (2009) 'Nucleotide Sequences and Modifications That Determine RIG-I/RNA Binding and Signaling Activities', *Journal of Virology*,

83(9), pp. 4174–4184. doi: 10.1128/JVI.02449-08.

Venkataraman, T. *et al.* (2007) 'Loss of DExD/H Box RNA Helicase LGP2 Manifests Disparate Antiviral Responses', *The Journal of Immunology*, 178(10), pp. 6444–6455. doi: 10.4049/jimmunol.178.10.6444.

Wang, H. *et al.* (2017) 'cGAS is essential for the antitumor effect of immune checkpoint blockade', *Proceedings of the National Academy of Sciences*, p. 201621363. doi: 10.1073/pnas.1621363114.

Weaver, S. C. (2017) 'Emergence of epidemic zika virus transmission and congenital zika syndrome: Are recently evolved traits to blame?', *mBio*, 8(1), pp. 1–5. doi: 10.1128/mBio.02063-16.

Weber, F. *et al.* (2006) 'Double-Stranded RNA Is Produced by Positive-Strand RNA Viruses and DNA Viruses but Not in Detectable Amounts by Negative-Strand RNA Viruses Double-Stranded RNA Is Produced by Positive-Strand RNA Viruses and DNA Viruses but Not in Detectable Amounts by Neg', *Journal of virology*, 80(10), pp. 5059–5064. doi: 10.1128/JVI.80.10.5059.

de Weerd, N. A. and Nguyen, T. (2012) 'The interferons and their receptors—distribution and regulation', *Immunology and Cell Biology*. Nature Publishing Group, 90(5), pp. 483–491. doi: 10.1038/icb.2012.9.

Welsch, S. *et al.* (2009) 'Composition and Three-Dimensional Architecture of the Dengue Virus Replication and Assembly Sites', *Cell Host and Microbe*. Elsevier Ltd, 5(4), pp. 365–375. doi: 10.1016/j.chom.2009.03.007.

West, A. P. *et al.* (2015) 'Mitochondrial DNA stress primes the antiviral innate immune response', *Nature*, 520(7548), pp. 553–557. doi: 10.1038/nature14156.

Wies, E. *et al.* (2013) 'Dephosphorylation of the RNA Sensors RIG-I and MDA5 by the Phosphatase PP1 Is Essential for Innate Immune Signaling', *Immunity*, 38(3), pp. 437–449. doi: 10.1016/j.immuni.2012.11.018.

Williams, B. R. (1999) 'PKR; a sentinel kinase for cellular stress', *Oncogene*, 18(45), pp. 6112–6120. doi: 10.1038/sj.onc.1203127.

Wu, B. *et al.* (2013) 'Structural basis for dsRNA recognition, filament formation, and antiviral signal activation by MDA5', *Cell*. Elsevier Inc., 152(1–2), pp. 276–289. doi: 10.1016/j.cell.2012.11.048.

Wu, B. *et al.* (2014) 'Molecular imprinting as a signal-activation mechanism of the viral RNA sensor RIG-I', *Molecular Cell*. Elsevier Inc., 55(4), pp. 511–523. doi: 10.1016/j.molcel.2014.06.010.

Wu, J. and Chen, Z. J. (2014) 'Innate Immune Sensing and Signaling of Cytosolic Nucleic Acids', *Annual Review of Immunology*, 32(1), pp. 461–488. doi: 10.1146/annurev-immunol-032713-120156.

Xu, H. *et al.* (2014) 'Structural basis for the prion-like MAVS filaments in antiviral innate immunity', *eLife*, 3, p. e01489. doi: 10.7554/eLife.01489.

XuFeng, R. *et al.* (2009) 'ADAR1 is required for hematopoietic progenitor cell survival via RNA editing', *Proceedings of the National Academy of Sciences*, 106(42), pp. 17763–17768. doi: 10.1073/pnas.0903324106.

Yang, H. *et al.* (2017) 'cGAS is essential for cellular senescence', *Proceedings of the National Academy of Sciences*, p. 201705499. doi: 10.1073/pnas.1705499114.

Yao, H. *et al.* (2015) 'ATP-Dependent effector-like functions of RIG-I-like receptors', *Molecular Cell*, 58(3), pp. 541–548. doi: 10.1016/j.molcel.2015.03.014.

Yockey, L. J. *et al.* (2016) 'Vaginal Exposure to Zika Virus during Pregnancy Leads to Fetal Brain Infection', *Cell*, 166(5), p. 1247–1256.e4. doi: 10.1016/j.cell.2016.08.004.

Yoneyama, M. *et al.* (2004) 'The RNA helicase RIG-I has an essential function in double-stranded RNA-induced innate antiviral responses', *Nature Immunology*, 5(7), pp. 730–737. doi: 10.1038/ni1087.

Yoo, Y.-S. *et al.* (2015) 'The mitochondrial ubiquitin ligase MARCH5 resolves MAVS aggregates during antiviral signalling', *Nature Communications*. Nature Publishing Group, 6, p. 7910. doi: 10.1038/ncomms8910.

Yu, C. Y. *et al.* (2012) 'Dengue virus targets the adaptor protein MITA to subvert host innate immunity', *PLoS Pathogens*, 8(6). doi: 10.1371/journal.ppat.1002780.

Zarnegar, B. J. *et al.* (2016) 'irCLIP platform for efficient characterization of protein-RNA interactions', *Nat Methods*, 13(6), pp. 489–492. doi: 10.1038/nmeth.3840.

Zeidler, J. *et al.* (2017) 'Non-Canonical Roles of Dengue Virus Non-Structural Proteins', *Viruses*, 9(3), p. 42. doi: 10.3390/v9030042.

Zellweger, R. M. and Shresta, S. (2014) 'Mouse models to study dengue virus immunology and pathogenesis', *Frontiers in Immunology*, 5(APR), pp. 1–9. doi: 10.3389/fimmu.2014.00151.

Zeng, W. *et al.* (2010) 'Reconstitution of the RIG-I pathway reveals a signaling role of unanchored polyubiquitin chains in innate immunity', *Cell*. Elsevier Ltd, 141(2), pp. 315–330. doi: 10.1016/j.cell.2010.03.029.

Zhao, B. *et al.* (2017) 'Structure and function of the Zika virus full-length NS5 protein', *Nature Communications*. Nature Publishing Group, 8, p. 14762. doi: 10.1038/ncomms14762.

Zhou, Z. *et al.* (2007) 'Type III Interferon (IFN) Induces a Type I IFN-Like Response in a Restricted Subset of Cells through Signaling Pathways Involving both the Jak-STAT Pathway and the Mitogen-Activated Protein Kinases', *Journal of Virology*, 81(14), pp. 7749–7758. doi: 10.1128/JVI.02438-06.

Zhou, Yangsheng *et al.* (2007) ‘Structure and Function of Flavivirus NS5 Methyltransferase’, *Journal of Virology*, 81(8), pp. 3891–3903. doi: 10.1128/JVI.02704-06.

Zompi, S. and Harris, E. (2012) ‘Animal models of dengue virus infection’, *Viruses*, 4(1), pp. 62–82. doi: 10.3390/v4010062.